BNWL-1967
UC-23

The Containment of $^{90}SrF_2$ at 800 to 1100°C Preliminary Results

November 1975

Prepared for the U.S. Energy Research and Development Administration under Contract E(45-1):1830

Battelle
Pacific Northwest Laboratories

BNWL-1967

DISCLAIMER

NOTICE

PACIFIC NORTHWEST LABORATORY
operated by
BATTELLE
for the
U.S. ENERGY RESEARCH AND DEVELOPMENT ADMINISTRATION
Under Contract E(45-1)-1830

Printed in the United States of America
Available from
National Technical Information Service
U.S. Department of Commerce
5285 Port Royal Road
Springfield, Virginia 22151
Price: Printed Copy $7.75; Microfiche $2.25

BNWL-1967
UC-23

THE CONTAINMENT OF $^{90}SrF_2$ AT 800 TO 1100°C PRELIMINARY RESULTS

by
H. T. Fullam

November 1975

Battelle
Pacific Northwest Laboratories
Richland, Washington 99352

THIS PAGE

WAS INTENTIONALLY

LEFT BLANK

ABSTRACT

A program is currently underway at PNL to develop the data needed to license $^{90}SrF_2$ for heat source applications. A major portion of the program involves determining the compatibility of $^{90}SrF_2$ with containment materials at elevated temperatures. The compatibility studies are divided into two phases: an initial series of short-term scouting tests lasting up to 4400 hr in which a number of containment materials were evaluated, and a subsequent series of long-term tests in which the three best containment materials identified in the short-term tests will be tested for up to 30,000 hr with WESF-produced $^{90}SrF_2$. This report summarizes the results of the first phase tests.

The short-term tests were carried-out at temperatures of 800, 1000 and 1100°C for 1500 and 4400 hr using both radioactive and nonradioactive strontium fluoride. Nine potential containment materials were evaluated in the tests: two refractory metals (tungsten and TZM); two cobalt base alloys (Haynes Alloy 25 and Haynes Alloy 188); and five nickel base alloys (Hastelloy C-276, Hastelloy X, Hastelloy N, Inconel 600 and Inconel 625).

Test results show that both of the refractory metals are very resistant to fluoride attack, and tungsten and TZM specimens exposed to $^{90}SrF_2$ exhibited little or no attack. Haynes Alloy 25 was the best of the Ni- and Co-base alloys, but attack up to a depth of 0.004 in. was observed in some Haynes Alloy 25 specimens exposed to $^{90}SrF_2$.

Based on the results of the short-term compatibility tests and several other factors, TZM, Haynes Alloy 25 and Hastelloy C-276, the present WESF capsule material, were selected for long-term testing with $^{90}SrF_2$.

CONTENTS

CONTENTS (contd)

LIST OF FIGURES

LIST OF FIGURES (contd)

LIST OF TABLES

LIST OF TABLES (contd)

THE CONTAINMENT OF $^{90}SrF_2$ AT 800 TO 1100°C
PRELIMINARY RESULTS

H. T. Fullam

1.0 INTRODUCTION

As part of the waste management program at the Energy Research Development Administration's (ERDA) Richland Operations complex, strontium is separated from the high-level nuclear fuel reprocessing waste, converted to the fluoride, and doubly encapsulated in small high-integrity containers for subsequent long-term storage under water. The fluoride conversion, encapsulation and storage takes place in the Waste Encapsulation and Storage Facility (WESF), which is operated for ERDA by the Atlantic Richfield Hanford Company (ARHCO).

The WESF $^{90}SrF_2$ capsules are approximately 2-5/8 in. diameter by 20 in. long. When filled with fuel-grade strontium fluoride of 50 to 55% ^{90}Sr isotopic content, the capsules contain initially about 150,000 Ci of ^{90}Sr. This is equivalent to a thermal output of about 1 kW/capsule. The density of the fluoride in the capsule is approximately 75% of the theoretical density and the power density is approximately 1.1 W/cm^3.

The encapsulated strontium fluoride represents an economical source of ^{90}Sr if the WESF capsule can be licensed for heat source applications under anticipated use conditions. Possible applications for $^{90}SrF_2$ heat sources include: electric power production using static and dynamic conversion systems, and heating of water and sewage systems in cold regions.

The Strontium Heat Source Development Program was started at the Pacific Northwest Laboratory (PNL) in 1973 to develop the information needed to permit licensing of $^{90}SrF_2$ sources, and more specifically the WESF $^{90}SrF_2$ capsules, for heat source applications. The program was sponsored initially by the former Atomic Energy Commission's Division of Applied Technology (DAT) and subsequently by ERDA's Division of Space Nuclear Systems (SNS).

It was apparent at the start of the Strontium Heat Source Development Program that considerable information was needed before $^{90}SrF_2$ sources could be licensed. The program plan calls for research studies extending into FY-1980. The major areas of research include:

- The chemical and metallurgical compatibility of containment materials with $^{90}SrF_2$ at elevated temperatures,
- Chemical and physical properties of $^{90}SrF_2$ and the effects of impurities on these properties,
- Necessary capsule property data such as mechanical strength and resistance to external corrosion.

Licensing of the $^{90}SrF_2$ heat sources will require assurance of containment of the $^{90}SrF_2$ during the service life of the source. The service life can be relatively short if the source is guaranteed retrievable. For the cases where the source is irretrievable, or the more practical cases where retrievability cannot be guaranteed, assurance must be provided that the $^{90}SrF_2$ is adequately contained until the ^{90}Sr decays to a negligible level. Since the ^{90}Sr has a half-life of approximately 29 years, a large heat source would require a decay period of several hundred years for the ^{90}Sr content to reach a negligible level. Assurance of adequate containment of the ^{90}Sr for such an extended period can only be provided by adequate knowledge of the kinetics of the reactions which occur between the $^{90}SrF_2$ and the containment material at the source temperature.

At the time the program was initiated there was only a limited amount of data available on the compatibility of $^{90}SrF_2$ with containment materials. The Martin Marietta Corporation evaluated the compatibility of nonradioactive SrF_2 with various materials at 925°C for periods up to 19 months.[1] As part of the research program to develop the WESF process, PNL evaluated the compatibility of $^{90}SrF_2$ with various containment materials at 400°C for up to 1 year, and nonradioactive SrF_2 with the same materials at 400 and 800°C for up to 3 years.[2] Based on information developed in the study, Hastelloy C-276 was selected as the containment material for the $^{90}SrF_2$ at WESF. The

data developed in these studies was not sufficient, however, to permit licensing of $^{90}SrF_2$ sources for elevated temperature use. Much more information was needed, particularly with regard to the effects of impurities and decay products on the compatibility of $^{90}SrF_2$ with containment materials, and the effects of fluoride attack on the mechanical properties of the containment materials. Therefore, a major portion of the Strontium Heat Source Development Program is devoted to obtaining the required compatibility data. For reasons to be discussed later, the compatibility studies are divided into two phases: a series of short-term scouting studies lasting up to 4400 hr, and longer-term tests lasting up to 30,000 hr. This report summarizes the results of the short-term scouting tests.

2.0 SUMMARY

A program is currently underway at PNL to develop the information required to license $^{90}SrF_2$ for heat source applications. Primary emphasis is on the $^{90}SrF_2$ produced by ARHCO at WESF. One area where additional data is needed is the compatibility of $^{90}SrF_2$ with containment materials at elevated temperatures. A major portion of the PNL program is devoted to obtaining the required compatibility data. The $^{90}SrF_2$ compatibility studies are divided into two phases: an initial series of short-term scouting tests lasting 1500 and 4400 hr followed by a series of long-term tests lasting up to 30,000 hr. The objective of the short-term scouting tests are twofold:

1. To evaluate a number of potential containment materials and select the best three for long-term testing.
2. Evaluate the effects of impurities on $^{90}SrF_2$ compatibility, and thus determine if additional purification steps are required in the WESF process to remove harmful impurities before the $^{90}SrF_2$ can be used in heat source service.

Four different grades of strontium fluoride were used in the short-term tests:

- High-purity nonradioactive SrF_2 containing less than 0.1 wt% total impurities,
- WESF-grade $^{90}SrF_2$, containing ~4.5 wt% cationic impurities, prepared by PNL using the WESF flowsheet and ^{90}Sr solution obtained from ARHCO,
- High-purity $^{90}SrF_2$, containing ~1.9 wt% cationic impurities, prepared by PNL,
- High-purity nonradioactive SrF_2 containing controlled levels of added impurities.

Each grade of SrF_2 was evaluated with nine different containment materials: two refractory metals (tungsten and TZM); two cobalt-base alloys (Haynes Alloy 25 and Haynes Alloy 188); and five nickel-base alloys (Hastelloy C-276, Hastelloy X, Hastelloy N, Inconel 600 and Inconel 625). The tests lasted 1500 and 4400 hr.

The tests with the SrF_2 containing added impurities were carried out at 1000°C, while the other grades of SrF_2 were tested at 800, 1000 and 1100°C. The couple test configuration utilized a test specimen of the containment material, 0.5 in. OD x 3/8 in. thick, buried in SrF_2 within a capsule of the same material as the test specimen. Couple interaction was determined by examination of the test specimen using metallographic techniques, scanning electron microscopy and electron microprobe analysis. Only compatibility data was obtained from the tests. No attempt was made to obtain mechanical property data from the test specimens, except for a limited number of microhardness measurements.

In analyzing the various test specimens it was found that the metal attack observed could be divided into two general types:

1. Chemical attack of the specimen which could be directly attributed to reaction with the fluoride, and includes such mechanisms as grain boundary attack (intergranular penetration), pitting, subsurface void formation and surface dissolution,
2. Microstructural changes in the metal which are not due to thermal aging. Typically this involves the disappearance of normal alloy precipitates, the formation of abnormal precipitates, or marked changes in grain size. Control specimens were tested at each set of conditions to distinguish between microstructural changes which resulted from thermal aging and those which resulted from interaction with the fluoride.

Both types of attack were found in most of the test specimens. In general, microstructural changes occurred to greater depths in the metals than did chemical attack.

Based on an overall evaluation of the short-term compatibility test data the following conclusions can be reached with regard to the containment of $^{90}SrF_2$ at 800 to 1100°C:

- The refractory metals tungsten and TZM provide the greatest resistance to fluoride attack of all the materials tested. In most of the refractory metal couples little or no attack of the test specimens could be

detected. Overall tungsten is slightly more resistant to attack than the TZM. However tungsten suffers a number of disadvantages not related to compatibility, and at the present time, of the two, TZM is the preferred containment material for $^{90}SrF_2$.

- Haynes Alloy 25 was the most resistant to fluoride attack of the seven Ni- and Co-base alloys tested. However, the Haynes Alloy 25 exhibited considerably more attack than the equivalent refractory metal specimens. Chemical attack was observed to a depth of up to 0.002 in. in some Haynes Alloy 25 specimens exposed to $^{90}SrF_2$, while microstructural changes occurred to a depth of 0.004 in. in some specimens.
- The other six Ni- and Co-base alloys were significantly less resistant to fluoride attack than the Haynes Alloy 25. Inconel 600, Hastelloy X and Hastelloy C-276 appear to be about equal in their resistance to fluoride attack, while the other three alloys, Hastelloy N, Haynes Alloy 188 and Inconel 625, are less resistant to attack.
- In general, greater attack was observed in the couples containing $^{90}SrF_2$ than in the couples containing nonradioactive SrF_2.
- In most cases, chemical attack of the test specimens did not increase appreciably with increasing exposure temperature to 1100°C, and there were instances where the attack was less at the higher temperatures. Microstructural changes due to fluoride attack were generally greater at the higher temperatures.
- The rate of metal attack appeared to decrease with time, but there was insufficient data to predict the shapes of the rate curves.
- A number of impurities were found to have a serious adverse effect on SrF_2 compatibility. The presence of SrO in the fluoride resulted in extensive chemical attack of the Ni- and Co-base alloys, but had little effect on the tungsten and TZM. Fluorides of multivalent cations, such as Fe and Cu, generally caused increased chemical attack of the containment materials tested. They also increased the depth of metal affected by changes in the microstructure. Surprisingly, water and nitrate ion had little effect on the compatibility of SrF_2. Fortunately,

the impurities which seriously affect $^{90}SrF_2$ compatibility are present only in low concentrations in the WESF $^{90}SrF_2$. It does not appear that it will be necessary to develop new or improved purification procedures for the present WESF process to reduce or remove these impurities.

Based primarily on the results of the short-term compatibility tests, as well as several other factors, TZM, Haynes Alloy 25 and Hastelloy C-276 were the three containment materials selected for long-term testing, with Inconel 600 and Hastelloy X as possible alternates. Tungsten was not selected because of the difficulties involved in using it in the WESF operation.

3.0 WESF PROCESS

A basic objective of the Strontium Heat Source Development Program is to develop the data needed to license the WESF $^{90}SrF_2$ capsule for heat source applications. The WESF process is subject to certain modifications and changes that can improve the utility of the ^{90}SrF capsule as a heat source. The compatibility testing program is intended to provide not only basic compatibility data on $^{90}SrF_2$ but also to indicate what changes in the WESF process may be necessary or desirable to improve the WESF $^{90}SrF_2$ capsule as a heat source.

The flowsheet for recovery of strontium from fuel reprocessing waste, conversion to the fluoride, and subsequent encapsulation of the fluoride is shown in Figure 1. In the process, strontium is separated from current Purex acid waste (CAW) or Purex acid sludge (PAS) by solvent extraction using di-2-ethyl-hexylphosphoric acid (HDEHP), tributyl phosphate (TBP) and normal paraffin hydrocarbon (NPH). The strontium is stripped from the organic phase with dilute nitric acid. The strontium is purified by a series of sulfate and hydroxide precipitation steps and stored as strontium nitrate in dilute nitric acid. The foregoing operations take place in B-Plant. Subsequent operations take place in WESF. Both plants are operated for ERDA by ARHCO.

The purified strontium nitrate solution serves as feed to the WESF process. All steps in the WESF process are batch operations. A given volume of strontium feed solution (containing 3 to 4 kg of Sr) is neutralized to pH 8 to 9 with sodium hydroxide solution. Solid sodium fluoride is added to the solution to precipitate strontium fluoride. The resulting slurry is digested at 80°C with air sparging and then filtered. The SrF_2 filter cake is washed with water, transferred to furnace boats, and fired at 1100°C in argon for several hours. After cooling, the SrF_2 is removed from the boats and crushed to -1/2 in. granules. The pulverized SrF_2 is loaded into a Hastelloy C-276 inner capsule using impact consolidation (pneumatic impaction) which is essentially a cold pressing operation. The loaded capsule is closed

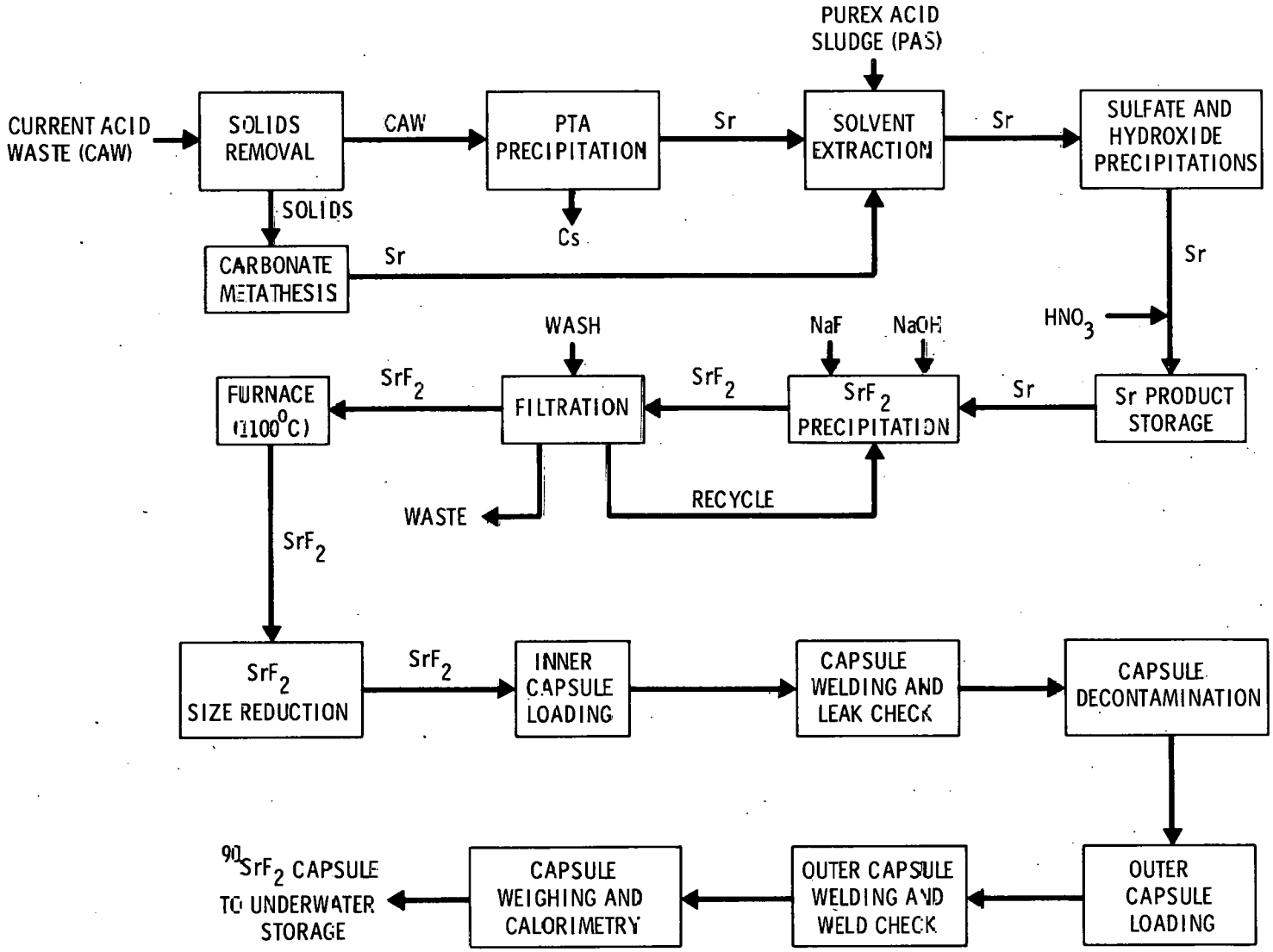

FIGURE 1. Simplified Flowsheet for the Preparation and Encapsulation of $^{90}SrF_2$ at ARHCO (WESF Process)

by tungsten inert gas (TIG) welding a lid in place, leak checked, and decontaminated. The cleaned inner capsule is then sealed in an outer capsule of Hastelloy C-276[(a)] by TIG welding. Integrity of the outer capsule weld is checked using ultrasonic techniques. The capsule is then weighed and the heat output determined in a calorimeter after which the capsule is sent to the storage basin for storage under water.

The composition of the SrF_2 is determined by analysis of samples from each batch. The SrF_2 content of each capsule is determined from weight measurements on the capsule. The ^{90}Sr content of the capsule is determined from the calorimeter measurements and isotopic analysis of the fluoride samples. Pertinent data on a typical WESF $^{90}SrF_2$ capsule containing fuel grade $^{90}SrF_2$ of 50 to 55% ^{90}Sr isotopic content are given in Table 1.

TABLE 1. Data on the WESF $^{90}SrF_2$ Capsule

Strontium Fluoride:	1. Purity ~95%		
	2. ^{90}Sr isotopic content - 50 to 55%		
	3. Density ~75% of theoretical density		
	4. Power density ~1.1 W/cm^3		
	5. Loading ~150,000 Ci		
Capsule Data:		Inner	Outer
1. Material		Hastelloy C-276	Hastelloy C-276
2. Inner Diameter		2.010 in.	2.385 in.
3. Outer Diameter		2.250 in.	2.625 in.
4. Length		19.050 in.	20.100 in.

In evaluating the potential use of the WESF $^{90}SrF_2$ capsule as a heat source, there are several aspects of the WESF encapsulation process which

(a) Plans call for the outer capsule material to be changed to 316L stainless steel as soon as the current stock of Hastelloy C-276 capsules is consumed.

should be considered. These involve process operations where modifications or changes may be possible to improve the potential usefulness of the WESF $^{90}SrF_2$ capsule:

1. Certain modifications in the capsule design may be possible which will make the WESF $^{90}SrF_2$ capsule more attractive for heat source applications without adversely affecting the encapsulation process. Possible modifications include:
   - changes in the encapsulating material--both the inner and outer capsules,
   - nominal changes in capsule dimensions (wall thickness, length, etc.),
   - changes in the capsule end cap design,
   - filling the gap between the inner and outer capsules with helium to improve heat transfer.

   A change in the inner capsule material may be required if the Hastelloy C-276 shows excessive attack by the strontium fluoride at anticipated heat source operating temperatures.

2. The composition of the WESF produced $^{90}SrF_2$ may vary between batches depending on the source of the feed material. Strontium feed solutions obtained from different sources such as different waste tanks, can contain varying amounts of impurities which can, in turn, affect the composition of the fluoride product. The composition of a typical feed solution is given in Table 2. While the types of impurities present in the various batches of feed do not vary significantly, the concentration of the impurities can vary over a considerable range. The processes used to purify the strontium feed solution are only partially effective, and some of the impurities in the feed precipitate with the strontium fluoride. Impurities which can be present in the WESF $^{90}SrF_2$, as encapsulated, and their probable forms and concentration ranges are shown in Table 3. The presence of impurities in the $^{90}SrF_2$ can affect its compatibility with containment materials at high temperature. A knowledge of the effects of the impurities on compatibility is desirable,

TABLE 2. Composition of a Typical ^{90}Sr Feed Solution

Element	Concentration (molar)
Sr	0.29
^{90}Sr	0.16
H^+	0.57
NO_3^-	3.4
Ag	<0.00004
Al	<0.0014
Ba	0.0012
Ca	0.0018
Cd	0.00005
Cr	0.0003
Cu	0.00002
Fe	0.0002
K	0.0003
Mn	<0.0005
Mg	0.0009
Na	2.06
Ni	<0.00009
Pb	0.0008
Rare Earths	0.002
Si	0.0012
Zr	Variable (decay product)

TABLE 3. Probable Impurities in WESF $^{90}SrF_2$

Impurity	Concentration Range (wt%)	Probable Form
Al	<0.5	AlF_3
Ba	0.1 -2.0	BaF_2
Ca	0.1 -2.0	CaF_2
Cd	<0.1	CdF_2
Cr	<0.2	CrF_3
Cu	<0.01	CuF_2
Fe	<0.1	FeF_3
H	<0.01	H_2O
K	<0.1	KF
Mg	0.05-0.5	MgF_2
Mn	<0.1	MnF_2
N	<0.01	NO_3^-
Na	1-4	NaF
Ni	<0.1	NiF_2
O	<0.05	H_2O
Pb	<0.2	PbF_2
R[(a)]	<2.0	RF_3
Si	<0.02	SiO_2 or $SiF_6^=$
Zr	Variable (decay product)	ZrF_4?

(a) Rare earths

especially for those impurities which are present in high concentrations, undergo valence changes or form easily reduced fluorides. If certain impurities are found to be deleterious to $^{90}SrF_2$ compatibility, their removal from the fluoride should be considered. Inclusion of additional purification steps in the WESF process to remove harmful impurities may be possible if deemed necessary.

3. The $^{90}SrF_2$ is loaded into the inner capsule by impact consolidation using a pneumatic impactor, and is essentially a cold pressing operation. This method of loading produces several effects in the loaded capsule. The loading operation stresses the capsule wall and, because the strontium fluoride does not flow readily under pressure, can result in damage to the inner capsule surface and some distortion of the capsule. As a result, potential containment materials are limited to those that can withstand the rigors of the loading operation. This eliminates from consideration as containment materials a number of materials and concepts which could possibly provide adequate compatibility with the fluoride at heat source operating temperatures. These include vapor deposited metal or ceramic films, thin metal liners and brittle materials.

   When the $^{90}SrF_2$ is pressed into the Hastelloy C-276 capsule there is intimate contact between the fluoride and the inner surface of the capsule. This differs from most heat sources in which the fuel is pelletized and slipped into the containment vessel. The increased contact observed in the WESF capsules could result in greater fluoride-clad interaction than would be observed in capsules containing fluoride pellets.

   The loading equipment available at WESF limits the fluoride density that can be achieved in the capsule to about 75% of theoretical density. It would be necessary to go to a different method of loading to achieve higher fluoride densities.

4. Much of the high-level reprocessing wastes at Hanford have been stored for many years. The ^{90}Sr isotopic content of these wastes can vary from as low as 25 to 30% to a maximum of greater than 50% depending on how long the wastes have been stored. The strontium currently being processed at WESF has an ^{90}Sr isotopic content of 25 to 30%. Processing of fuel-grade strontium is not scheduled to start until the second quarter of FY-1976.

4.0 THEORETICAL ANALYSIS OF $^{90}SrF_2$ COMPATIBILITY

The possible reactions which can occur between a radioisotope fuel, such as $^{90}SrF_2$, and a containment material can be predicted on the basis of thermodynamic considerations. Calculation of the Gibbs free energy of reaction (ΔG_R°) can provide an estimate of the potential for a given reaction to occur (but provides no information on reaction kinetics). Therefore, a thermodynamic analysis of potential $^{90}SrF_2$-container reactions can provide useful information to help in selecting potential containment materials for compatibility testing. For the thermodynamic analysis to be of real value, however, it is necessary that all potential reactions be evaluated. This requires that all existing and potential compounds in the systems be identified and that thermochemical data be available for all compounds. Carrying out a rigorous thermodynamic analysis can be a relatively easy task for a simple system which involves only a few components, but can be extremely difficult or impossible for very complex systems. Unfortunately presently conceived systems containing WESF $^{90}SrF_2$ falls into the latter category.

In attempting a thermodynamic analysis of any system containing $^{90}SrF_2$ it is necessary to know what strontium compounds can exist in the system. Strontium is reported to form two fluorides: SrF and SrF_2. The monofluoride, SrF, is reported to form only at high temperatures in the gas phase, and should not be stable at the temperatures encountered in a $^{90}SrF_2$ heat source (<1200°C). Therefore, SrF need not be considered in any theoretical analysis of $^{90}SrF_2$ containment. Strontium fluoride, SrF_2, is one of the most stable fluorides (and compounds) known, having a reported free energy of formation (ΔG_f°) of approximately -136 and -116 kcal/g-atom of fluorine at 25 and 1200°C, respectively. Only the fluorides of lithium, calcium and barium (and possibly some rare earths) possess similar stabilities. The free energies of formation at 25°C for a number of simple fluorides are given in Table 4. Most of the ΔG_f° values given in the table were estimated by various theoretical techniques and are not based on experimental measurements. The accuracy of the free energy data is subject

TABLE 4. Free Energy of Formation of Some Fluorides[a] at 25°C (in kcal/g-atom of fluorine)

Fluoride[b]	$-\Delta G_f^\circ$[c] kcal/g-atom of F	Fluoride[b]	$-\Delta G_f^\circ$[c] kcal/g-atom of F
AgF	44	NbF_5	64
AlF_3	113	NdF_3	134
AsF_3	63	NiF_2	74
AuF_3	28	OsF_2	46
BF_3	90	PF_3	54
BaF_2	137	PbF_2	74
BeF_2	104	PdF_2	56
BiF_3	67	PrF_3	132
CF_4	40	PtF_3	40
CaF_2	140	RbF	126
CdF_2	77	ReF_3	51
CeF_3	133	RhF_2	54
CoF_2	74	RuF_5	56
CrF_2	86	SF_6	40
CsF	124	SbF_3	67
CuF_2	59	ScF_3	117
DyF_3	129	SeF_6	37
ErF_3	130	SiF_4	94
EuF_2	121	SmF_3	129
FeF_2	79	SnF_2	73
GaF_3	80	SrF_2	138
GdF_3	138?	TaF_2	85
GeF_2	80	TbF_3	129
HF	65	TeF_6	47
HfF_3	111	ThF_4	114
HgF_2	42	TiF_3	100
HoF_3	126	TlF	60
InF_3	78	TmF_3	120
IrF_4	47	UF_3	107
KF	129	VF_3	85
LaF_3	134	WF_4	58
LiF	139	YF_3	127
LuF_3	137?	YbF_3	124
MgF_2	128	ZnF_2	82
MoF_5	63	ZrF_4	108
NaF	129		

(a) Most of the values were taken from Rosenqvist,[3] Glassner,[4] Smithells,[5] and Kubaschewski and Evans.[6]
(b) Only the most stable fluoride at 25°C of each element is listed.
(c) Most of the ΔG_f° values given were estimated by theoretical techniques and are not based on experimental measurements.

to question and the values given in Table 4 have been rounded off to the nearest whole number. Strontium is reported to form only a few complex fluorides, such as $SrSiF_6$ and $SrPbF_6$ and a limited number of intermetallic compounds. Very little thermochemical data are available on the intermetallics or complex fluorides which do exist. The limited data available indicate that strontium has very low solubility in most metals.

Because strontium fluoride is extremely stable, the pure compound should be relatively unreactive with potential containment materials. Reactive metals such as Li, Ca and Ba and the individual rare earths metals are not considered as practical containment materials. Reactions of the type,

$$aSrF_2 + M \longrightarrow aSr + MF_{2a} \qquad (1)$$

where M is any metal, should be thermodynamically unfavorable up to at least 1200°C assuming a closed system and all condensed phases at unit activity. Dissolution of the strontium metal in M could reduce the activity of the strontium. However, it appears quite unlikely that the solubility of strontium in the containment materials of interest would be sufficient to reduce the activity.

Since the monofluoride is not stable at the conditions under consideration, reactions of the type shown in Equation (2) need not be considered.

$$aSrF_2 + M \longrightarrow aSrF + MF_a \qquad (2)$$

Strontium does form some complex fluorides but in every case the strontium has an oxidation state of +2. Therefore reactions of the type in Equation (3) are not possible.

$$aSrF_2 + bM \longrightarrow Sr_aM_bF_{2a} \qquad (3)$$

However, it is possible that reactions as shown in Equation (4) could occur (using Si as an example).

$$3SrF_2 + Si \longrightarrow SrSiF_6 + 2Sr \qquad (4)$$

Unfortunately thermochemical data for the complex fluorides are not available. To make Equation (4) thermodynamically favorable at 25°C the

free energy of formation of the $SrSiF_6$ would have to be at least -138 kcal/g-atom of fluorine, which appears unlikely. However, the possibility of reactions similar to Equation (4) occurring must be considered, and the more negative the free energy of formation of the metal fluoride (i.e., SiF_4) the more likely the reaction is to be thermodynamically favorable.

The possibility of reactions involving the formation of intermetallic compounds of strontium must be considered.

$$aSrF_2 + bM \longrightarrow Sr_aM_{b-1} + MF_{2a} \qquad (5)$$

For Equation (5) to be thermodynamically favorable the free energy of formation of the intermetallic compound must be sufficiently negative to overcome the difference in free energies of formation of SrF_2 and the metal fluoride. Therefore, the more negative ΔG_f° for the metal fluoride is the less negative ΔG_f° for the intermetallic compound has to be to make the reaction favorable. Magnesium forms a very stable fluoride and is one of the few metals which is reported to form intermetallic compounds with strontium.[5] One can postulate the reaction

$$SrF_2 + 3Mg \longrightarrow Mg_2Sr + MgF_2 \qquad (6)$$

For Equation (6) to be energetically favorable at 25°C the free energy of formation of Mg_2Sr would have to be more negative than -20 kcal/mole. The ΔG_f° for Mg_2Sr has not been reported in the literature. The heat of formation of Mg_2Sr is reported to be only -5.1 kcal/mole,[5] and it is extremely unlikely that ΔG_f° could approach -20 kcal/mole. Therefore, Equation (6) should be thermodynamically unfavorable.

It is theoretically possible that components of the metal phase could dissolve in the solid strontium fluoride. However, little is known of metal solubility in the fluoride, and it is difficult to predict if measurable metal dissolution could occur below the melting point of the fluoride.

In discussing Equations (1) through (5) it was assumed that the reactant M was present at unit activity (as a separate and discrete phase).

If M is the constituent of an alloy, and is present in solid solution or as a compound (i.e., carbide, intermetallic compounds, etc.), then the reactions would be thermodynamically less favorable because of the free energy associated with compound formation or solid solution.

In analyzing a system containing $^{90}SrF_2$ it is necessary to consider the decay products formed.

$$^{90}SrF_2 \longrightarrow [^{90}Y \cdot F_2] \longrightarrow {}^{90}Zr \cdot F_2 + Q + 2e \qquad (7)$$

The equilibrium quantity of ^{90}Y in the system is very small and can be ignored. Zirconium difluoride (ZrF_2) has been reported in the literature[7] but is said to disproportionate at elevated temperatures.

$$2ZrF_2 \longrightarrow ZrF_4 + Zr \qquad (8)$$

It is impossible to define at this time what the decay products would be in a $^{90}SrF_2$ system held at elevated temperatures. Any ZrF_2 present should disproportionate, but this has not been demonstrated experimentally. Any theoretical analysis of a $^{90}SrF_2$ system should, therefore, consider ZrF_2, ZrF_4 and zirconium metal as possible decay products. It is possible that the ZrF_2 or ZrF_4 could react with the $^{90}SrF_2$ to form a complex fluoride, but no complex fluorides containing Sr and Zr have been reported. The ZrF_2 and ZrF_4 are thermodynamically less stable than the SrF_2. Therefore, reactions of the types shown in Equations (1) through (5) involving the zirconium fluorides and containment materials are more likely to be thermodynamically favorable than the equivalent reactions involving SrF_2.

WESF-produced $^{90}SrF_2$ can contain a great many impurities (see Table 3). The available analytical data identify only the elemental constituents and not the chemical compounds. The data indicate, however, that the cationic impurities are present primarily as fluorides. It can be assumed that the impurities are present as simple fluorides but this has not been demonstrated experimentally, and X-ray diffraction patterns for nonradioactive SrF_2 prepared by the WESF flowsheet and containing the same elemental impurities were far too complex to interpret. It is likely, however, that

some or all of the impurity fluorides are present as solid solutions or complex fluorides with the $^{90}SrF_2$, ZrF_2, ZrF_4 or each other. Without knowing the chemical compounds present it is impossible to analyze the system rigorously. If one assumes the impurity fluorides are present as simple fluorides of unit activity then the potential for reactions between the impurity fluorides and containment materials can be estimated. By referring to Table 4 it can be seen that most of the impurity fluorides are much less stable than SrF_2, and reactions of the types shown in Equations (1) through (5) involving the less stable impurity fluorides are more likely to be thermodynamically favorable than those involving SrF_2. The overall net effect is for most impurities to increase the possibility of attack of the containment material.

The ZrF_2 and zirconium metal, which may be present as decay products, represent fairly strong reducing agents. The possibility of reactions between the ZrF_2 or zirconium metal and the less stable impurity fluorides must be considered. Equations (9) through (12) are typical of the types of reactions which may be possible.

$$ZrF_2 + MF_2 \longrightarrow ZrF_4 + M \qquad (9)$$

$$ZrF_2 + 2MF_2 \longrightarrow MZrF_6 + M \qquad (10)$$

$$Zr + 2MF_2 \longrightarrow ZrF_4 + 2M \qquad (11)$$

$$2Zr + 2MF_2 \longrightarrow ZrF_4 + ZrM_2 \qquad (12)$$

The metals formed by reduction of the fluorides could in turn react with the containment material to form solid solutions or intermetallic compounds. Similarly the zirconium metal could react directly with the containment material.

The $^{90}SrF_2$ contains a small amount of oxygen (<500 ppm). The analytical data show most of the oxygen is present as water. However, small amounts of metal oxides may be present. Therefore, any thermodynamic analysis of a $^{90}SrF_2$ system should include potential reactions involving

water and the metal oxides. The ZrF_2 or zirconium metal, as it forms, could react with the water and less stable metal oxides, and these reactions must be considered as well.

From the above discussion it can be seen that any WESF $^{90}SrF_2$-container system is extremely complex, especially if the container material is a Ni- or Co-base alloy, most of which have a large number of constituents. Ni- and Co-base alloys in the solution heat-treated form have their constituents present primarily in solid solution. Thermal aging of the alloy, as would occur with a $^{90}SrF_2$ heat source, produces reactions which result in compound formation (carbides, intermetallics, etc.). The compounds formed in a given alloy can vary with aging time and temperature.

The complexity of any WESF $^{90}SrF_2$ system combined with the lack of thermochemical data on the complex fluorides, intermetallics, carbides, etc. makes a rigorous thermodynamic analysis of any WESF $^{90}SrF_2$-container system impossible at the present time. By making a number of simplifying assumptions it is possible to carry out an elementary thermodynamic analysis of WESF $^{90}SrF_2$ containment. Such an analysis is of limited value in selecting potential containment materials for compatibility testing, but can be of use as an aid in interpreting the compatibility test results.

Nine containment materials were evaluated in the short-term compatibility tests: two refractory metals, two cobalt-base alloys and five nickel-base alloys. An elementary thermodynamic analysis was performed on each of the container-WESF $^{90}SrF_2$ systems, and is presented in the Appendix. The reactions predicted by the thermodynamic calculations were confirmed in a general way by the experimental results. However, it is apparent that because of the simplifying assumptions required, the thermodynamic analysis does not present a true picture of the reactions involved in the WESF $^{90}SrF_2$-container systems.

5.0 OBJECTIVES

The short-term compatibility tests represent the first phase of a compatibility program that is intended to identify containment materials for $^{90}SrF_2$ that will permit its use in heat source applications. The principal effort is directed at developing the data required to license WESF-produced $^{90}SrF_2$ and the WESF capsule. The basic objectives of the short-term tests were twofold:

1. To evaluate a variety of potential containment materials with strontium fluoride in a series of short-term scouting tests and develop sufficient data to allow selection of the 2 or 3 best materials for long-term compatibility testing,
2. To evaluate the effects of impurities on the compatibility of strontium fluoride with containment materials and determine if additional purification steps are needed in the WESF process to produce a fluoride product that can be adequately contained in heat source applications.

Compatibility testing can be very costly and time consuming, especially when highly radioactive materials such as ^{90}Sr are involved. Much of the cost is directly related to analysis and evaluation of the test couples. Because of the costs involved, the number of couples that could be tested was limited. In designing the experimental tests to accomplish the objectives listed above, two basic approaches were considered: to test a small number of couples over a limited range of conditions and analyze each very thoroughly, or test a large number of couples over a wide range of conditions and reduce the analytical effort devoted to each couple. The approach selected was to test a large number of couples and rely primarily on metallographic examination (optical microscopy) to evaluate fluoride-metal interaction.

6.0 EXPERIMENTAL

6.1 TEST PARAMETERS

The short-term compatibility tests were designed to accomplish the objectives set forth in Section 5.0. The experimental conditions for the tests are summarized in Table 5. The bases used in selecting the test conditions are discussed below. The short-term tests were divided into four series of tests each using a different grade of SrF_2 plus a fifth series involving the testing of reference specimens without SrF_2 present.

The four grades of strontium fluoride were used in the tests to determine the effects of impurities, radiation and decay products on the compatibility of SrF_2 with containment materials. (Descriptions of the four grades of fluoride are given in Section 6.2.2.) High-purity nonradioactive SrF_2 (containing <1000 ppm total impurities) was tested as a reference against which the other fluoride compositions could be compared. Duplicate couples containing the high-purity SrF_2 were tested for each set of conditions.

Mixtures of high-purity nonradioactive SrF_2 with controlled levels of added impurities were tested to determine the effects of specific impurities on SrF_2 compatibility. The fluoride-impurity mixtures used in the tests are shown in Table 6. Selection of the impurities to be studied was based on analysis of $^{90}SrF_2$ prepared by the WESF flowsheet at PNL using a typical ^{90}Sr feed solution obtained from ARHCO (WESF-produced $^{90}SrF_2$ was not available when the tests were started). The concentrations of impurities used in the test mixtures were greater than those expected in the WESF $^{90}SrF_2$ in order to accelerate possible effects. It was impossible to test all of the impurities expected in the WESF $^{90}SrF_2$ because of the great many test couples required. The tests were limited to those impurities which should be present in the WESF $^{90}SrF_2$ in large concentrations, such as Na, Ca, and Ba, and those impurities which thermodynamic calculations indicated should be especially troublesome, such as Cu, Fe, and Mn. The tests with fluoride-impurity mixtures were carried out at only one temperature, 1000°C. Single

TABLE 5. Experimental Conditions for the Short-Term Compatibility Tests

1. Grades of Strontium Fluoride Tested
   a. High-purity nonradioactive SrF_2 (<1000 ppm impurities)
   b. WESF-grade $^{90}SrF_2$ (~4.5 wt% impurities)
   c. High-purity $^{90}SrF_2$ (~1.9 wt% impurities)
   d. High-purity nonradioactive SrF_2 with controlled levels of added impurities
2. Containment Materials Evaluated
   a. Hastelloy C-276
   b. Hastelloy X
   c. Hastelloy N
   d. Haynes Alloy 25
   e. Haynes Alloy 188
   f. Inconel 600
   g. Inconel 625
   h. TZM
   i. Tungsten
3. Test Temperatures
   a. 800°C (1472°F)
   b. 1000°C (1832°F)
   c. 1100°C (2012°F)
4. Test Duration
   a. 1500 hr (~2 months)
   b. 4400 hr (~6 months)
5. Metal Surface to Fuel Volume Ratio
   a. 4.5 cm^{-1}
6. Number of Couples Tested
   a. High-purity nonradioactive SrF_2-duplicate couples for each set of conditions (108 couples)
   b. WESF $^{90}SrF_2$ (54 couples)
   c. High-purity $^{90}SrF_2$ (54 couples)
   d. High-purity nonradioactive SrF_2 with controlled levels of added impurities (216 couples)
   e. Reference metal samples tested at 800, 1000 and 1100°C (27 total)

TABLE 6. Compositions of SrF_2-Impurity Mixtures Used in the Short-Term Compatibility Tests

	Composition	wt%
1.	Sr^{+2} (as SrF_2)[(a)]	95
	Na^+ (as NaF)	5
2.	Sr^{+2} (as SrF_2)	95
	Ca^{+2} (as CaF_2)	1.67
	Mg^{+2} (as MgF_2)	1.67
	Ba^{+2} (as BaF_2)	1.66
3.	Sr^{+2} (as SrF_2)	98
	Mn^{+2} (as MnF_2)	2
4.	Sr^{+2} (as SrF_2)	98
	Pb^{+2} (as PbF_2)	2
5.	Sr^{+2} (as SrF_2)	98
	Cu^{+2} (as CuF_2)	2
6.	Sr^{+2} (as SrF_2)	98
	Fe^{+3} (as FeF_3)	2
7.	Sr^{+2} (as SrF_2)	98
	Al^{+3} (as AlF_3)	2
8.	Sr^{+2} (as SrF_2)	99
	O^{-2} (as SrO)	1
9.	Sr^{+2} (as SrF_2)	99.95
	NO_3^- [as $Sr(NO_3)_2$]	0.05
10.	SrF_2	99.95
	H_2O	0.05

(a) High-purity nonradioactive SrF_2, containing <1000 ppm total impurities, used in preparing the mixtures.

couples were tested for each set of conditions except for the fluoride mixtures containing water or nitrate where duplicate couples were tested.

High-purity $^{90}SrF_2$ was tested to estimate the effects of radiation and decay product buildup on the compatibility of SrF_2 with containment materials. The fluoride had a ^{90}Sr isotopic content of 55%. Unfortunately the high-purity $^{90}SrF_2$ contained about 1.9 wt% impurities, principally Na, that could have affected the results obtained, making it difficult to estimate the effects of radiation and decay products or compatibility. Single couples containing high-purity $^{90}SrF_2$ were tested for each set of conditions.

WESF-grade $^{90}SrF_2$ was tested to allow an early evaluation of the potential problems expected in containing $^{90}SrF_2$ which contains significant amounts of process impurities as well as decay products. The ^{90}Sr isotopic content of the fluoride was 55%. The $^{90}SrF_2$ was prepared by the WESF flowsheet using typical ^{90}Sr feed solution obtained from ARHCO. It would have been highly desirable to use WESF-produced $^{90}SrF_2$ but the plant had not yet started up when the tests were initiated. Single couples were tested for each set of conditions.

The containment materials tested were limited to nine: tungsten, TZM, Haynes Alloy 25, Haynes Alloy 188, Hastelloy C-276, Hastelloy X, Hastelloy N, Inconel 600 and Inconel 625. Selection of the specific materials to be tested was based on several factors including: thermodynamic considerations, results of prior SrF_2 compatibility studies and adaptability of the materials to the WESF process. A detailed description of the selection process is given in Section 6.2.3.

The tests were carried out at temperatures of 800, 1000 and 1100°C. When the program was started, a review of potential applications for $^{90}SrF_2$ heat sources was made. This review indicated that $^{90}SrF_2$ could be used with both static and dynamic conversion systems. Advanced concepts for both types of systems called for capsule-fuel interface temperatures, under normal operating conditions, in the range of 800 to 1000°C, and temperatures up to 1100°C under accident conditions. The test temperatures were selected to bracket the range of expected capsule operating and accident temperatures.

The tests were conducted for 1500 and 4400 hr. It was felt that 4400 hr was the shortest test period that would provide a reasonable comparison of the various containment materials, and allow a valid evaluation of the effects of impurities on compatibility. Two time periods were used to obtain preliminary estimates of reaction kinetics and the forms of the rate equations.

An important variable in the design of any compatibility test couple is the ratio of exposed container material surface to the core material volume (S/V). The WESF capsule has a surface to volume ratio of about 0.83 cm^{-1}. It was impractical to reproduce this value in the short-term compatibility test couples because of the many couples required. The couple design used for the tests had a S/V ratio of 4.5 cm^{-1} and this was not varied. The effect of varying the S/V ratio on compatibility will be evaluated in the long-term tests.

In addition to the fluoride couples, individual metal control samples were tested at each temperature to determine the effect of time and temperature on the microstructures of the containment materials. The samples were tested without SrF_2 present and served as references to compare with the metal specimens from the fluoride couples.

Overall, a total of 432 fluoride couples were used in the short-term tests including 108 couples containing $^{90}SrF_2$.

6.2 PREPARATION OF TEST COUPLES

The procedures used in preparing the compatibility test couples were designed to duplicate the WESF process as close as reasonably possible. The strontium fluoride used in the tests was prepared using the WESF flowsheet. The radioactive fluoride was prepared from a partially purified ^{90}Sr solution obtained from ARHCO, which was typical of the feed to the WESF operation. While the design of the test couples differed substantially from the WESF capsule, the procedures used in loading and welding the couples were similar to those used at WESF. All operations involving radioactive fluoride were carried out in hot cells.

6.2.1 Couple Fabrication

The design of the couples used in the short-term compatibility tests is shown in Figure 2. Basically the couple consists of a small metal test specimen packed in strontium fluoride within a metal capsule. The capsule and test specimen are the same material. All metal components of the couples were machined from bar stock. All test specimens, of a given material, that were used in the tests were prepared from a single lot of material which was well-characterized as to chemical composition and physical properties. Each test specimen was 1/2 in. diameter and approximately 3/8 in. thick. The flat faces of each specimen were ground and polished to a metallographic finish using 0.3 micron (μ) alumina for the final polish. After fabrication the metal components of the couples were cleaned in an ultrasonic bath using trichloroethylene, washed with acetone, dried in air and stored in sealed containers until needed.

Strontium fluoride was loaded into the test capsules by step pressing using a hydraulic press. The procedure used with the nonradioactive SrF_2 was as follows:

> The components of the couples were placed in a small argon atmosphere gloved box which surrounded the ram of a hydraulic press. The capsule to be loaded was pressed into a hardened steel die block. A small amount of SrF_2 (4 to 5 g) was placed in the capsule and compacted using a steel plunger (Figure 3). The plunger was removed and a second increment of SrF_2 added to the capsule and compacted. The test specimen was placed on top of the fluoride layer and centered to prevent contact with the capsule wall. Additional fluoride was added and compacted in 4 to 5 g increments until the capsule was filled to the desired level. The capsule lid was pressed into place and the capsule ejected from the die block. The capsule was then transferred in a sealed container to an argon atmosphere welding box where it was closed by TIG welding the lid in place. Using this procedure the void space in the capsule was filled with argon.

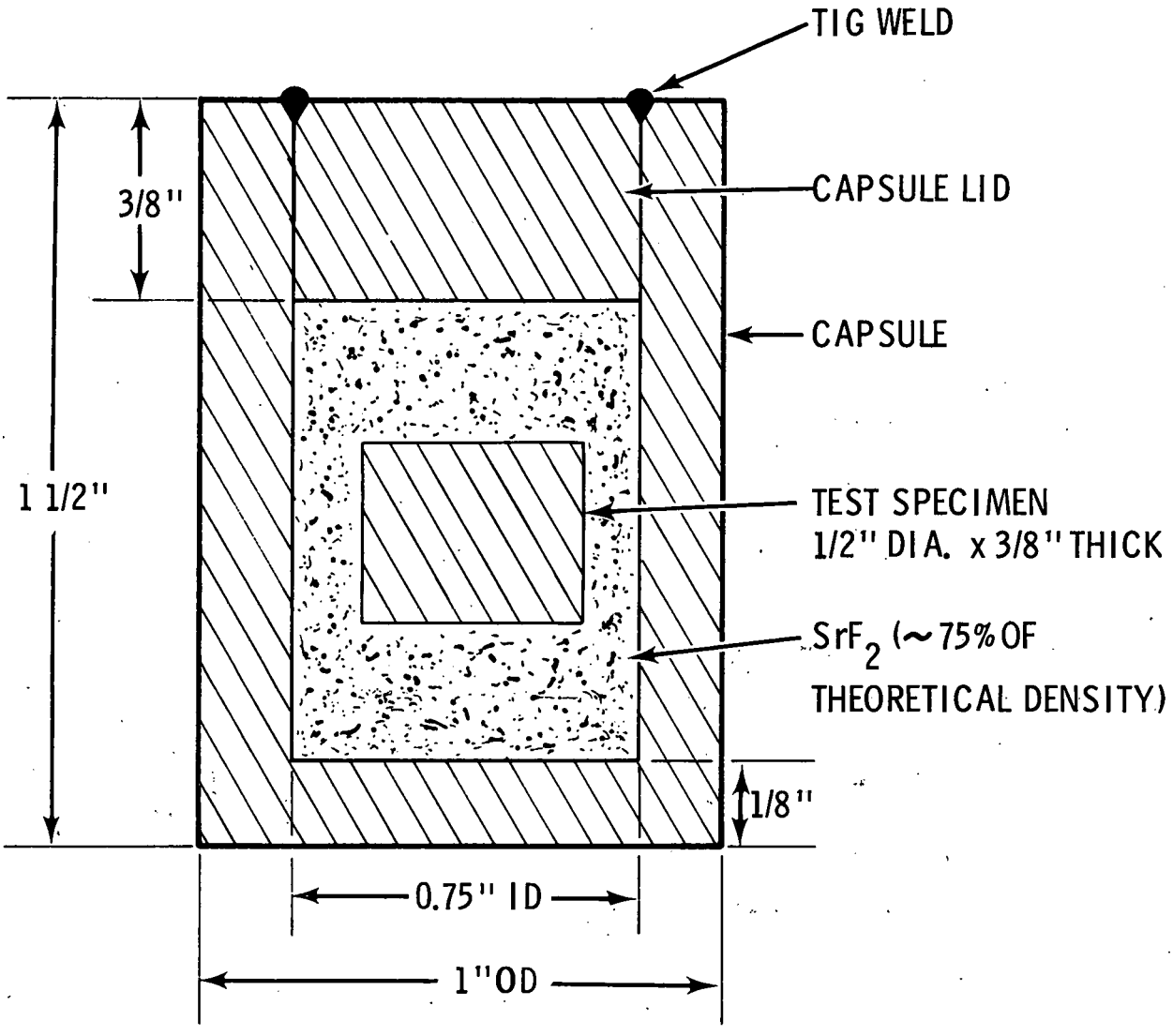

NOTES:
1. CAPSULE, LID AND TEST SPECIMEN ARE SAME MATERIAL
2. METAL COMPONENTS MACHINED FROM BAR STOCK
3. FLAT FACES OF TEST SPECIMENS POLISHED TO METALLOGRAPHIC FINISH
4. SrF_2 STEP PRESSED INTO CAPSULE

FIGURE 2. Design of the Compatibility Couples Used in the Short-Term Tests

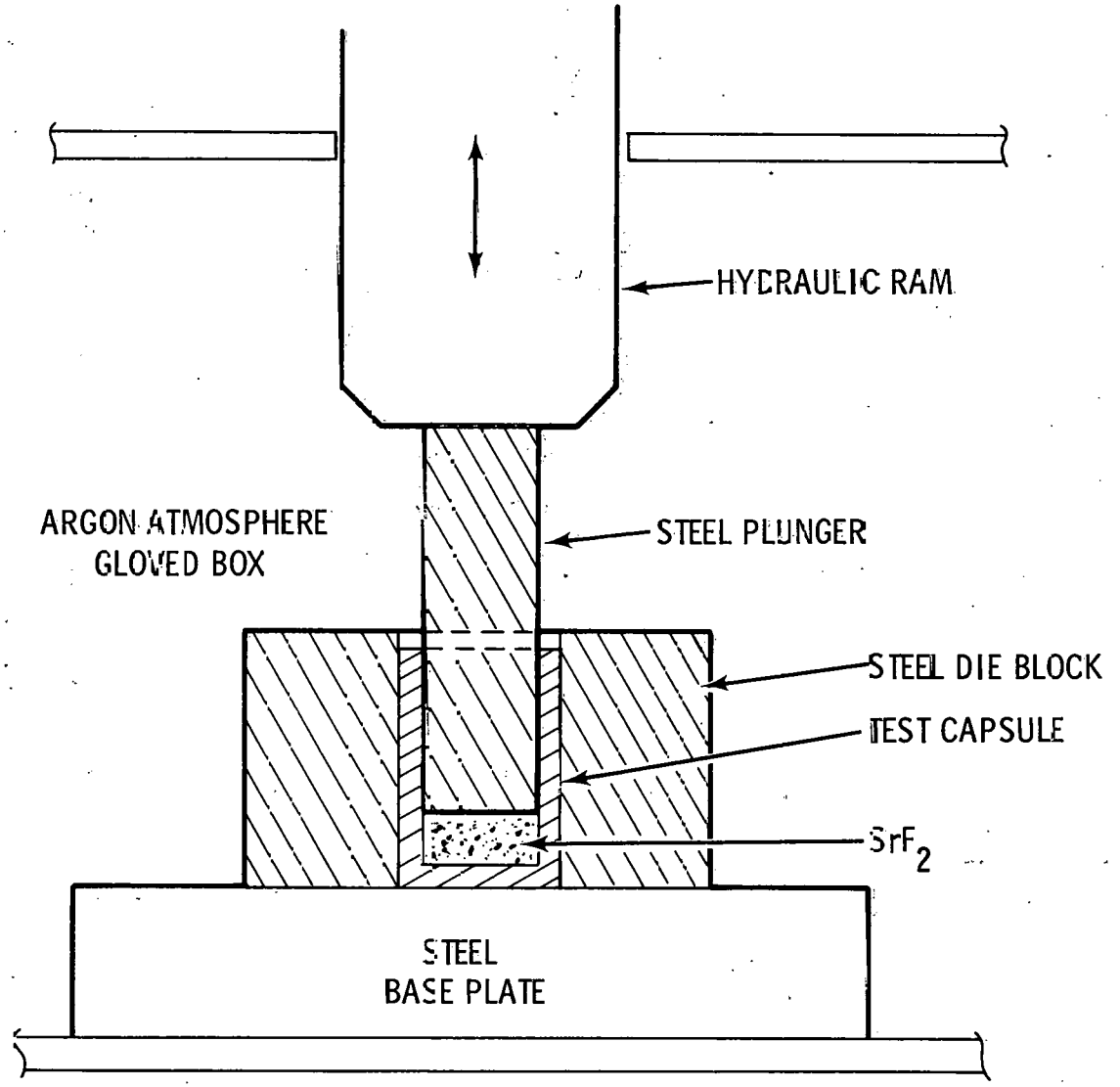

FIGURE 3. Equipment for Loading SrF_2 Into the Test Capsules

A similar procedure was used to fabricate the radioactive couples except the loading and welding operations were carried out in air-atmosphere hot cells. A small press constructed from a hydraulic jack was used to compact the fluoride. The capsules were sealed by TIG welding. Since the radioactive couples were assembled in an air atmosphere, the void space in the capsule was filled with air. The difference in internal atmosphere between the radioactive and nonradioactive couple might have some effect on the metal attack but the effect should be very slight.

In the loading operations the fluoride was compacted to a density of about 75% of theoretical density, approximately the density of the $^{90}SrF_2$ in the WESF capsules. A pressure of 9-10 TSI was sufficient to give the desired fluoride density.

Testing of the couples was carried out in air atmosphere muffle furnaces. To protect the couples from external oxidation during testing they were sealed in protective jackets of Inconel 600 as shown in Figure 4. Each jacket contained up to eight couples. Alumina tubes and spacers were used to prevent contact between the couples and the Inconel 600.

6.2.2 Preparation of Strontium Fluoride

Four grades of strontium fluoride were used in the short-term compatibility tests:

- High-purity nonradioactive SrF_2 containing less than 1000 ppm total impurities,
- WESF-grade $^{90}SrF_2$ containing approximately 4.5 wt% cation impurities,
- High-purity $^{90}SrF_2$ containing approximately 1.9 wt% cation impurities,
- High-purity nonradioactive SrF_2 with controlled levels of added impurities.

The high-purity nonradioactive SrF_2 was prepared from reagent-grade strontium nitrate by a procedure approximating the WESF flowsheet:

> Strontium nitrate was dissolved in distilled water and the pH of the solution raised to 9 using reagent-grade sodium hydroxide. Any

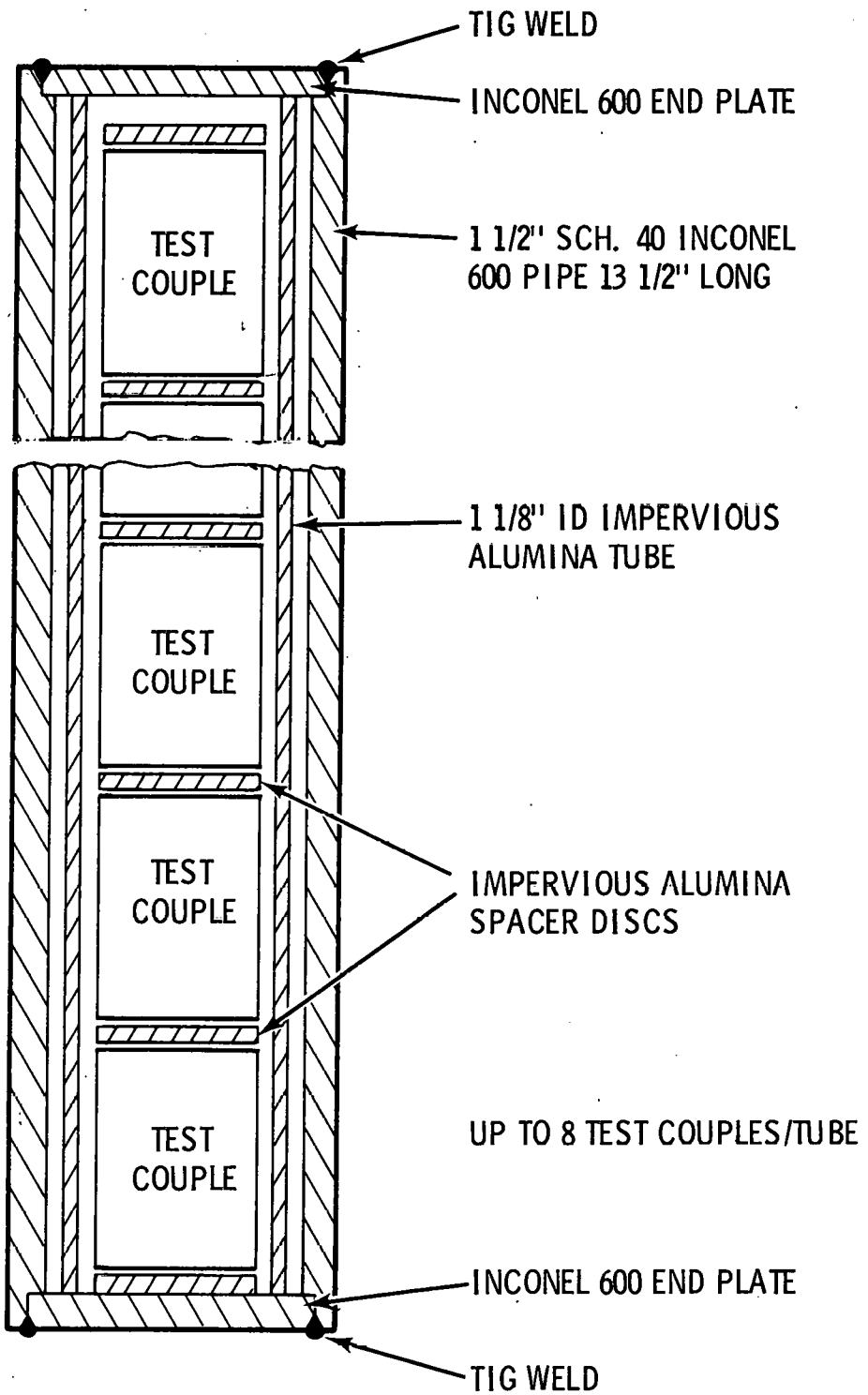

FIGURE 4. Protective Jackets for Test Couples

solids that formed were removed by filtration after which reagent-grade solid sodium fluoride was added to precipitate SrF_2. After digesting for 1 hr at 80°C, the slurry was filtered and the cake washed thoroughly with boiling distilled water. The SrF_2 cake was vacuum dried at 140°C, ball-milled to -100 mesh and fired in alumina trays at 1100°C for 16 hr in an air atmosphere. After cooling, the SrF_2 was ball-milled to -100 mesh and sealed in plastic bottles until needed.

The high-purity fluoride was prepared in several batches and the batches combined and thoroughly blended.

The high-purity SrF_2 was analyzed by several methods including spark source mass spectroscopy, emission spectroscopy, neutron activation, flame photometry, atomic absorption and wet chemistry. The results obtained are shown in Table 7. The material was found to contain less than 1000 ppm total impurities with sodium (300 ppm) and calcium (220 ppm) being the principal impurities. The oxygen content was 50 ppm, and the data showed the bulk of the oxygen was present as water.

The WESF-grade $^{90}SrF_2$ was prepared by PNL using ^{90}Sr solution obtained from ARHCO. The analysis of the ^{90}Sr solution is given in Table 8. The ^{90}Sr isotopic content of the feed was 55.1%. The fluoride was prepared using the same procedure used in preparing the high-purity nonradioactive SrF_2. The fluoride was prepared in 18 batches and the batches were combined and blended. The product was analyzed by emission spectroscopy, atomic absorption, flame photometry and wet chemistry, and the results obtained are shown in Table 9. Unfortunately methods were not available for analyzing for anion impurities in $^{90}SrF_2$. On a cation basis the WESF-grade $^{90}SrF_2$ contained about 4.5 wt% impurities. Sodium and rare earths were the major impurities.

High-purity $^{90}SrF_2$ was prepared from the same solution used to prepare the WESF-grade $^{90}SrF_2$. The Sr solution was purified by chromatographic ion exchange prior to preparation of the fluoride. The procedure used in preparing the high-purity $^{90}SrF_2$ was identical to that used in preparing the WESF-grade $^{90}SrF_2$. The analysis of the high-purity $^{90}SrF_2$ is given in Table 10. Cation impurities in the material amounted to 1.9 wt% with sodium being the principal impurity.

TABLE 7. Analysis of Nonradioactive SrF_2 Used in the Short-Term Compatibility Tests(a)

Element	Concentration (ppm)	Element	Concentration (ppm)	Element	Concentration (ppm)
H	7	Ga	ND	Nd	ND
Li	1	Ge	5	Sm	ND
Be	<1	As	5	Eu	ND
B	<1	Se	ND	Gd	ND
C	10	Br	ND	Tb	ND
N	5	Rb	2	Dy	ND
O	50	Y	40	Ho	ND
Na	300	Zn	<10	Er	ND
Mg	10	Nb	<10	Tm	ND
Al	70	Mo	ND	Yb	ND
Si	15	Te	ND	Lu	ND
P	1	Ru	ND	Hf	<10
S	10	Rh	ND	Ta	<10
Cl	4	Pd	ND	W	ND
K	20	Ag	<10	Re	ND
Ca	220	Cd	ND	Os	ND
Sc	<1	In	ND	Ir	ND
Ti	20	Sn	ND	Pt	ND
V	<1	Sb	ND	Au	<1
Cr	30	Te	ND	Hg	ND
Mn	10	I	<10	Tl	ND
Fe	75	Cs	15	Pb	ND
Co	15	Ba	20	Bi	ND
Ni	5	La	1	Th	ND
Cu	4	Ce	ND	U	ND
Zn	5	Pr	ND		

(a) Values given are the average values from the analysis of three separate samples (using two or more procedures for most elements).

ND indicates element is below the detectable limit. In most cases the detectable limit is <1 ppm.

TABLE 8. Composition of ^{90}Sr Feed Solution

Total Sr	=	16.2 g/l
^{90}Sr	=	8.93 g/l
H^+	=	0.7M
NO_3^-	=	2.5M

Isotopic Analysis:

^{84}Sr	=	0.10 atom %
^{86}Sr	=	0.57
^{87}Sr	=	0.40
^{88}Sr	=	43.80
^{90}Sr	-	55.10

Impurity Analysis:

Element	Moles/Mole Sr
Al	0.013
Ba	0.003
Ca	0.015
Cd	<0.0006
Cr	<0.003
Cu	<0.0002
Fe	<0.003
Mg	<0.004
Mn	<0.001
Na	5.7
Ni	<0.005
Pb	0.007
RE(a)	0.010
Zr	<0.004

(a) Rare Earths

TABLE 9. Analysis of WESF-Grade $^{90}SrF_2$ Used in the Short-Term Compatibility Tests

Element	Concentration (wt%)	Element	Concentration (wt%)
Al	<0.01	Mn	<0.01
Ba	0.35	Na	2.0
Ca	0.48	Ni	<0.01
Cd	0.04	P	ND
Co	ND[a]	Pb	0.015
Cr	<0.01	Si	<0.005
Cu	0.01	Sn	ND
Fe	0.03	Zn	ND
K	ND	Zr	ND
Mg	0.20	RE[b]	1.7

(a) ND - not detected (the detectable limit for most elements ~0.01%)
(b) RE - rare earths

TABLE 10. Analysis of High-Purity $^{90}SrF_2$ Used in the Short-Term Compatibility Tests

Element	Concentration (wt%)	Element	Concentration (wt%)
Al	0.25	Mn	0.0005
Ba	0.002	Na	1.32
Ca	0.006	Ni	0.002
Cd	0.0007	P	ND
Co	ND[a]	Pb	0.006
Cr	0.003	Si	ND
Cu	<0.0005	Sn	ND
Fe	0.022	Zn	ND
K	0.004	Zr	ND
Mg	0.0036	RE[b]	ND

(a) ND - not detected (the detectable limit for most elements ~0.01%)
(b) RE - rare earths

High-purity nonradioactive SrF_2 containing controlled levels of added impurities was prepared using the high-purity SrF_2 described above. The required composition was prepared by combining the high-purity SrF_2 with the appropriate amount of impurity fluoride. The fluoride mixture was then ball-milled for several hours to insure thorough blending.

A different procedure was used to prepare the mixture containing water. The water was added to the test couples as the high-purity SrF_2 was being compacted into the capsule. First a small weighed amount of SrF_2 was pressed into the capsule (see Section 6.2.1). Then a known volume of water, sufficient to give the desired concentration, was added to the capsule using a micropipette. A second increment of SrF_2 was compacted into the capsule. The test specimen was inserted and the rest of the SrF_2 added. The capsule lid was pressed in place and the capsule sealed by TIG welding. Analysis of fluoride from a welded couple indicated that, within experimental error, little or no water was lost during the loading and welding operation.

6.2.3 Containment Materials

The nine containment materials evaluated in the short-term compatibility test, and their compositions, are listed in Table 11. For a given alloy the concentration of a specific component can vary significantly from one alloy heat to another. The compositions given in Table 11 are for the test specimens all of which, for a given material, were prepared from a single heat. The test capsules and lids were machined from different heats of materials and their compositions varied somewhat from those given in Table 11.

Selection of the containment materials to be evaluated in the short-term compatibility tests represented a critical decision point in the Strontium Heat Source Development Program. Cost considerations prevented the testing of a wide variety of materials, and time considerations made it imperative that the materials selected for short-term testing provided the maximum possibility of achieving the program objectives. To be suitable

TABLE 11. Chemical Composition of Containment Materials Evaluated in the Short-Term Compatibility Tests(a)

	Composition, wt%								
Element	Hastelloy C-276 Solution Heat Treated at 2100°F	Hastelloy X ASM-5754 Solution Heat Treated at 1950°F	Hastelloy N Solution Heat Treated at 2165°F	Haynes Alloy 25 ASM 5759D Solution Heat Treated	Haynes Alloy 188 Solution Heat Treated at 2100°F	Inconel 600 Hot Finished Pickled and Annealed	Inconel 625 ASM-5666 Hot Finished and Annealed	TZM Wrought Bar Stress Relieved 3/4 hr at 2300°F	Tungsten Arc Cast
Al			0.16				0.21		
B		0.001	0.01						
C	0.005	0.09	0.07	0.11	0.08	0.07	0.04	0.019	
Cb							3.62		
Co	1.36	1.85	0.16	Bal	Bal				
Cr	15.05	21.38	6.21	20.25	21.80	15.73	21.99		
Cu			0.30			0.12			
Fe	6.20	18.94	4.73	2.40	1.56	7.54	3.44	0.001	
La					0.05				
Mo	15.65	8.88	16.81				8.93		
Mn	0.49	0.62	0.59	1.65	1.12	0.17	0.05		
Ni	Bal	Bal	Bal	10.80	22.3	76.12	61.17	<0.001	
P	0.015	0.015	0.01	0.014	0.010				
S	0.008	0.006	0.01	0.005	0.006	0.007	0.007		
Si	<0.01	0.47	0.72	0.25	0.31	0.22	0.24		
Ti			0.24				0.28	0.44	
V	0.24								
W	3.50	0.44	0.42	14.90	14.05				99.9
Zr								0.087	

(a) Compositions listed are as given in the Certified Reports of Chemical Analysis supplied with each lot of material

as a containment material for $^{90}SrF_2$ in heat source applications, a material should not only be compatible with the $^{90}SrF_2$ under source operating conditions but provide other source requirements as well. These can include such requirements as oxidation resistance, seawater corrosion resistance and good high temperature strength characteristics. In addition, the material should be adaptable for use in the WESF process which requires loading of the capsule by impact consolidation. Containment materials which best meet the fluoride compatibility requirement may not provide other source and/or WESF-process requirements. Since the $^{90}SrF_2$ will be doubly encapsulated consideration can be given to the use of dissimilar materials for the inner and outer capsules; the inner capsule material to provide fluoride compatibility and WESF process needs and the outer material to provide other source requirements. In selecting the materials for evaluation in the short-term scouting tests, therefore, primary emphasis was placed on fluoride compatibility and adaptability to the WESF process.

Selection of the materials to be tested from the many potential candidates was based on a review of the following considerations:

- An elementary thermodynamic analysis of SrF_2 containment,
- Results obtained in earlier SrF_2 compatibility programs at the Martin Co.[1] and PNL,[2]
- Other experimental programs involving metal fluorides at high temperatures including the Molten Salt Reactor Program at ORNL, the fluoride volatility programs at ORNL, ANL and BMI, and miscellaneous electrolytic studies involving fused fluoride salts,
- Adaptability of the containment material to the WESF process,
- Potential heat source operating requirements (i.e., temperature, etc.),
- Probable licensing requirements (i.e., IAEA Safety Series No. 33, 10 CFR Parts 20 and 71).

After evaluating the various factors involved, the nine materials listed in Table 11 were selected for testing. Anticipated compatibility with $^{90}SrF_2$ was the principal basis for selecting the nine materials, and

in some instances overrode other considerations. For example, previous work has shown Haynes Alloy 25 is compatible with SrF_2 at 400 to 900°C, and it was selected for testing even though thermal aging reactions in the alloy at 650 to 900°C greatly reduce its impact strength and ductility.[8,9] A number of other materials were considered for testing but were rejected for various reasons. Examples of the types of materials considered and rejected are given in Table 12.

TABLE 12. Potential Containment Materials Considered for Testing and Rejected

316L Stainless Steel	Incoloy 800	Multimet
Hastelloy B	Incoloy 825	Vanadium
Hastelloy F	TD Nickel	Columbium
Hastelloy S	TD NiCr	Tantalum
Hastelloy T	N-155	Ta-10W
Haynes 152	Rene 41	T-111
Inconel 601	Rene Y	Molybdenum
Inconel 617	Waspalloy	Mo-50% Re
Inconel 713	Nichrome 5	W-25% Re
Inconel X-750	Nio-O-Nel 185	Graphite

6.3 COUPLE TESTING

All of the short-term compatibility tests were carried out in resistance heated air-atmosphere muffle furnaces. Several furnaces were required because of the large number of couples to be tested, the different temperature requirements, and the need to test both radioactive and nonradioactive couples. Each furnace was equipped with a solid-state proportioning controller and Platinel II thermocouple capable of maintaining the temperature within ±2°C of the set point. In addition, each furnace was equipped with a second calibrated thermocouple, either Platinel II or Pt/Pt-13% Rh, which

was monitored continuously with a strip chart recorder and periodically with a digital millivoltmeter. The second thermocouple was positioned in approximately the same location in the furnace chamber as the controller thermocouple. Each controller was equipped with thermocouple break protection to turn off the power if the control thermocouple failed.

Prior to use, the temperature profile in each furnace chamber was measured using a calibrated Platinel II thermocouple. At a control temperature of 1100°C the maximum deviations observed were +5°C and -12°C. At 800 and 1000°C the deviations were slightly less.

In testing couples containing radioactive compounds the problem exists of determining the actual test specimen-compound interface temperature. This temperature can be substantially above the furnace temperature depending on the design and heat output of the couple. Use of a protective jacket serves to increase the temperature difference. Heat transfer calculations showed the furnace control temperatures should be 762, 972 and 1077°C to give the desired average interface temperatures of 800, 1000 and 1100°C.

Few difficulties were encountered during the various short-term tests. A control thermocouple failed during the 1100°C tests with high-purity $^{90}SrF_2$ and had to be replaced. Downtime was approximately 36 hr. A more serious problem occurred in the 1500-hr tests with nonradioactive SrF_2 containing added impurities. On the day the tests were to be terminated a furnace controller failure allowed some of the couples to overheat to approximately 1200°C for about 4 hr. The effects of overheating on the test couples is discussed in Section 7.1.4. The temperature excursion occurred due to failure of two separate systems in the controller. The SCR power module failed, allowing continuous power input, and at the same time the overtemperature control switch failed. To prevent similar incidents in other tests, each furnace was equipped with a second overtemperature switch. The switch operated off the strip-chart recorder used to monitor the furnace temperature and was separated from the furnace controller. The switches were set up to shut off power to the furnace if the temperature exceeded a predetermined level.

6.4 COUPLE EVALUATION

When a series of tests was completed the couples were cooled and removed from their protective jacket. Each couple was examined for signs of external oxidation and then sectioned using an abrasive saw, taking care not to damage the test specimen. The SrF_2 and test specimen were removed from the capsule and separated. In almost every case some SrF_2 adhered to the test specimen and could not be removed completely without damage to the specimen surface. The problem was especially severe with the radioactive fluoride.

The nonradioactive test specimens were sectioned longitudinally and one half was mounted in plastic for subsequent examination. The radioactive specimens were mounted on edge in plastic and ground to the midpoint for examination. With some couples the capsule was sectioned and a portion showing the weld area was mounted in plastic for metallographic examination.

Attack of the nonradioactive test specimens was evaluated using optical microscopy, scanning electron microscopy (SEM) and electron microprobe analysis (EM). Microhardness measurements were obtained on some of the test specimens. Attack of the radioactive test specimens was evaluated primarily by optical microscopy.

Initially it was hoped that additional data on fluoride-metal interaction could be obtained by chemical analyses of the SrF_2 and test specimens and by dimensional and weight changes of the test specimens, but these hopes proved to be unwarranted. Chemical analysis of the SrF_2 and metal specimens by various techniques provided little useful information. Any changes in composition observed were always less than the precision of the analytical procedures used. The use of X-ray diffraction to identify reaction products was also unsuccessful and was abandoned. Weight and dimensional changes of the test specimens were of little value. Strontium fluoride adhering to the metal specimens made weight changes meaningless, and attempts to remove the fluoride without affecting the metal surface were unsuccessful. It was

also found that when the SrF_2 was step-pressed into the test capsule during the loading operation, some distortion of the test specimen resulted. This distortion made any subsequent dimensional measurements on the test specimens of little value.

7.0 RESULTS AND DISCUSSION

Evaluation of metal-fluoride interaction in a given couple was based on examination of the metal test specimen. Metal attack was determined from the specimen photomicrographs and electron microprobe data. It was difficult to obtain an exact measure of the metal attack from the micrographs and microprobe data, and the results presented in the following tables are estimates of the depth of metal affected. In most couples the metal attack was nonuniform. The micrographs and electron microprobe data were obtained from those areas of the test specimens showing maximum attack, and the data reported in the tables represent, in each case, the maximum attack observed.

Various types of metal attack were observed in the different test couples, and usually two or more types were found in each couple. In general, however, the attack mechanisms can be divided into two basic types. Two estimates of metal attack are reported for each couple, one for each type of attack. Although the nomenclature may be misleading the two types of attack have been designated as: chemical attack, and changes in specimen microstructure. While the two types of attack are probably interdependent, there was insufficient analytical data available to identify the interrelationships.

Chemical attack is defined as those attack mechanisms which are directly attributable to attack of the specimen by the fluoride and includes such mechanisms as grain boundary attack (intergranular penetration), pitting, subsurface void formation and generalized attack of the metal surface. It can also include selective dissolution of alloy components in the solid fluoride phase. Typical examples of chemical attack are shown in Figure 5. Changes in microstructure are defined as those affected areas where the specimen morphology differs significantly from that of the bulk of the specimen and from the reference specimen; and can consist of various structural changes such as the disappearance of normal alloy precipitates, the formation of abnormal precipitates, and marked changes in grain size.

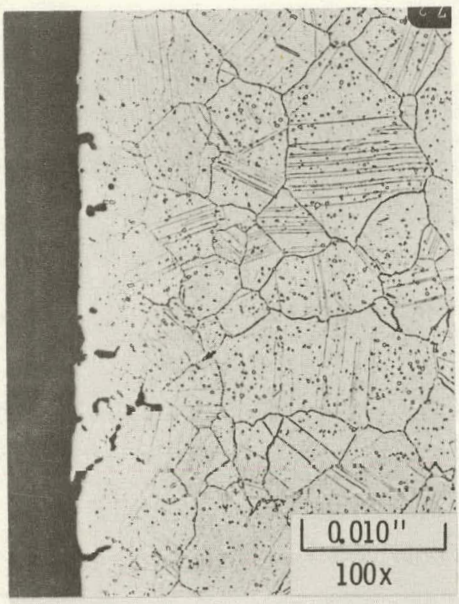

(a) Haynes 25 / SrF_2 + SrO (Impurity)
1000°C, 4000 Hours

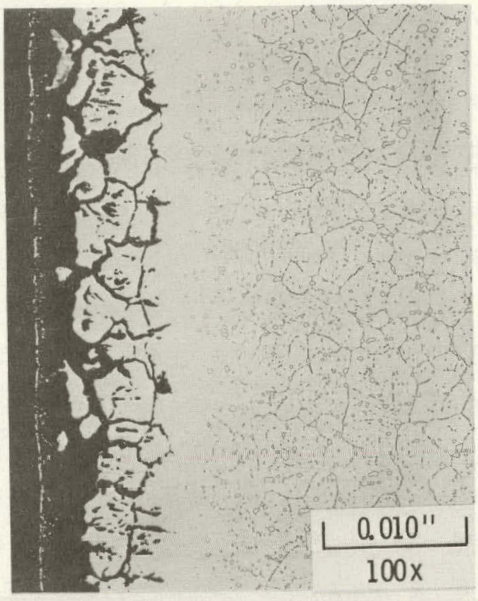

(b) Hastelloy X / SrF_2 + SrO (Impurity)
1000°C, 4400 Hours

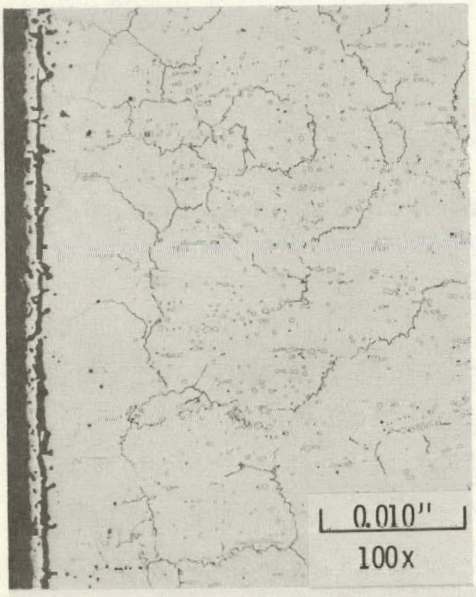

(c) Hastelloy N / SrF_2 + NaF (Impurity)
1000°C, 4400 Hours

(d) Hastelloy C-276 / SrF_2 + MnF_2 (Impurity)
1000°C, 4400 Hours

FIGURE 5. Typical Examples of Chemical Attack

Typical examples of microstructural changes are shown in Figure 6. In the Hastelloy C-276 specimen, which had contacted SrF_2 containing FeF_3, there is a surface layer several mils thick where the normal alloy precipitates have almost completely disappeared. The Inconel 625 specimen exposed to SrF_2-CuF_2 has a surface layer where the normal alloy precipitates have largely disappeared. However, the specimen also contains a much narrower surface layer where abnormal precipitates are present as discrete globular inclusions.

The effect of microstructural changes on the usefulness of a given alloy as a containment material for $^{90}SrF_2$ is difficult to assess without mechanical property data such as tensile strength, toughness and ductility. Chemical attack of the alloy will definitely decrease the usefulness of a given alloy. This may not necessarily be the case with microstructural changes, however. The disappearance of normal alloy precipitates may increase the ductility and toughness of the affected zone, while the formation of abnormal precipitates could reduce toughness and ductility.

7.1 RESULTS

The short-term compatibility tests were divided into four series of tests each using a different grade of strontium fluoride. A great deal of experimental data was obtained from the tests. Providing a comprehensive and meaningful evaluation of the data requires considerable effort. To simplify the presentation the basic experimental data and general analyses of the results are provided in this section, while the specifics of the individual metal-fluoride systems are discussed in Section 7.2.

7.1.1 High-Purity Nonradioactive SrF_2

The metal attack found in couples containing high-purity nonradioactive strontium fluoride is summarized in Table 13. Several conclusions are apparent from the test data:

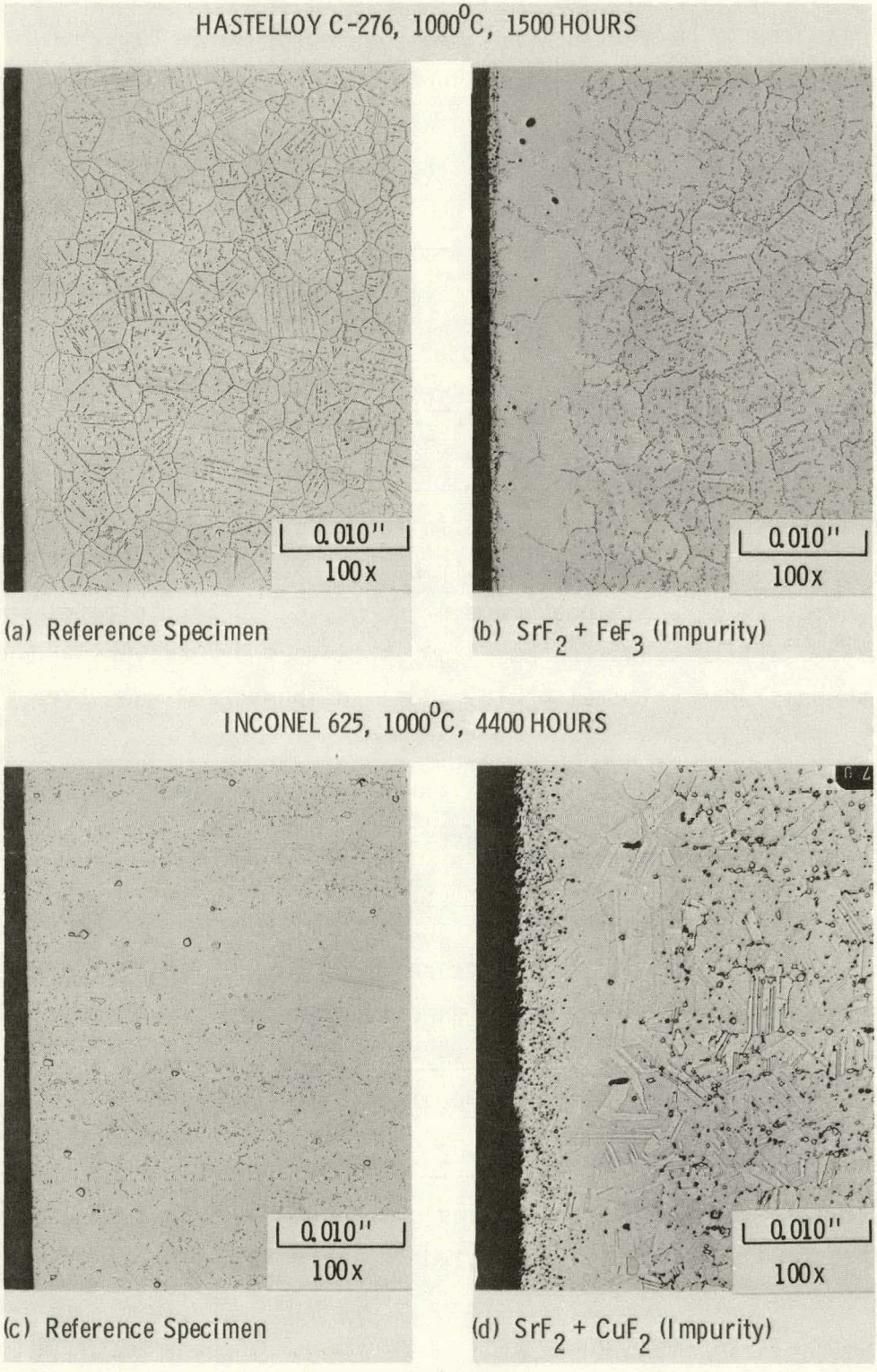

FIGURE 6. Typical Examples of Changes in Specimen Microstructure

TABLE 13. Metal Attack Observed in Couples Containing High-Purity Nonradioactive SrF_2

Material Tested	Test Temperature (°C)	Depth of Metal Affected, mils			
		Chemical Attack		Change in Microstructure	
		1500 hr	4400 hr	1500 hr	4400 hr
Hastelloy C-276	800	1	2	1	1
	1000	4	7	1	2
	1100	6	8	0	2
Hastelloy X	800	1	<1	2	2
	1000	1	1	2	1
	1100	2	1	1	4
Hastelloy N	800	1	4	2	5
	1000	3	3	5	5
	1100	<1	1	5	6
Haynes Alloy 25	800	<<1	1	<1	<1
	1000	<<1	1	<1	1
	1100	<<1	1	1	2
Haynes Alloy 188	800	2	1	2	2
	1000	2	3	0	0
	1100	2	4	1	1
Inconel 600	800	0	<1	3	6
	1000	<1	<1	5	7
	1100	<1	1	0	4
Inconel 625	800	1	1	1	2
	1000	3	3	4	4
	1100	2	3	0	0
TZM	800	0	0	0	<1
	1000	0	0	0	<1
	1100	0	0	0	<1
Tungsten	800	0	0	0	<1
	1000	0	0	0	<1
	1100	0	0	0	<1

- The refractory metals, tungsten and TZM, provide the greatest resistance to attack by the high-purity nonradioactive SrF_2. There was no evidence of chemical attack in any of the refractory metal couples and only slight indications of microstructural changes.
- Attack varied considerably between the various Ni- and Co-base alloys with Haynes Alloy 25 showing the least attack. Surprisingly the Haynes Alloy 188, which is quite similar to Haynes Alloy 25 in chemical composition, showed considerably more attack than the latter alloy.
- Except for Hastelloy C-276, metal attack did not increase substantially with increasing exposure temperature. In the case of Hastelloy N the chemical attack was less at 1100°C than at the lower temperature. There were several instances where microstructural changes were less at 1100°C than at the lower temperatures. This is probably because dissolution of precipitates occurs in many Ni- and Co-base alloys at temperatures above about 1000°C.
- Although the number of data points are limited, the overall results indicate that the rate of metal attack by the fluoride decreases with time.

Microhardness measurements were obtained on the 1500-hr test specimens and on the reference samples. The measurements were taken at 25 μ (∿1 mil) increments from the edge of the specimen. The hardness data are given in Table 14. The data show a general softening of the alloys with increased exposure temperature. The effects of SrF_2 attack on hardness appear to be quite complex and are difficult to interpret. These effects are covered in more detail in the discussion of the individual alloy systems. Microhardness measurements were obtained on some of the 4400-hr test specimens, and the results were very similar to those obtained with the 1500-hr specimens.

Overall, the microhardness measurements provided relatively little information, and hardness data were not obtained in the other series of tests.

TABLE 14. Microhardness Measurements on Metal Specimens Exposed to High-Purity Nonradioactive Strontium Fluoride for 1500 hr

Alloy	Microhardness DPHN (Average) 1 mil	2 mil	3 mil	4 mil
Hastelloy C-276				
As Received	357	311	285	268
Control 800°C(a)	351	325	317	302
Control 1000°C	262	266	273	268
Control 1100°C	192	215	215	219
Sample 800°C	339	342	302	302
Sample 1000°C	243	260	268	260
Sample 1100°C	201	192	204	199
Hastelloy X				
As Received	203	190	203	203
Control 800°C	238	262	262	253
Control 1000°C	215	230	243	240
Control 1100°C	168	180	181	190
Sample 800°C	237	243	243	237
Sample 1000°C	206	219	219	222
Sample 1100°C	185	209	213	210
Hastelloy N				
As Received	342	354	360	383
Control 800°C	264	264	276	292
Control 1000°C	235	238	254	237
Control 1100°C	181	190	221	212
Sample 800°C	236	246	269	255
Sample 1000°C	205	198	205	216
Sample 1100°C	208	208	199	199
Haynes Alloy 25				
As Received	306	311	303	302
Control 800°C	373	387	373	383
Control 1000°C	317	363	345	348
Control 1100°C	270	294	299	302
Sample 800°C	389	387	394	383
Sample 1000°C	348	348	345	304
Sample 1100°C	258	260	249	248
Haynes Alloy 188				
As Received	260	266	268	268
Control 800°C	283	294	294	297
Control 1000°C	266	266	266	264
Control 1100°C	227	260	267	243
Sample 800°C	319	316	304	334
Sample 1000°C	229	239	231	245
Sample 1100°C	245	253	254	258

(a) Control specimens tested at temperature without SrF_2.

TABLE 14 (Contd)

Alloy	Microhardness DPHN (Average) 1 mil	2 mil	3 mil	4 mil
Inconel 600				
As Received	205	209	217	221
Control 800°C	202	210	209	217
Control 1000°C	134	159	159	164
Control 1100°C	157	161	161	163
Sample 800°C	176	181	182	193
Sample 1000°C	138	142	150	146
Sample 1100°C	146	158	161	150
Inconel 625				
As Received	363	322	304	285
Control 800°C	336	335	348	339
Control 1000°C	228	238	217	217
Control 1100°C	190	195	204	205
Sample 800°C	339	366	373	354
Sample 1000°C	203	217	230	228
Sample 1100°C	178	196	195	195
TZM				
As Received	264	272	281	270
Control 800°C	309	325	306	314
Control 1000°C	---	---	---	---
Control 1100°C	271	270	279	283
Sample 800°C	311	302	302	290
Sample 1000°C	297	302	302	302
Sample 1100°C	319	311	298	292
Tungsten				
As Received	420	429	437	437
Control 800°C	390	397	390	394
Control 1000°C	459	459	464	473
Control 1100°C	446	468	454	454
Sample 800°C	468	459	473	468
Sample 1000°C	383	413	425	425
Sample 1100°C	423	397	394	425

7.1.2 High-Purity $^{90}SrF_2$

Compatibility data obtained with the couples containing high-purity $^{90}SrF_2$ are summarized in Table 15. In general, the results confirm those obtained with the high-purity nonradioactive SrF_2. One troublesome factor was encountered with the high-purity $^{90}SrF_2$ couples. There were several instances where the 1500-hr test specimens exhibited more attack than the equivalent 4400-hr test specimens. This phenomenon was not observed nearly as often in the other series of tests. Several important conclusions can be reached from the results obtained with high-purity $^{90}SrF_2$:

- Tungsten and TZM provide the greatest resistance to attack while Haynes 25 is the best of the Ni- and Co-base alloys.
- Increasing the exposure temperature has relatively little overall effect on metal attack, and there were several instances where attack by the high-purity $^{90}SrF_2$ was less at 1100°C than at lower temperatures.
- The rate of metal attack decreased with time.
- On an overall basis there was considerably more metal attack in the couples containing high-purity $^{90}SrF_2$ than in those containing the high-purity nonradioactive SrF_2. Among the Ni- and Co-base alloys, microstructural changes occurred to much greater depths in the $^{90}SrF_2$ couples than in the equivalent nonradioactive couples. With the limited data available, it is impossible to determine if the increased attack found in the $^{90}SrF_2$ couples is due to radiation effects or the presence of impurities and decay products. However, indications are that in most cases the increased attack is due primarily to the impurities and decay products.

7.1.3 WESF-Grade $^{90}SrF_2$

The results obtained with couples containing WESF-grade $^{90}SrF_2$ are presented in Table 16. In general the results confirm those obtained with the high-purity fluorides. Although the WESF-grade $^{90}SrF_2$ contains substantially more impurities than the high-purity $^{90}SrF_2$, the overall metal attack was not appreciably greater. In the case of Hastelloy C-276 both

TABLE 15. Metal Attack in Couples Containing High-Purity $^{90}SrF_2$

Material Tested	Test Temperature (°C)	Depth of Metal Affected, mils			
		Chemical Attack		Change in Microstructure	
		1500 hr	4400 hr	1500 hr	4400 hr
Hastelloy C-276	800	4	2	6	6
	1000	2	4	5	15
	1100	4	6	12	6
Hastelloy X	800	1	2	5	5
	1000	2	4	10	15
	1100	5	4	20	22
Hastelloy N	800	4	5	10	8
	1000	6	8	16	16
	1100	2	(a)	5	(a)
Haynes Alloy 25	800	<1	<1	3	2
	1000	<1	1	3	3
	1100	1	2	4	3
Haynes Alloy 188	800	4	5	10	13
	1000	6	3	12	5
	1100	2	2	5	5
Inconel 600	800	1	3	4	8
	1000	2	(a)	6	(a)
	1100	2	2	4	4
Inconel 625	800	6	3	10	5
	1000	4	(a)	13	(a)
	1100	5	2	15	15
TZM	800	0	1	0	0
	1000	0	<1	0	0
	1100	<1	1	0	0
Tungsten	800	0	0	0	0
	1000	<1	<<1	0	0
	1100	<1	<1	0	0

(a) Three test specimens were inadvertently destroyed before examination.

TABLE 16. Metal Attack in Couples Containing WESF-Grade $^{90}SrF_2$

Material Tested	Test Temperature (°C)	Depth of Metal Affected, mils			
		Chemical Attack		Change in Microstructure	
		1500 hr	4400 hr	1500 hr	4400 hr
Hastelloy C-276	800	2	2	3	3
	1000	2	3	5	8
	1100	3	3	5	6
Hastelloy X	800	1	3	4	4
	1000	1	1	6	4
	1100	3	3	6	10
Hastelloy N	800	4	6	7	6
	1000	7	9	20	12
	1100	6	(a)	8	(a)
Haynes Alloy 25	800	1	1	2	2
	1000	1	1	2	3
	1100	1	2	2	2
Haynes Alloy 188	800	1	2	2	4
	1000	3	4	7	10
	1100	1	2	8	5
Inconel 600	800	1	3	4	11
	1000	1	2	8	14
	1100	2	2	7	12
Inconel 625	800	1	4	4	8
	1000	2	5	20	18
	1100	4	5	18	14
TZM	800	<1	<1	0	0
	1000	<1	<1	1	0
	1100	<1	<1	0	0
Tungsten	800	0	0	0	0
	1000	0	<1	0	0
	1100	1	<1	0	0

(a) Test specimen inadvertently destroyed before examination.

chemical attack and microstructural changes were less in the WESF-grade $^{90}SrF_2$ couples than in the high-purity $^{90}SrF_2$ couples. Again tungsten and TZM were attacked least by the fluoride, and Haynes Alloy 25 was the best of the Ni- and Co-base alloys. Metal attack did not increase appreciably with temperature above 1000°C, and the rate of attack appeared to decrease with time.

7.1.4 Nonradioactive SrF_2 with Added Impurities

The results obtained with couples containing high-purity nonradioactive SrF_2 with controlled levels of added impurities are presented in Table 17. In the 1500-hr tests a number of couples were accidentally overheated to approximately 1200°C for about 4 hr on the day the tests were to be terminated. Results obtained with the overheated couples are indicated with an (a) in Table 17. The overheating produced marked changes in the microstructures of the Ni- and Co-base alloys, such as very large grain size and dissolution of precipitates, which made it impossible to evaluate the effect of strontium fluoride on the microstructure. Overheating the couples for a period of only 4 hr at the end of a 1500-hr test would not be expected to increase the chemical attack of the test specimens significantly. However, the overheating did make it difficult to estimate the degree of chemical attack of the Ni- and Co-base alloys because of the marked changes in the microstructure of the specimens. The values given in Table 17 for chemical attack of the overheated specimens are, at best, rough approximations of the depth of metal affected.

Several facts are apparent from a review of the data presented in Table 17:

- On an overall basis the addition of impurities to high-purity nonradioactive SrF_2 increased metal attack, with changes in the microstructure of the Ni- and Co-base alloys being especially sensitive to the presence of impurities in the SrF_2.

TABLE 17. Metal Attack in Couples Containing SrF_2-Impurity Mixtures at 1000°C

Material Tested	Impurity Added	Depth of Metal Affected, mils			
		Chemical Attack		Change in Microstructure	
		1500 hr	4400 hr	1500 hr	4400 hr
Hastelloy C-276	NaF	1(a)	1	-	3
	MnF_2	2	1	3	4
	PbF_2	2(a)	1	-	3
	CuF_2	1	2	8	15
	FeF_3	2	1	8	8
	AlF_3	<1(a)	<1	-	4
	$(Ca\text{-}Ba\text{-}Mg)F_2$	1	1	3	3
	SrO	12	10	12	10
	$Sr(NO_3)_2$	1(a)	1	-	10
	H_2O	4(a)	1	-	5
Hastelloy X	NaF	<1	<1	3	2
	MnF_2	4(a)	1	-	5
	PbF_2	1(a)	1	-	4
	CuF_2	30(a)	4	-	12
	FeF_3	1	3	12	22
	AlF_3	<1	1	4	3
	$(Ca\text{-}Ba\text{-}Mg)F_2$	<1(a)	1	-	4
	SrO	15(a)	8	-	10
	$Sr(NO_3)_2$	5(a)	1	-	4
	H_2O	1(a)	1	-	5
Hastelloy N	NaF	2	2	10	10
	MnF_2	2	3	2	5
	PbF_2	3	3	6	8
	CuF_2	3(a)	4	-	20
	FeF_3	6(a)	8	-	15
	AlF_3	<1	1	3	10
	$(Ca\text{-}Ba\text{-}Mg)F_2$	<1	1	3	4
	SrO	25	35	28	35
	$Sr(NO_3)_2$	2(a)	2	-	15
	H_2O	2	1	5	5
Haynes Alloy 25	NaF	<1	1	3	2
	MnF_2	<1(a)	<1	-	3
	PbF_2	<1	1	4	3
	CuF_2	2(a)	1	-	18
	FeF_3	2(a)	3	-	20
	AlF_3	<1	<1	3	4
	$(Ca\text{-}Ba\text{-}Mg)F_2$	<1	1	2	1
	SrO	5	7	0	3
	$Sr(NO_3)_2$	1(a)	2	-	0
	H_2)	1	1	0	0
Haynes Alloy 188	NaF	<1	1	0	3
	MnF_2	<1(a)	1	-	5
	PbF_2	1	2	5	4
	CuF_2	1(a)	2	-	13
	FeF_3	2(a)	1	-	7

(a) Indicates couples accidentally overheated to 1200°C for about 4 hr.
- No meaningful estimate of changes possible because of overheating.

TABLE 17. (contd)

Material Tested	Impurity Added	Depth of Metal Affected, mils			
		Chemical Attack		Change in Microstructure	
		1500 hr	4400 hr	1500 hr	4400 hr
Haynes Alloy 188 (continued)	AlF_3	<1	<1	<1	2
	$(Ca-Ba-Mg)F_2$	<1	1	1	3
	SrO	12	20	0	10
	$Sr(NO_3)_2$	1(a)	<1	-	5
	H_2O	<1(a)	1	-	2
Inconel 600	NaF	1(a)	1	-	1
	MnF_2	2	1	5	3
	PbF_2	1	1	3	10
	CuF_2	1	3	3	8
	FeF_3	2(a)	4	-	8
	AlF_3	1	1	0	1
	$(Ca-Ba-Mg)F_2$	1	1	3	1
	SrO	20	10	0	0
	$Sr(NO_3)_2$	3(a)	1	-	12
	H_2O	1(a)	1	-	1
Inconel 625	NaF	1	1	4	12
	MnF_2	1	2	8	10
	PbF_2	1	1	6	6
	CuF_2	6(a)	2	-	12
	FeF_3	2(a)	4	-	13
	AlF_3	1	<1	6	6
	$(Ca-Ba-Mg)F_2$	5(a)	1	-	10
	SrO	7(a)	10	-	18
	$Sr(NO_3)_2$	3(a)	1	-	10
	H_2O		2		5
TZM	NaF	<<1(a)	<<1	0	0
	MnF_2	<<1(a)	<1	0	0
	PbF_2	<1	<1	0	0
	CuF_2	2(a)	6	2	6
	FeF_3	2(a)	3	2	3
	AlF_3	<<1	<1	0	0
	$(Ca-Ba-Mg)F_2$	<<1	<<1	0	0
	SrO	<1	<1	0	0
	$Sr(NO_3)_2$	<<1(a)	<<1	0	0
	H_2O	<1	<<1	0	0
Tungsten	NaF	<<1	<1	0	0
	MnF_2	<1(a)	<1	0	0
	PbF_2	0(a)	<1	0	0
	CuF_2	2	1	0	0
	FeF_3	<<1	<1	0	0
	AlF_3	0(a)	<1	0	0
	$(Ca-Ba-Mg)F_2$	<<1	<1	0	0
	SrO	<1	<1	0	0
	$Sr(NO_3)_2$	0(a)	<1	0	0
	H_2O	<1(a)	0	0	0

(a) Indicates couples accidentally overheated to 1200°C for about 4 hr.
- No meaningful estimate of changes possible because of overheating.

- On an individual basis, SrO, copper (Cu) and iron (Fe) caused the most marked increase in metal attack by SrF_2. The addition of SrO to the fluoride resulted in a large increase in chemical attack of all the Ni- and Co-base alloys, while the addition of copper and iron resulted in substantial increases in the depth of metal exhibiting microstructural changes. The presence of copper or iron also increased the chemical attack of TZM severalfold and tungsten to a lesser degree.
- The presence of nitrate ion or water in the fluoride had a suprisingly small effect on metal attack. This may be because both nitrate and water were added to the fluoride in comparatively small concentrations.
- On an overall basis tungsten provided the greatest resistance to attack by the fluoride-impurity mixtures. TZM was almost as good except when copper or iron was present in the fluoride.
- Of the Ni- and Co-base alloys, it was difficult to select one as providing the best overall resistance to the fluoride-impurity mixtures. Haynes Alloy 25 and Hastelloy C-276 probably provided the best overall resistance to chemical attack, but they suffered as badly as the other Ni- and Co-base alloys from changes in microstructure.
- As was the case with the other series of tests, the rate of metal attack appeared to decrease with time.

7.2 DISCUSSION

The data presented in the previous section show the extent of metal attack observed in the various test couples. The data provide no indication however, of the attack mechanism(s) involved in the different couples. In the following sections each metal-fluoride system is discussed individually, and an attempt has been made to interpret the available data and identify the attack mechanisms whenever possible. Unfortunately the systems involved are quite complex, and with the limited amount of analytical data available, it is very difficult to define the reactions taking place in the various couples in more than qualitative terms. In many instances interpretation

of the metallographic data is difficult, and conclusions reached with regard to attack mechanisms and microstructural charges are tentative. For this reason micrographs of many of the test specimens have been included in the report.

7.2.1 Tungsten-SrF_2

The tungsten test specimens were fabricated from arc-cast rod, except for a few which were prepared from wrought bar. The latter specimens were tested to determine if there was a significant difference in SrF_2 compatibility between the two types of tungsten. The arc-cast tungsten, as received from the vendor, had a very large grain size which contributed to the brittleness of the material. Microscopic examination showed the presence of microcracks throughout the structure of the arc-cast material. The wrought tungsten had a smaller grain size, no apparent microcracks and, not suprisingly, appeared to be much less brittle than the arc-cast materials. Photomicrographs of the two types of tungsten, as received from the vendor, are shown in Figure 7.

The arc-cast tungsten was sufficiently brittle that when the test couples were fabricated some of the test specimens fractured or cracked during the loading operation. This problem was not observed with test specimens fabricated from the wrought tungsten.

Aging of tungsten specimens at temperatures up to 1100°C produced no significant change in the microstructure. Very slight bulk precipitation was evident at 800°C with very little change up to 1100°C. Grain size stability was excellent with no appreciable increase in grain size with either the arc-cast or wrought specimens. Very high magnification photomicrographs (3000X) indicated some extremely small voids to a depth of about 3 mils in the arc-cast specimens heated to 1000 and 1100°C, while hardness measurements indicated a slight hardening compared to the "as received" material. The porosity may be due to the loss of impurity species from the metal.

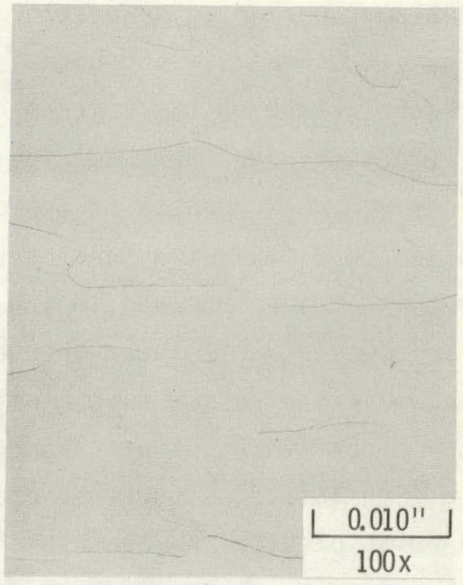

(a) Arc Cast Bar

(b) Wrought Bar

FIGURE 7. Microstructure of Arc-Cast and Wrought Tungsten Specimens As Received from the Vendor

All of the compatibility results indicate that tungsten is quite resistant to attack by strontium fluoride at temperatures up to 1100°C, being far better in this regard than the Ni- and Co-base alloys tested and slightly better than TZM. Where attack of the test specimens did occur it usually consisted of chemical attack, and there were only slight indications of changes in microstructure. Photomicrographs of typical tungsten specimens that had been tested with the different grades of strontium fluoride are shown in Figure 8. The only attack observed in the couples containing high-purity nonradioactive SrF_2 was a very slight change in microstructure at the specimen surface in couples tested for 4400 hr. Slightly greater attack was found in the couples containing WESF-grade or high-purity $^{90}SrF_2$. Chemical attack predominated with little evidence of changes in microstructure. There was some evidence of pitting and grain boundary attack. There was little discernible difference between the two grades of $^{90}SrF_2$ in their attack of the tungsten.

In the tests with SrF_2-impurity mixtures, only copper appeared to increase the metal attack significantly. Attack by the other fluoride-impurity mixtures was similar to that observed in the $^{90}SrF_2$ couples. In the couples containing copper, the attack was markedly greater with pitting and grain boundary attack predominating. Electron microprobe data indicated some diffusion of copper into the grain boundaries of the tungsten.

Based on elementary thermodynamic considerations (see Section 11.0), it is predicted that tungsten would be compatible with all of the fluorides in the WESF $^{90}SrF_2$ except those of copper and Fe(III). The experimental data confirmed the predicted reaction of tungsten with CuF_2, but the predicted reaction with FeF_3 was not observed experimentally. There are several possible explanations of why the tungsten and FeF_3 did not react to a significant degree in the test couples:

- The thermodynamic calculations are incorrect and a reaction is not to be expected,
- The rate of the chemical reaction is very slow,
- The reaction is limited by diffusion mechanisms.

(a) High Purity Nonradioactive SrF_2
1100°C, 4400 Hours

(b) Nonradioactive SrF_2 + CuF_2 (Impurity)
1000°C, 4400 Hours

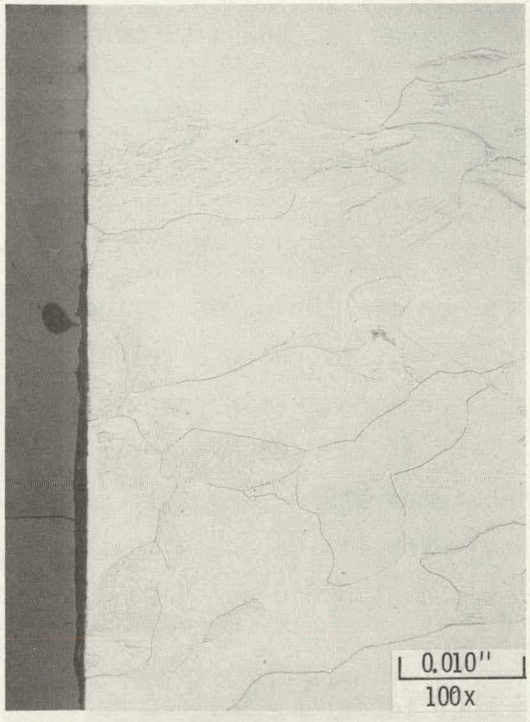

(c) WESF Grade $^{90}SrF_2$
1000°C, 4400 Hours

(d) High Purity $^{90}SrF_2$
1100°C, 4400 Hours

FIGURE 8. Tungsten Specimens After Exposure to Different Grades of Strontium Fluoride

While the results show that tungsten provides the greatest resistance to fluoride attack of all the materials tested, other considerations affect its usefulness as a containment material for $^{90}SrF_2$. Like all refractory metals, tungsten has poor oxidation resistance at high temperatures. Up to 600 to 700°C an oxide coating (WO_3), which is fairly protective, forms on tungsten. Above 700°C scaling of the protective oxide layer occurs and oxidation increases. At still higher temperatures the WO_3 vaporizes and melts and oxidation of the tungsten increases drastically. Tungsten is difficult to fabricate and weld, and has a relatively high ductile-brittle transition temperature. The exact temperature depends on metal purity, microstructure and deformation rate. Tungsten provides good seawater corrosion resistance and possesses good strength at high temperatures, but is quite sensitive to impact loads. The thermal conductivity of tungsten is much higher than that of the Ni- and Co-base alloys, and its greater density provides substantially more shielding for a given thickness of material.

7.2.2 TZM-SrF_2

The TZM test specimens were fabricated from wrought bar which had been stress relieved at 2300°F for 3/4 hr. Photomicrographs of the "as received" material showed a highly elongated grain structure typical of wrought materials (Figure 9). Exposure to temperatures up to 1100°C for periods up to 4400 hr produced no significant change in the microstructure (Figure 9). No grain growth was apparent in any of the specimens except possibly a slight amount in specimens heated for 4400 hr at 1100°C. No grain boundary precipitation occurred during aging at any temperature, and only slight very fine bulk precipitation was apparent. Overall, hardness appeared to increase slightly when the material was heated at 800°C and then decreased slightly at higher temperatures.

TZM is easier to fabricate and weld than tungsten, and its ductile-brittle transition temperature is much lower. TZM possesses good high temperature strength characteristics but suffers from low ductility at low temperatures. Welding normally raises the ductile-brittle transition

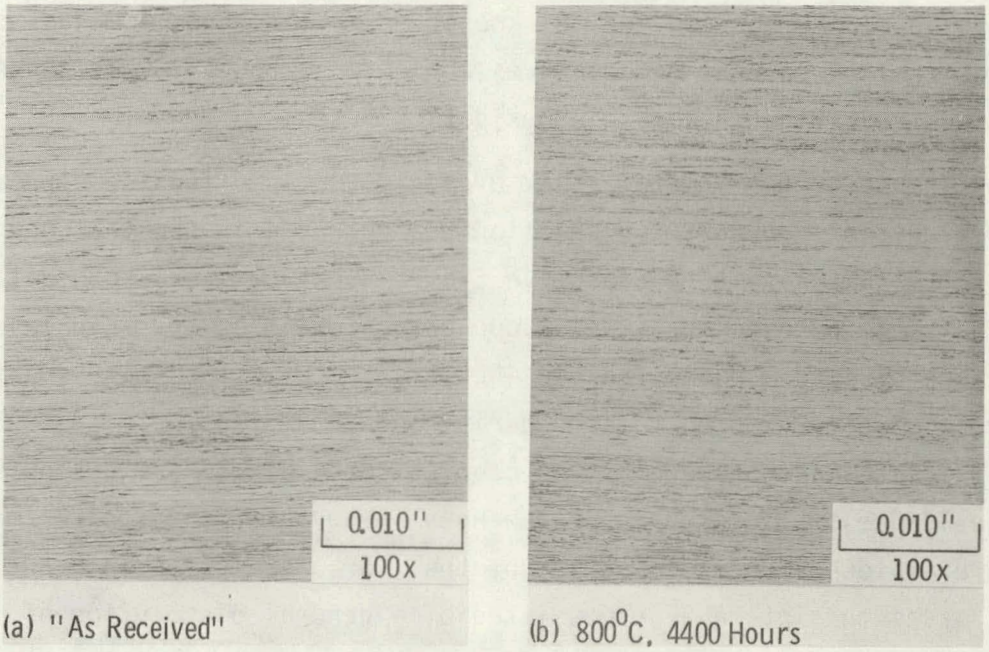

(a) "As Received"

(b) 800°C, 4400 Hours

(c) 1100°C, 4400 Hours

FIGURE 9. Effect of Temperature on the Microstructure of TZM

temperature of TZM and close control of the welding operation is required. The thermal conductivity of TZM approaches that of tungsten, but it provides much less shielding for a given thickness. Like tungsten, TZM has poor oxidation resistance. At temperatures above about 550 to 600°C the oxide volatilizes resulting in very high oxidation rates.

Resistance of the TZM to attack by the strontium fluoride approaches that of tungsten. Very little reaction was observed in the test couples containing high-purity nonradioactive SrF_2. Electron microprobe data indicated a slight increase in titanium concentration in a very thin layer at the surface of specimens tested for 4400 hr. Metal attack was slightly greater in couples exposed to high-purity and WESF-grade $^{90}SrF_2$. Only chemical attack was observed in the couples containing $^{90}SrF_2$, and there was no evidence of microstructural changes in any of the test specimens. Typical examples of chemical attack by the $^{90}SrF_2$ are given in Figure 10. In most cases the interaction consisted of a general dissolution of the metal surfaces with pitting and some grain boundary attack.

In the tests with the SrF_2-impurity mixtures only slight metal attack was observed except for the mixtures containing copper and iron. In the latter cases the attack was several times greater than was observed in the other TZM couples (Figure 11). When copper or iron was present in the SrF_2 there was extensive chemical attack of the TZM with heavy pitting, grain boundary attack and subsurface void formation. From the micrographs it appears that some recrystallization of molybdenum has occurred at the surface of the specimens. Electron microprobe data showed extensive diffusion of iron or copper into the alloy grains and along the grain boundaries. The data indicate the copper and iron were reduced to the free metals which then diffused into the alloy. The presence of the impurity could account for the apparent recrystallization of the molybdenum. Much less attack was observed in the couples containing the other fluoride-impurity mixtures. Where attack did occur it normally involved pitting and grain boundary attack.

(a) High Purity $^{90}SrF_2$
800°C, 4400 Hours

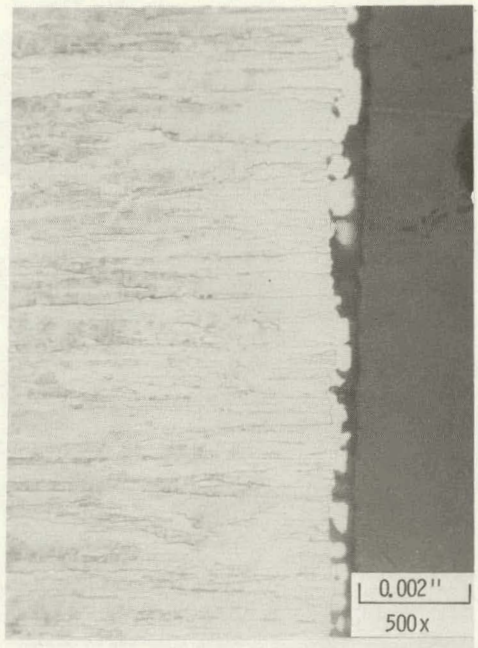

(b) High Purity $^{90}SrF_2$
1100°C, 4400 Hours

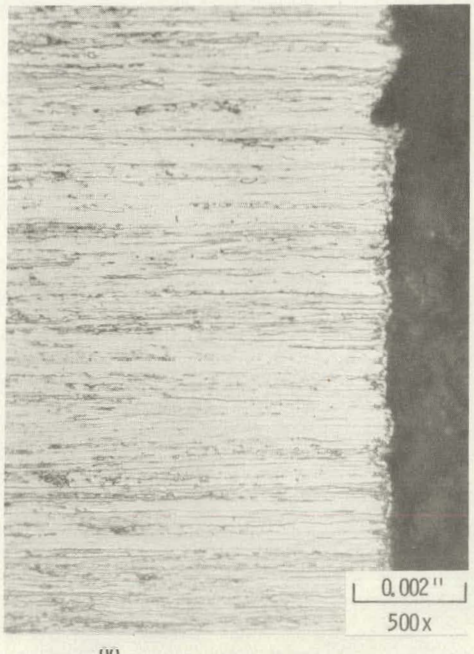

(c) WESF $^{90}SrF_2$
800°C, 4400 Hours

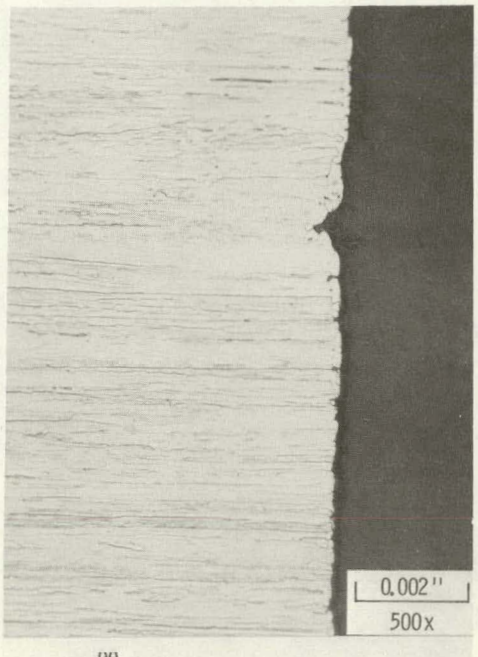

(d) WESF $^{90}SrF_2$
1100°C, 4400 Hours

FIGURE 10. TZM Specimens Exposed to $^{90}SrF_2$

(a) SrF_2 - NaF
4400 Hours

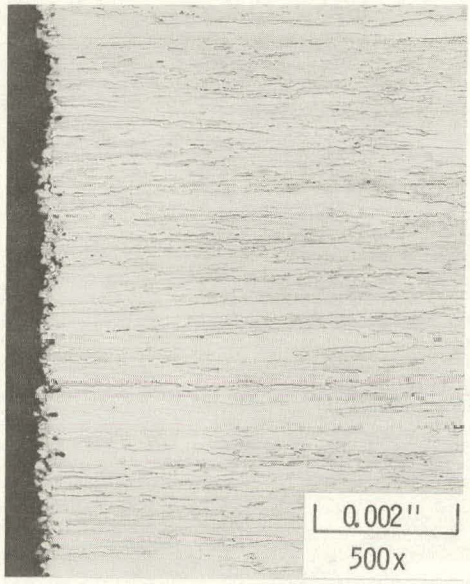

(b) SrF_2 - SrO
4400 Hours

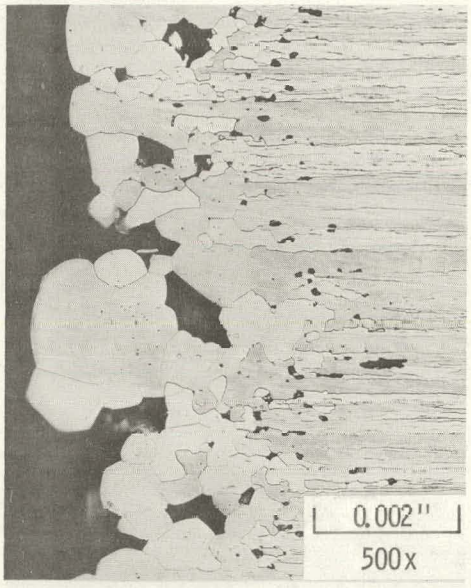

(c) SrF_2 - CuF_2
4400 Hours

(d) SrF_2 - FeF_3
4400 Hours

FIGURE 11. TZM Specimens Exposed to SrF_2-Impurity Mixtures at 1000°C

In none of the couples was there an indication of reaction between the TZM and SrF_2. Attack which was observed in the various TZM couples could be attributed to the presence of less stable fluoride impurities in the SrF_2. The thermodynamic analysis of the TZM-WESF $^{90}SrF_2$ system indicated that the components of the TZM would not react with SrF_2 but should react with the less stable fluorides such as CuF_2, FeF_3 and PbF_2. In general the experimental data confirm the theoretical calculations, although there is insufficient data to show if the molybdenum in the TZM reacted with the less stable fluorides or if only the zirconium and titanium reacted.

7.2.3 Haynes Alloy 25-SrF_2

The Haynes Alloy 25 test specimens were fabricated from bar stock which had been solution heat-treated (per ASM 5759D). Microstructure of the "as received" material was typical of the solution heat-treated alloy showing scattered carbides not taken into solution and annealing twins in the grains (Figure 12a). Aging of the alloy at 800°C for up to 4400 hr produced continuous precipitates along the grain boundaries, localized precipitates on twin boundaries and heavy bulk precipitation (Figure 12b). From electron microprobe data and the photomicrographs the precipitates appear to consist primarily of M_6C carbide phase (W, Cr, Co) and Laves phase [$(Co)_2$ (W, Cr)] with some $M_{23}C_6$ carbide phase. The microprobe data also indicated the presence of a significant quantity of molybdenum (up to 1.8%) in the carbide and Laves phase; molybdenum is not reported as a constituent of the alloy by the manufacturer. Aging at 1000°C produced M_6C and some $M_{23}C_6$ carbides in the grain boundaries, along twin boundaries and in the grain matrices; the Laves phase is more abundant (Figure 12c). Aging at 1100°C resulted in the disappearance of the twins and dissolution of most of the carbide phases, but the Laves phase remained (Figure 12d).

Grain size stability of the Haynes Alloy 25 was excellent, and there was little evidence of grain growth in samples aged up to 4400 hr at 1100°C. Hardness of the alloy increased with aging temperature up to 1000°C and then decreased markedly at 1100°C.

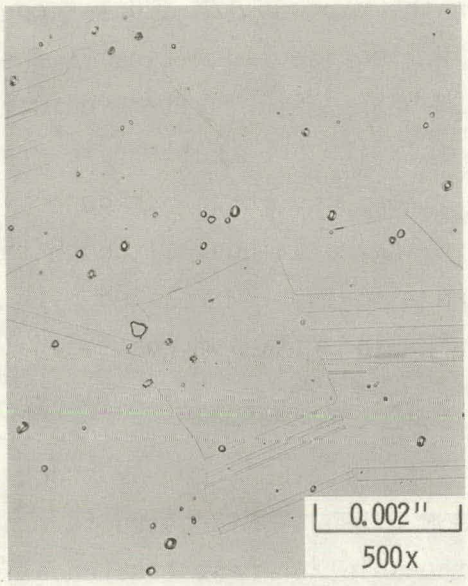

(a) "As Received"

(b) Aged at 800°C
4400 Hours

(c) Aged at 1000°C
4400 Hours

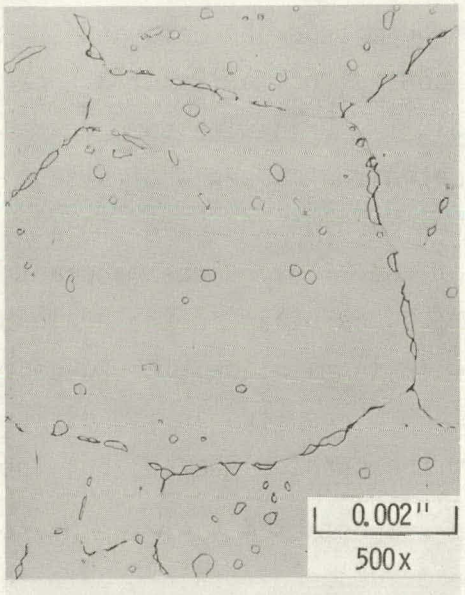

(d) Aged at 1100°C
4400 Hours

FIGURE 12. The Effect of Temperature on the Microstructure of Haynes Alloy 25

Aging of Haynes Alloy 25 in the temperature range of 650 to 900°C results in a severe loss of toughness and ductility.[8,9] Typically the notch impact energy at 25°C decreases from 70 ft-lb to less than 10 ft-lb when the alloy is aged at 800°C for 100 hr. The loss of toughness and ductility is reported to be due to the presence of the Laves and carbide phases.[9]

Haynes Alloy 25 showed the greatest overall resistance to fluoride attack of any of the other Ni- and Co-base alloys tested but was considerably less resistant than tungsten or TZM. Only slight attack of the alloy was found in the couples containing high-purity nonradioactive SrF_2. The level of attack did not increase significantly with increasing exposure temperature. Chemical attack did not exceed 1 mil and consisted of pitting and grain boundary attack, with limited subsurface void formation in the specimens tested at 1100°C (Figure 13). There was no indication of strontium diffusion into the grain boundaries or matrices, but some strontium was found in the voids. High magnification photomicrographs (3000X) revealed very fine porosity to a depth of 1 mil in the 1100°C specimens which was not present in specimens tested at lower temperatures. Electron microprobe data indicated a depletion of Laves phase to a depth of up to 2 mils in all specimens exposed to the high-purity nonradioactive SrF_2. This depletion is not readily apparent in the photomicrographs.

Tests with WESF-grade and high-purity $^{90}SrF_2$ produced significantly more attack of the Haynes Alloy 25 than the nonradioactive SrF_2. Chemical attack increased only slightly, but there was a marked increase in the depth of metal affected by changes in microstructure.

Photomicrographs of Haynes Alloy 25 specimens exposed to $^{90}SrF_2$ are shown in Figure 14. Specimens exposed to the radioactive fluoride exhibited a general dissolution of the metal surface with some grain boundary attack and pitting. Chemical attack appeared to increase slightly with increasing exposure temperature. The depth of metal affected by microstructural changes did not appear to increase to any marked degree with increasing

(a) 800°C, 4400 Hours

(b) 1000°C, 4400 Hours

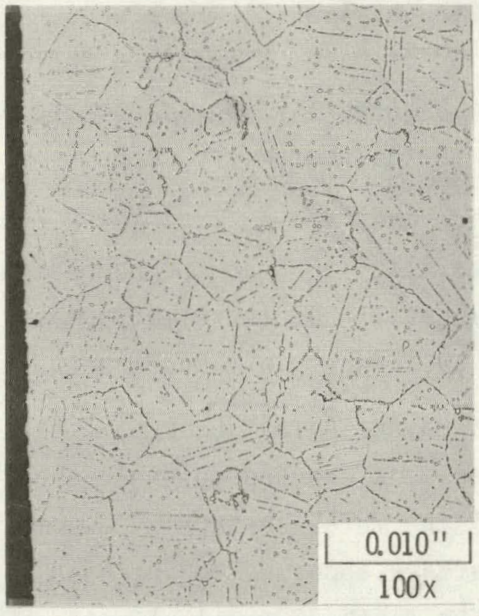

(c) 1100°C, 4400 Hours

FIGURE 13. Haynes Alloy 25 Specimens Exposed to High-Purity Nonradioactive SrF_2

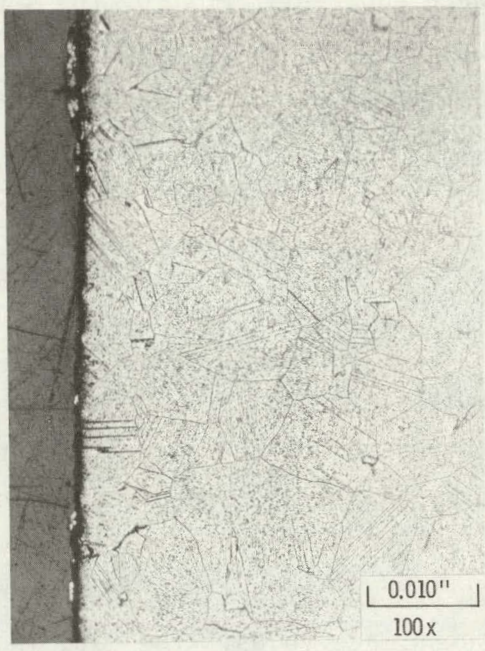

(a) WESF $^{90}SrF_2$
800°C, 4400 Hours

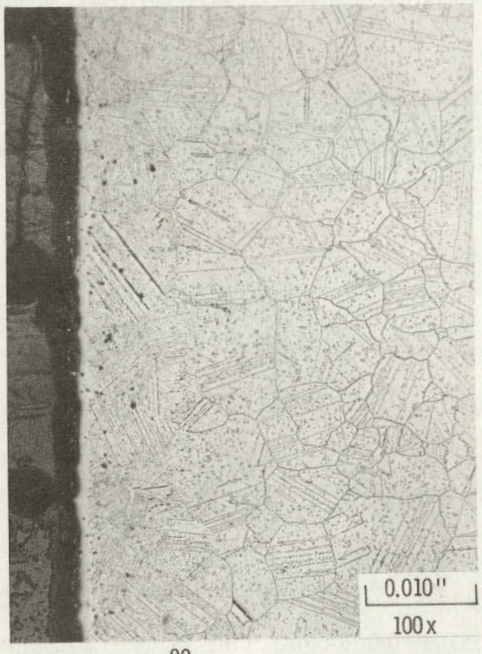

(b) High Purity $^{90}SrF_2$
1000°C, 4400 Hours

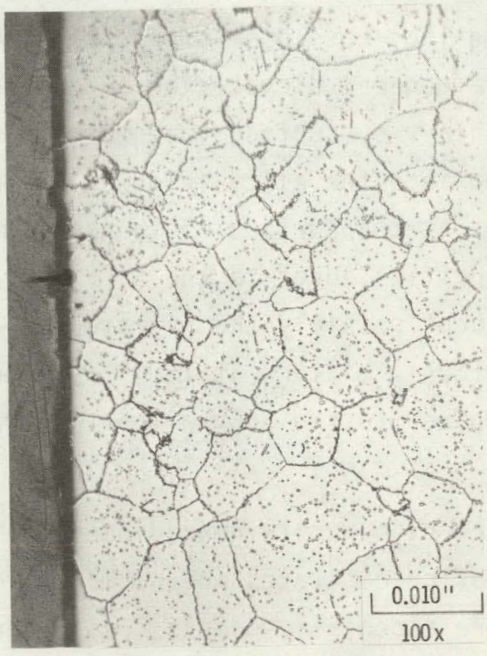

(c) WESF $^{90}SrF_2$
1100°C, 4400 Hours

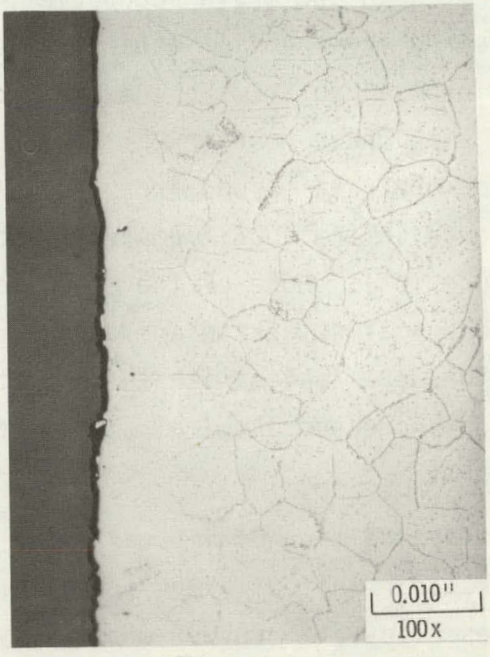

(d) High Purity $^{90}SrF_2$
1100°C, 4400 Hours

FIGURE 14. Haynes Alloy 25 Specimens Exposed to $^{90}SrF_2$

temperature. Two different effects were apparent. Most of the specimens exposed to $^{90}SrF_2$ exhibited a thin surface layer where normal alloy precipitates were largely depleted. The affected layers also contained large discrete spheroidal precipitates which were not found in the body of the test specimens or in the reference specimens. The nature of the spheroidal precipitates was not determined.

The tests with SrF_2-impurity mixtures showed that only two of the impurities increased the chemical attack of the Haynes Alloy 25 significantly, but most of them produced changes in the alloy microstructure. The addition of SrO to the SrF_2 greatly increased the chemical attack with the test specimens exhibiting grain boundary attack and subsurface void formation to a depth of several mils (Figure 15a). Microprobe data showed diffusion of strontium along the grain boundaries and a high concentration of strontium along the edges of the subsurface voids. The data indicate the attack is probably due to reactions between the SrO and carbide precipitates in the grain boundaries. The addition of FeF_3 to SrF_2 also increased the chemical attack (Figure 15b) but less so than the SrO. Specimens exposed to SrF_2-FeF_3 exhibited a general dissolution of the metal surface with grain boundary attack and heavy subsurface void formation. Microprobe data showed iron diffusion into the alloy (Figure 16b) and a decrease in the cobalt concentrations at the surface of the specimen (Figure 16f). None of the other impurities added to the SrF_2 increased the chemical attack to any degree except possibly the nitrate ion. Four couples were tested with the SrF_2-$Sr(NO_3)_2$ mixture at 1000°C and only one showed increased chemical attack compared to the SrF_2 without nitrate present.

The addition of impurities to the high-purity nonradioactive SrF_2 generally resulted in the formation of precipitates not normally found in Haynes Alloy 25. Copper and iron were especially bad in this regard, and abnormal precipitates were observed to depths of 18 to 20 mils in specimens exposed to SrF_2 containing FeF_3 or CuF_2 for 4400 hr at 1000°C (Figure 15b-c).

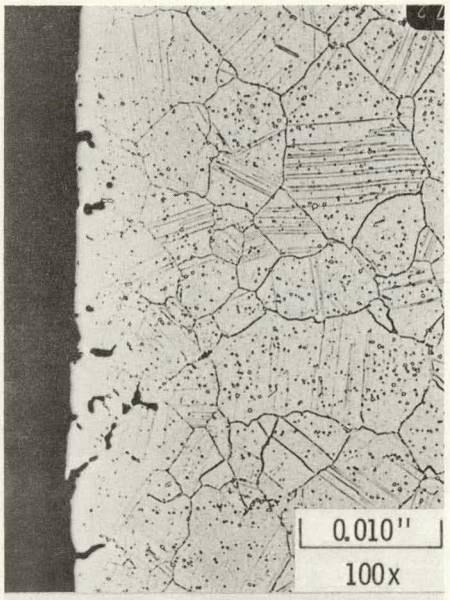

(a) SrF_2 - SrO
4400 Hours

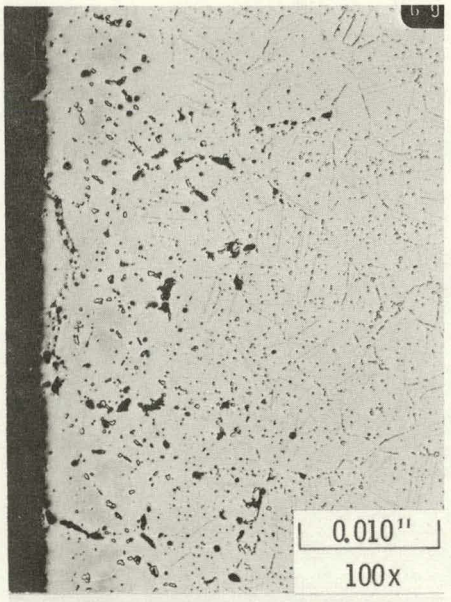

(b) SrF_2 - FeF_3
4400 Hours

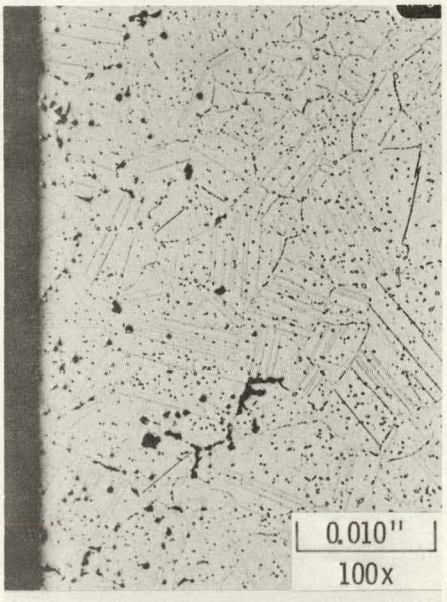

(c) SrF_2 - CuF_2
4400 Hours

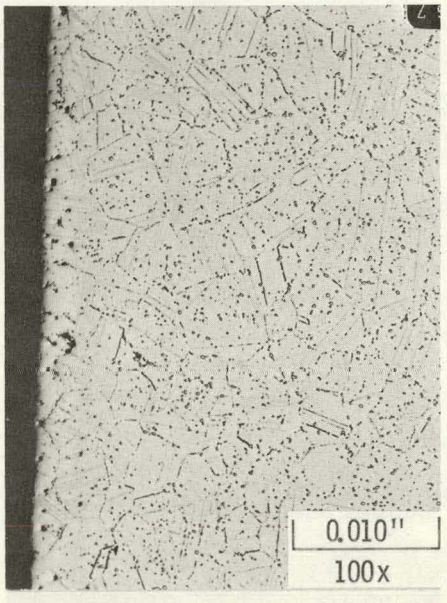

(d) SrF_2 - PbF_2
4400 Hours

FIGURE 15. Haynes Alloy 25 Specimens Exposed to SrF_2-Impurity Mixtures at 1000°C

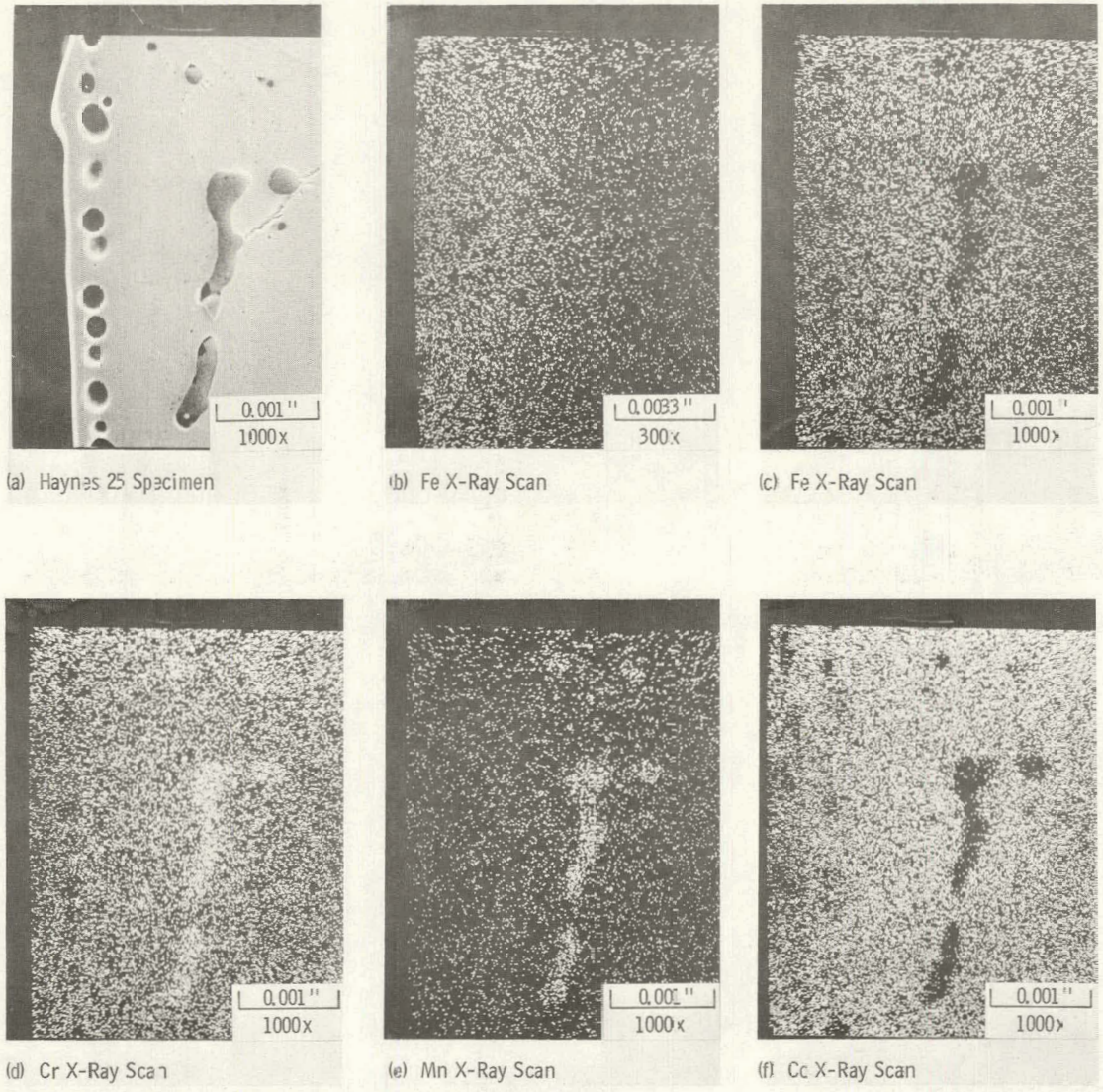

(a) Haynes 25 Specimen (b) Fe X-Ray Scan (c) Fe X-Ray Scan

(d) Cr X-Ray Scan (e) Mn X-Ray Scan (f) Co X-Ray Scan

FIGURE 16. Microstructure of Haynes Alloy 25 Exposed to SrF_2-FeF_3 at 1000°C and Electron Microprobe Scans of the Affected Areas

In the case of specimens exposed to FeF_3, electron microprobe data showed these precipitates to be composed primarily of chromium and manganese (Figure 16), while the precipitates in the specimens exposed to CuF_2-SrF_2 were high in chromium and tungsten. The microprobe data also showed copper had diffused into the grain boundaries and matrices as had the iron.

Specimens exposed to the other impurity-fluoride mixtures also exhibited abnormal precipitates. (For example, Figure 15d shows a test specimen exposed to SrF_2-PbF_2.) However, there was no indication of diffusion of the cation associated with the impurity fluoride into any of the test specimens, except those exposed to CuF_2 and FeF_3. Microprobe data indicated no abnormalities in the composition of the Haynes Alloy 25, and the composition of the abnormal precipitates could not be identified.

The theoretical analysis of the Haynes Alloy 25-$^{90}SrF_2$ system predicted that the alloy should be resistant to attack by pure SrF_2, but that the alloy should react with some impurities in the $^{90}SrF_2$ such as CuF_2 and FeF_3. The experimental results tended to confirm these predictions, although the calculation would lead one to expect more attack of the alloy by the WESF-grade $^{90}SrF_2$ than was actually observed. The results do show that the presence of less stable fluorides, such as CuF_2 and FeF_3, in the SrF_2 does increase attack of the alloy as predicted.

In addition to providing considerable resistance to attack by strontium fluoride, Haynes Alloy 25 possesses certain other features, such as good oxidation resistance and good seawater corrosion resistance, which make it a desirable containment for the fluoride. However, the potential usefulness of Haynes Alloy 25 as a containment material for $^{90}SrF_2$ is severely limited by the aging effects observed when the alloy is heated to temperatures in the range of 650 to 900°C.

7.2.4 Haynes Alloy 188-SrF_2

The Haynes Alloy 188 test specimens were prepared from bar stock which had been solution heat-treated at 2100°F. The alloy is a modification of Haynes Alloy 25 with increased nickel content for structural stabilization

and the addition of a small amount of lanthanum to provide improved oxidation resistance. The microstructure of the "as received" material was typical of that of the solution heat-treated alloy showing some M_6C carbide phase precipitate (Figure 17). Aging response of the Haynes Alloy 188 was similar to that of Haynes Alloy 25, although precipitate formation was generally less (Figure 17). Thermal aging at 800°C resulted in continuous grain boundary precipitates ($M_{23}C_6$ and M_6C) and moderate bulk precipitation with a limited amount of Laves phase. At 1000°C the precipitation was less, with some M_6C, and $M_{23}C_6$ carbides and Laves phase present. Aging at 1100°C resulted in further dissolution of the carbide precipitates.

Grain size of the "as received" alloy was smaller than that of the Haynes Alloy 25. Grain size stability was excellent up to 1000°C but some grain growth occurred at 1100°C. Hardness readings for the Haynes Alloy 188 were consistently less than for the Haynes Alloy 25. Hardness of the aged material increased with exposure temperature up to 1000°C but decreased sharply at 1100°C.

Work at ORNL[9] showed that Haynes Alloy 188 suffers a loss of toughness and ductility similar to Haynes Alloy 25 when aged at 650 to 900°C. The reduced toughness and ductility with thermal aging is attributed to the formation of both carbide and Laves phases.

The Haynes Alloy 188 provided significantly less resistance to fluoride attack than the Haynes Alloy 25. Exposure to high-purity nonradioactive SrF_2 produced localized pitting and grain boundary attack with some subsurface void formation (Figure 18). The level of attack appeared to increase with temperature, especially with the 4400-hr couples. Examination of the test specimens with the scanning electron microscope revealed the presence of very fine voids to depths up to 4 mils which were not present in the thermally aged reference specimen. The fine voids could not be detected in the low magnification (100 and 500X) photomicrographs. Grain boundary attack in the 1000 and 1100°C couples was very localized and occurred to depths of 3 to 4 mils. Microprobe data indicated the attack occurred in areas having high concentrations of Laves phase. No diffusion of strontium into the alloy was found although some strontium was found in the voids.

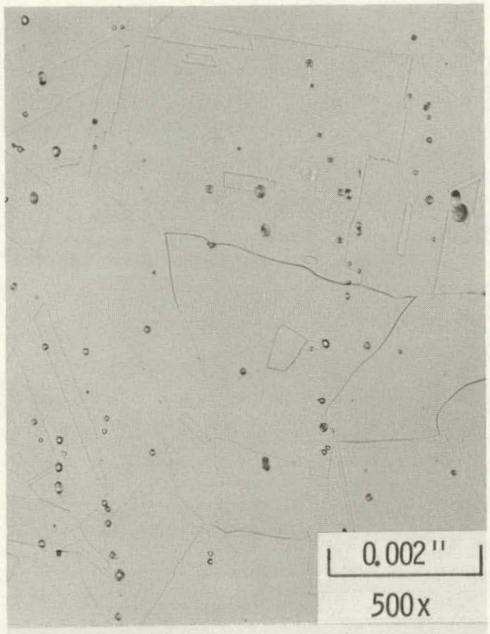

(a) As Received

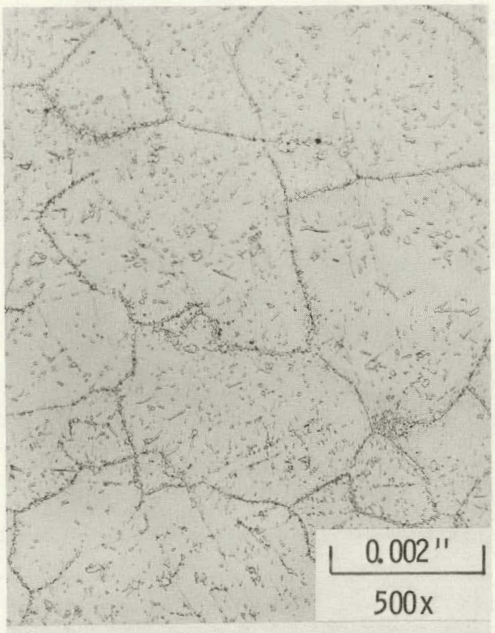

(b) Aged at 800°C, 4400 Hours

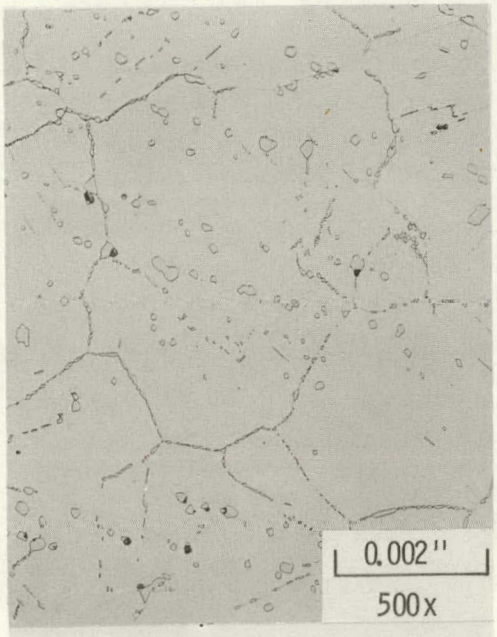

(c) Aged at 1000°C, 4400 Hours

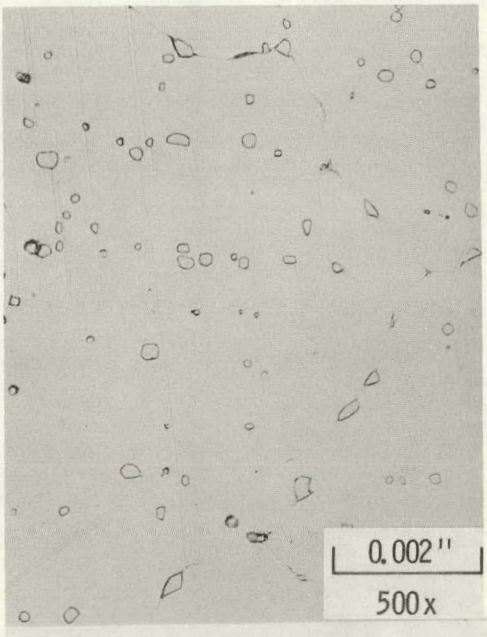

(d) Aged at 1100°C, 4400 Hours

FIGURE 17. Microstructure of Haynes Alloy 188

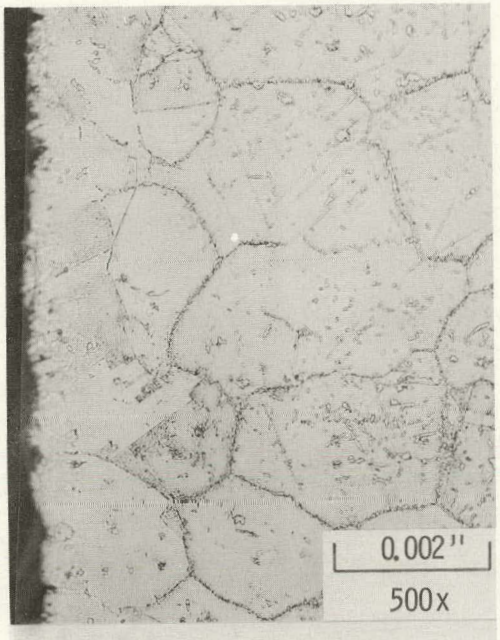

(a) 800°C, 4400 Hours

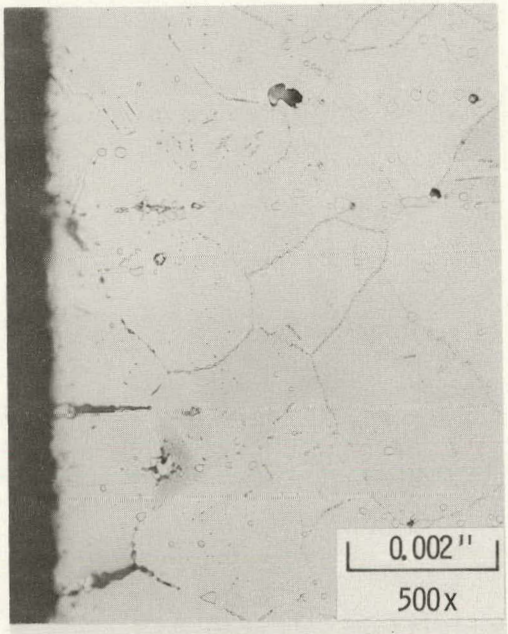

(b) 1000°C, 4400 Hours

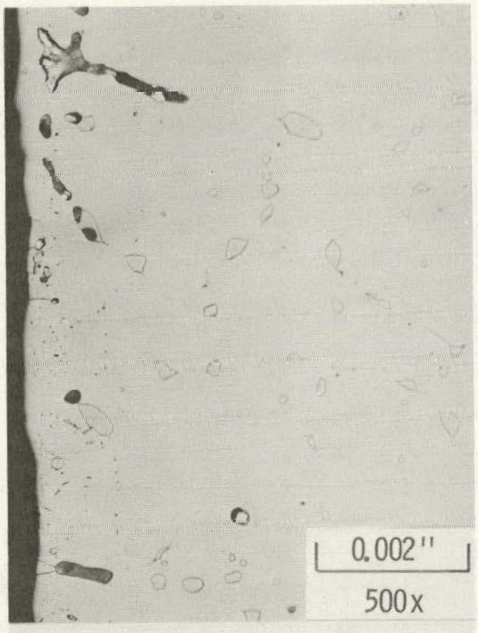

(c) 1100°C, 4400 Hours

FIGURE 18. Haynes Alloy 188 Specimens Exposed to High-Purity Nonradioactive SrF_2

Exposure of the Haynes Alloy 188 to WESF-grade and high-purity $^{90}SrF_2$ increased the chemical attack only slightly as compared to the nonradioactive SrF_2, but the depth of metal affected by microstructural changes was greatly increased. Overall, greater alloy attack was found in the couples containing high-purity $^{90}SrF_2$ than in the WESF-grade $^{90}SrF_2$ couples. The level of metal attack appeared to be less at 1100°C than at the lower temperatures and the type of attack observed appeared to vary with temperature (Figure 19). Test specimens exposed to WESF-grade and high-purity $^{90}SrF_2$ at 800°C exhibited a general dissolution of the metal surface with extensive grain boundary attack and a depletion of normal alloy precipitates to a considerable depth. Exposure to the radioactive fluorides at 1000°C resulted in heavy grain boundary attack and subsurface void formation but without the general surface dissolution observed in the 800°C specimens. Abnormal precipitates were found to depths up to 10 to 12 mils in the 1000°C specimens. At 1100°C metal attack was reduced somewhat from that found at the lower temperatures. Grain boundary attack was less; there was little evidence of subsurface void formation; and the abnormal precipitates found in the 1000°C specimens were much less apparent. There was a thin layer ($\sim$2 mils thick) at the metal surface which appeared to have a very high concentration of finely dispersed Laves phase. Below this was a layer several mils thick in which the normal alloy precipitates were depleted.

The addition of impurities to high-purity nonradioactive SrF_2 produced anomalous results. In general chemical attack was reduced, except for the case of SrO, while the microstructural changes were somewhat greater as compared to the high-purity SrF_2. As was the case with Haynes Alloy 25, the addition of SrO to the SrF_2 greatly accelerated the attack of the Haynes Alloy 188. Grain boundary attack and subsurface void formation were evident to depths of 20 mils (Figure 20a). Microprobe data indicated no diffusion of strontium into the alloy, but did show a disappearance of normal intragranular precipitates in the affected zone.

The addition of relatively stable fluorides such as NaF, (Ba, Ca, Mg)F_2 and AlF_3 to the SrF_2 reduced the chemical attack significantly (Figure 20b),

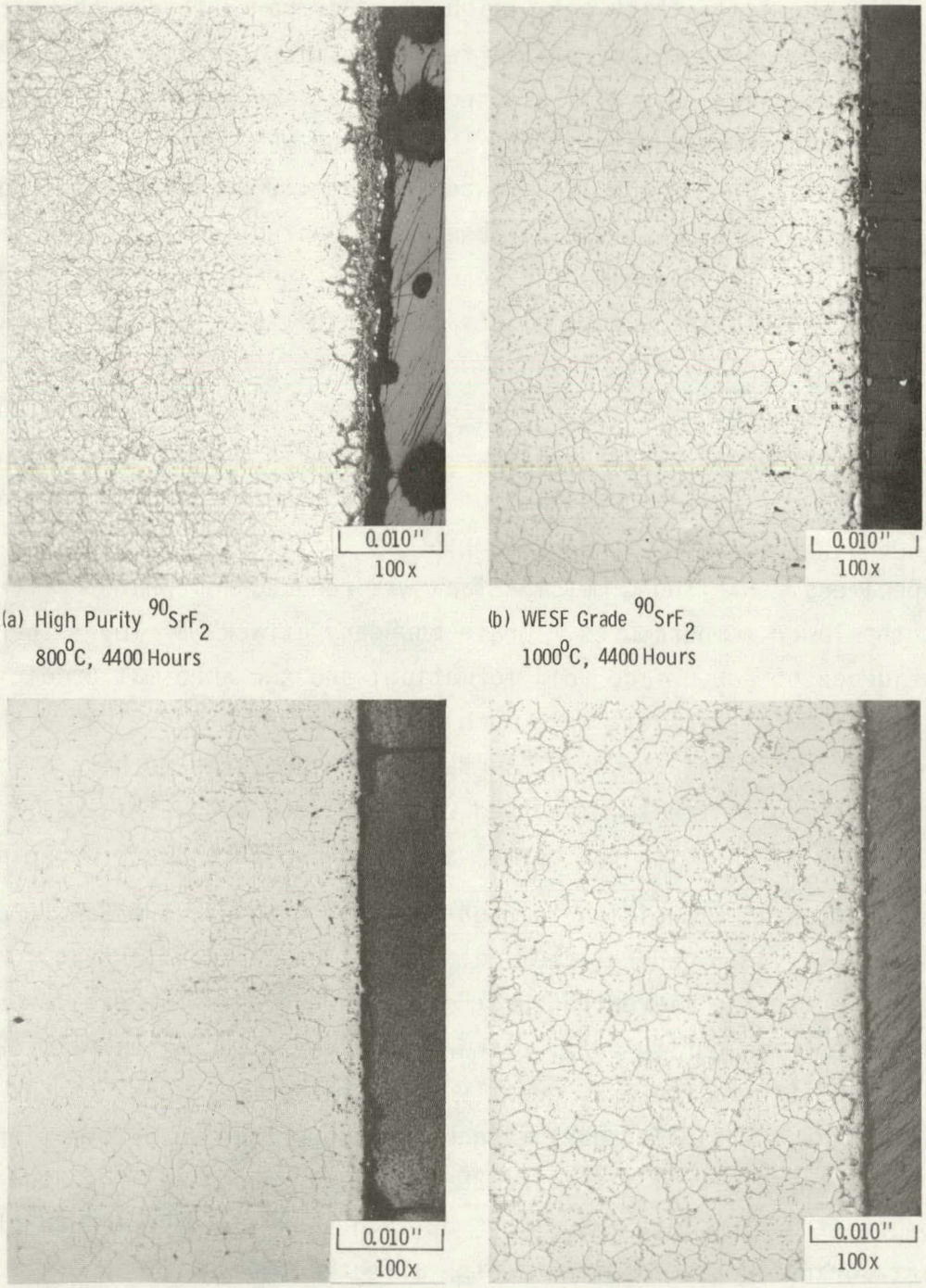

(a) High Purity $^{90}SrF_2$
800°C, 4400 Hours

(b) WESF Grade $^{90}SrF_2$
1000°C, 4400 Hours

(c) High Purity $^{90}SrF_2$
1000°C, 4400 Hours

(d) WESF Grade $^{90}SrF_2$
1100°C, 4400 Hours

FIGURE 19. Haynes Alloy 188 Specimens Exposed to $^{90}SrF_2$

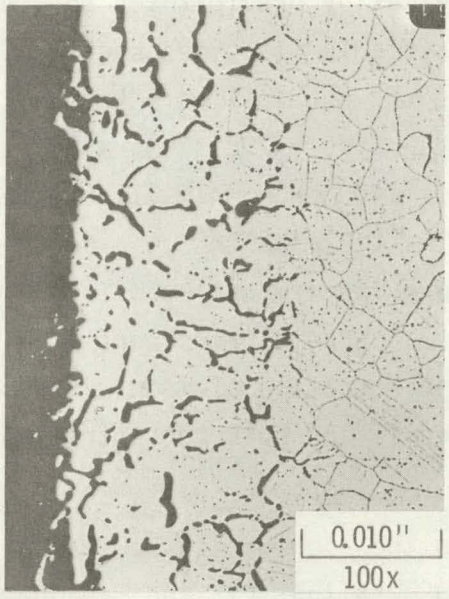

(a) SrF_2 + SrO
4400 Hours

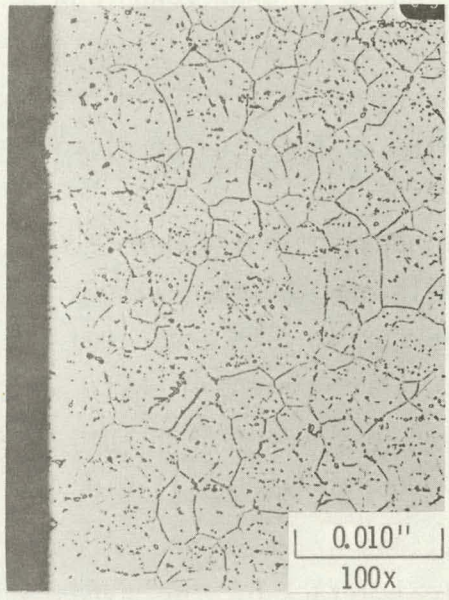

(b) SrF_2 + (Ba, Ca, Mg) F_2
4400 Hours

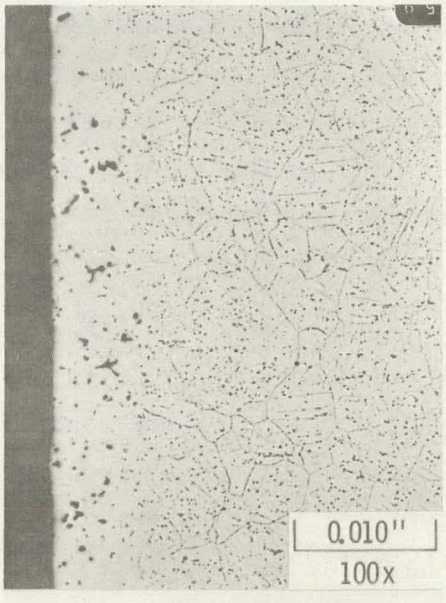

(c) SrF_2 + FeF_3
4400 Hours

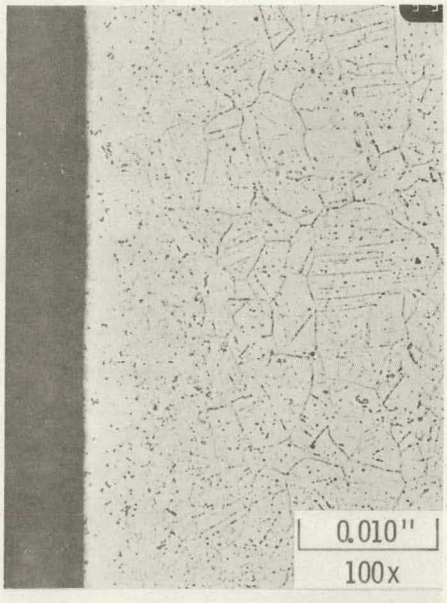

(d) SrF_2 + Sr $(NO_3)_2$
4400 Hours

FIGURE 20. Haynes Alloy 188 Specimens Exposed SrF_2-Impurity Mixtures at 1000°C

and resulted in a large reduction of normal alloy precipitates to a depth of 3 to 4 mils. Even the addition of less stable fluorides such as CuF_2, MnF_2 and FeF_3 to the SrF_2 did not increase the chemical attack but did increase the effects on the microstructure. Figure 20c shows a Haynes Alloy 188 specimen exposed to SrF_2-FeF_3 for 4400 hr. Only slight chemical attack is apparent but abnormal precipitates are apparent to a depth of about 7 mils and the normal precipitates are largely depleted in the same zone. Microprobe data indicated the abnormal precipitates were high in manganese, chromium and nickel. A high concentration of iron was found at the surface of the specimen which decreased to the bulk concentration over a zone approximately 5 mils wide.

Additions of water and nitrate ion to the high-purity SrF_2 also reduced the chemical attack of the Haynes Alloy 188. Slight pitting was observed in specimens exposed to nitrate (Figure 20d) or water, but the attack was minimal. Some disappearance of alloy precipitates occurred over a narrow zone below the metal surface.

Overall, the results obtained with Haynes Alloy 188 are difficult to explain. The data show that additions of impurities to high-purity non-radioactive SrF_2, with one exception, reduced the chemical attack of the alloy. Similarly less chemical attack was found in specimens exposed to WESF-grade $^{90}SrF_2$ compared to specimens exposed to high-purity $^{90}SrF_2$. No reasonable explanations for these results have been found.

The theoretical analysis of the Haynes Alloy 188-WESF $^{90}SrF_2$ system indicated the alloy should be quite similar to Haynes Alloy 25 in its resistance to fluoride attack, except for the presence of lanthanum. The thermodynamic calculations showed the lanthanum should be a strong reducing agent and could react with many of the impurities in the WESF $^{90}SrF_2$. While the experimental results show that the alloy is less resistant to fluoride attack than the Haynes Alloy 25, none of the data indicated that the presence of lanthanum was a cause of the increased reactivity.

The testing of Haynes Alloy 188 as a containment material for SrF_2 was originally undertaken because it was reported to have improved thermal aging properties compared to Haynes Alloy 25. The recent results obtained at ORNL show that the alloy suffers the same detrimental thermal aging effects as Haynes Alloy 25. This combined with its reduced resistance to fluoride attack makes the alloy a less acceptable container material for $^{90}SrF_2$ than the Haynes Alloy 25.

7.2.5 Hastelloy C-276-SrF_2

The Hastelloy C-276 test specimens were fabricated from wrought bar stock that had been solution heat-treated at 2100°F and rapidly quenched. The microstructure of the "as received" alloy is shown in Figure 21a. There is very little indication of precipitated second phases, with annealing twins being the predominate feature. Grain size is relatively large. Thermal aging at 800°C produced continuous grain boundary precipitation and heavy bulk precipitation (Figure 21b). The precipitates appear to be predominantly carbide phase with possibly some mu phase $[(Fe,Co)_7(Mo,W)_6]$ present. Microprobe data show the precipitates to be enriched in molybdenum, tungsten and chromium with the molybdenum concentration of the matrix being sharply reduced from the nominal concentration (8 to 10% versus a nominal 16%). Aging at 1000°C resulted in less precipitate formation, and the composition of the precipitates was more indicative of a M_6C type carbide (Figure 21c). Again the precipitates were enriched in molybdenum and the concentration of molybdenum in the matrix was reduced to 8 to 10%. When the alloy was aged at 1100°C for 1500 hr it was found that very little precipitate formation occurred (Figure 21d). Aging for 4400 hr, however, resulted in significant precipitate formation, but less than occurred at 1000°C (Figure 21e). The precipitates appear to be M_6C type carbide phase.

Grain size stability at 800 and 1000°C was excellent, but considerable grain growth occurred at 1100°C. Hardness of the "as received" material was higher than expected for the solution heat-treated material. The hardness may have resulted from preparation of the test specimen, since the

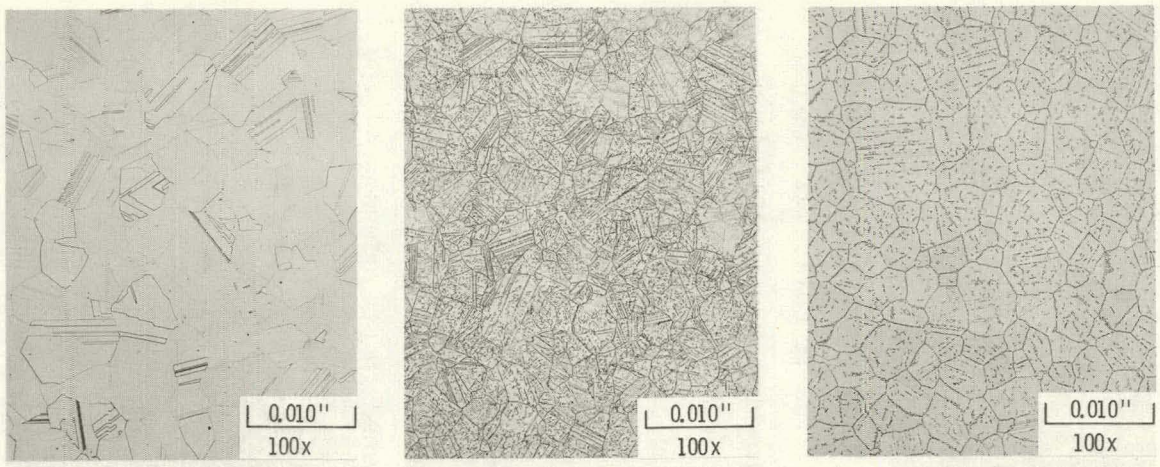

(a) "As Received" (b) 800°C, 4400 Hours (c) 1000°C, 4400 Hours

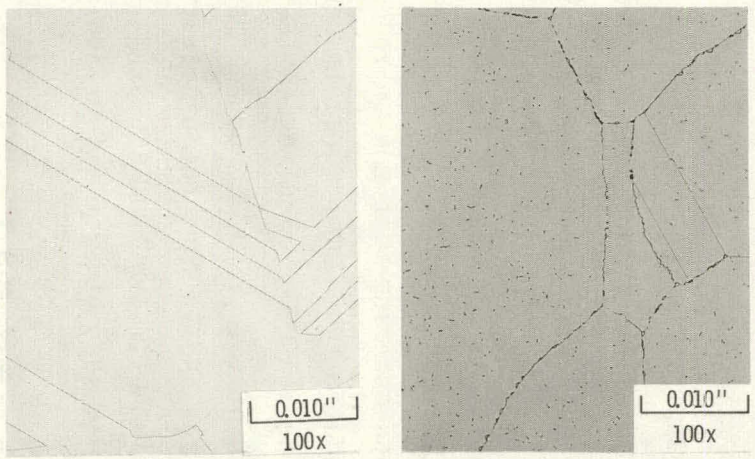

(d) 1100°C, 1500 Hours (e) 1100°C, 4400 Hours

FIGURE 21. Effect of Thermal Aging on the Microstructure of Hastelloy C-276

hardness decrease was substantial from the surface toward the center of the specimen. Aging at 800°C increased the hardness while aging at the higher temperatures decreased the hardness.

Exposure of Hastelloy C-276 to high-purity nonradioactive SrF_2 resulted in extensive metal attack which increased sharply with increased exposure temperature (Figure 22). Grain boundary attack and subsurface void formation were the predominant forms of attack at all temperatures. Changes in microstructure were less extensive, although some abnormal precipitates were present in the various specimens tested. These precipitates were high in chromium and nickel. Electron microprobe data showed extensive diffusion of strontium along the affected grain boundaries, and a thin surface layer where strontium had diffused into the alloy matrix. The mechanism of the grain boundary attack has not been fully identified but appears to involve reaction(s) of SrF_2 with (Mo,W,Cr) carbide in the grain boundaries. Exposure of the Hastelloy C-276 to the high-purity nonradioactive strontium fluoride had no noticeable effect on the hardness of the alloy.

Hastelloy C-276 exposed to WESF-grade or high-purity $^{90}SrF_2$ exhibited less chemical attack than the specimens exposed to high-purity nonradioactive SrF_2. However, changes in the microstructure occurred to much greater depths. Overall, less chemical attack was observed in the WESF-grade $^{90}SrF_2$ couples than in the couples containing high-purity $^{90}SrF_2$. Specimens exposed to the radioactive strontium fluoride suffered general surface dissolution with some grain boundary attack and subsurface void formation (Figure 23). Grain boundary attack was far less than that found in the nonradioactive couples especially at the higher temperatures. Abnormal precipitates were found in all specimens but were more extensive at the higher temperatures. The nature of the precipitates was not determined. The effect of temperatures on metal attack was much less pronounced with the radioactive fluoride than with the nonradioactive SrF_2.

With one exception, the addition of impurities to the high-purity nonradioactive SrF_2 reduced the chemical attack of the Hastelloy C-276. The

(a) 800°C, 4400 Hours

(b) 1000°C, 4400 Hours

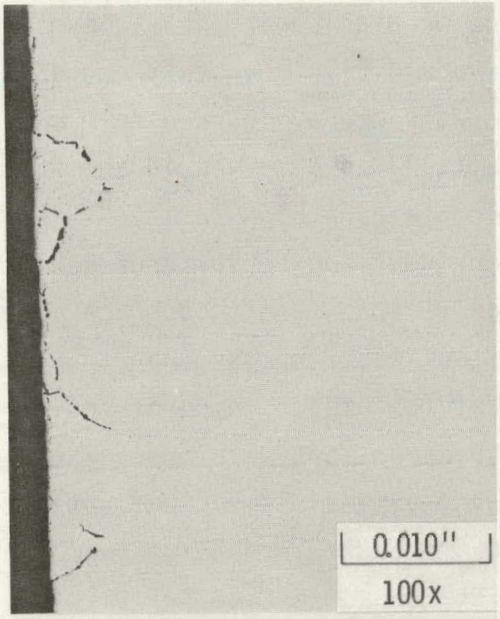

(c) 1100°C, 1500 Hours

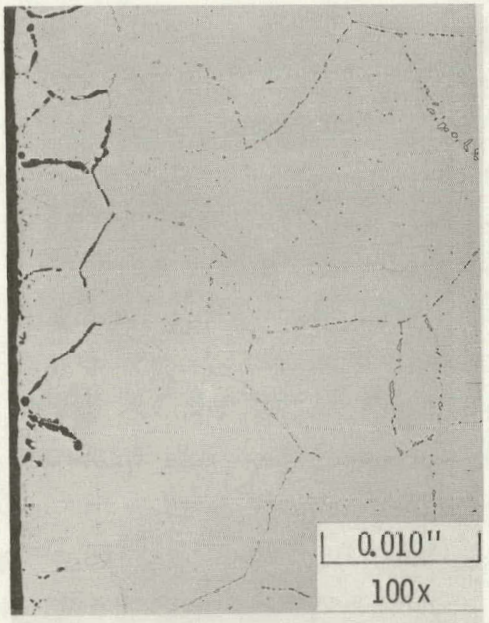

(d) 1100°C, 4400 Hours

FIGURE 22. Hastelloy C-276 Specimens Exposed to High-Purity Nonradioactive SrF_2

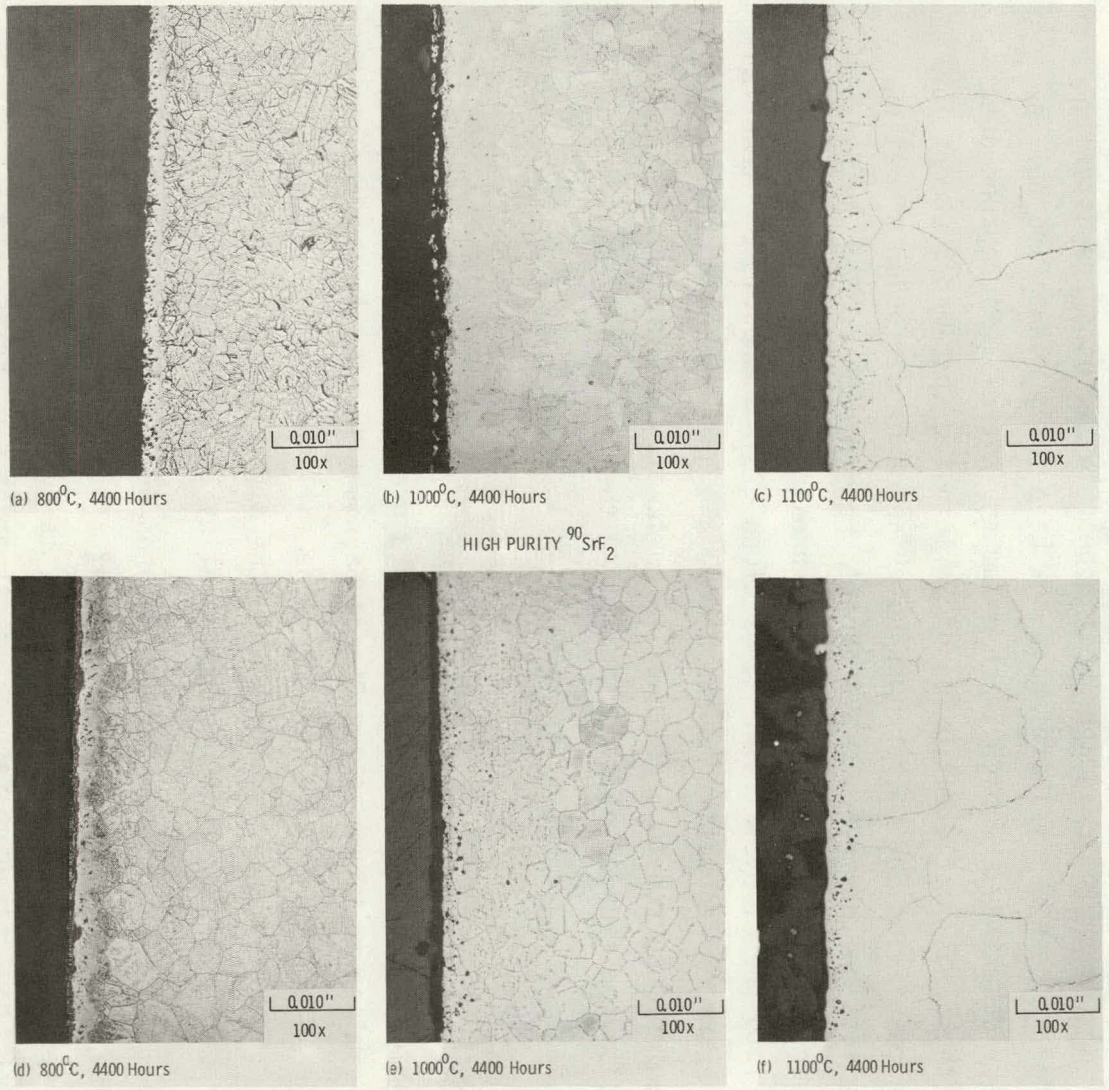

FIGURE 23. Hastelloy C-276 Specimens Exposed to $^{90}SrF_2$

grain boundary attack and void formation that was so extensive in couples containing high-purity nonradioactive SrF_2 was far less prevalent in the couples containing the SrF_2-impurity mixtures, except when SrO was present. However, the addition of impurities did serve to increase the depth of metal affected by changes in microstructure. Typical examples of Hastelloy C-276 specimens exposed to SrF_2-impurity mixtures are shown in Figure 24. In several of the photomicrographs what appear to be voids are actually precipitates. These precipitates have not been fully identified but in almost every case they are high in chromium and nickel. Microprobe data indicated there was little diffusion of Sr into the specimens, except for the couple containing SrO. There was no evidence of diffusion of cation impurities into the Hastelloy C-276 except when iron or copper was present in the fluoride. When copper or iron was present there was significant diffusion into the alloy matrix but not along grain boundaries. Strontium oxide was extremely corrosive to the alloy, and grain boundary attack and void formation occurred to a depth of 10 to 12 mils. Microprobe data indicated extensive diffusion of strontium along the grain boundaries.

There is no ready explanation of why the presence of impurities (except SrO) in the SrF_2 reduced the chemical attack of the Hastelloy C-276. However, a similar effect was observed with the Haynes Alloy 188. Based on thermodynamic considerations only, one would predict that Hastelloy C-276 should be similar to Haynes Alloy 25 and Haynes Alloy 188 in its resistance to fluoride attack. It is obvious from the data that Haynes Alloy 25 provides far more resistance to attack than the other two alloys. The basis for the greater resistance of the Haynes Alloy 25 has not been identified.

Hastelloy C-276 has a number of features, which makes it an attractive container material for $^{90}SrF_2$, exclusive of fluoride compatibility. It is extremely resistant to seawater corrosion, is quite resistant to oxidation up to 1000°C, has fair high temperature strength properties, and suffers less from thermal aging effects than the two Haynes alloys. The Hastelloy C-276 is also fairly easy to fabricate and weld. Against these advantages must be balanced its fairly poor resistance to attack by the $^{90}SrF_2$.

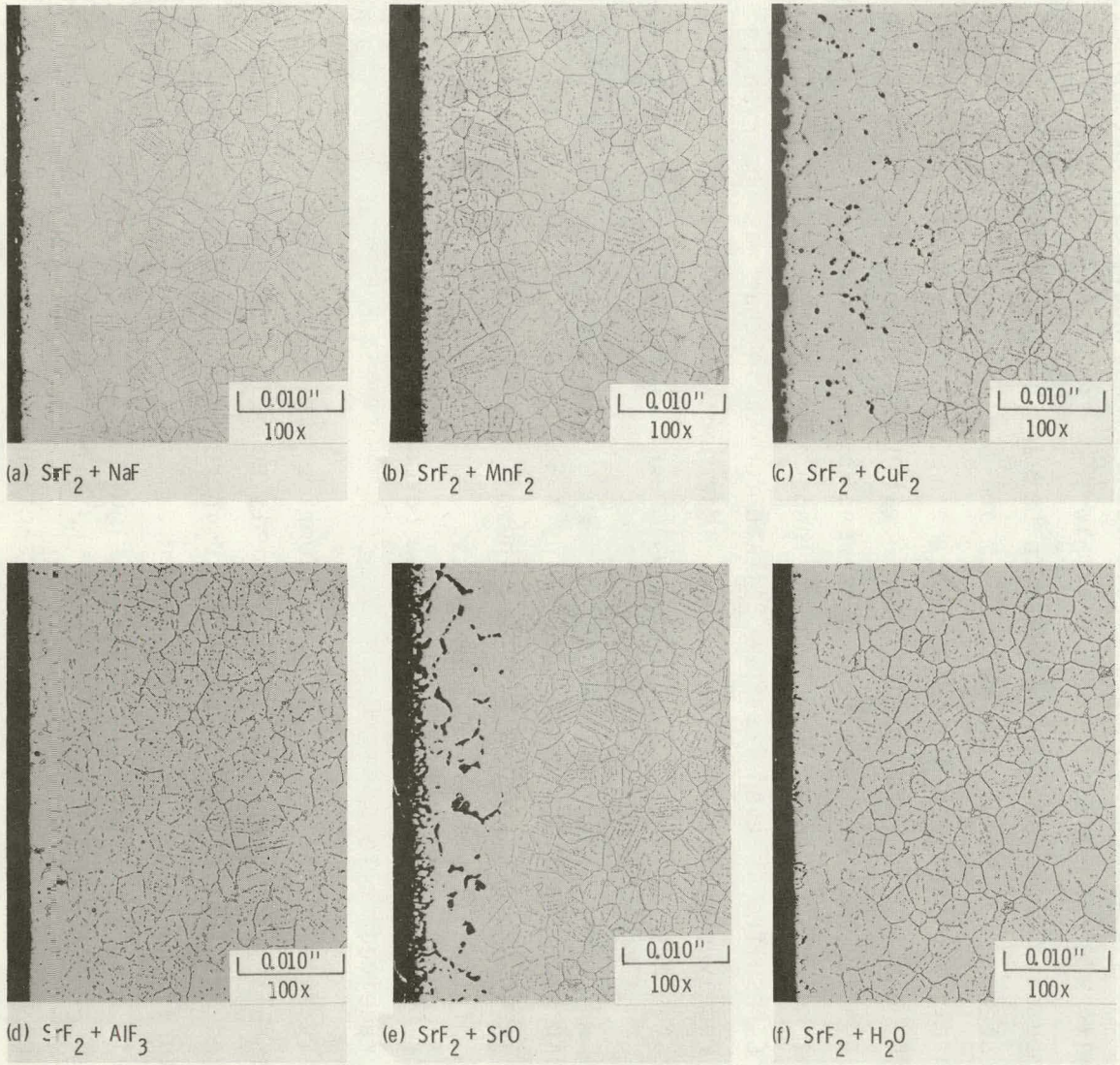

FIGURE 24. Hastelloy C-276 Specimens Exposed to SrF_2-Impurity Mixtures at 1000°C for 4400 hr

7.2.6 Hastelloy X-SrF_2

The Hastelloy X test specimens were fabricated from bar stock which had been solution heat-treated at 1950°F (per ASM 5754). The microstructure of the "as received" material is typical of the solution heat-treated alloy with carbide phase precipitates in the grain matrices (Figure 25a). Thermal aging at 800°C produced continuous grain boundary and heavy bulk precipitates, principally M_6C carbide phase with possibly some sigma phase (Figure 25b). Microprobe data show the carbide phase to be very high in molybdenum and tungsten. As a result the molybdenum and tungsten concentrations of the alloy matrix are considerably less than the nominal concentrations. Aging at 1000°C resulted in less precipitate formation, with only the M_6C carbide phase present. Much of the finely dispersed precipitates found in the grain matrix of material aged at 800°C are no longer present (Figure 25c). Aging at 1100°C resulted in even less precipitate formation than was observed in the "as received" material (Figure 25d). Microprobe data indicate that the precipitates are probably M_6C carbides which are high in molybdenum and tungsten.

Grain size stability of the Hastelloy X was good up to 1000°C, but some grain growth occurred at 1100°C. Thermal aging at 800°C increased the hardness of the alloy about 50 DPHN units. Aging at higher temperatures decreased the hardness, and at 1100°C the hardness was less than that of the "as received" alloy.

Resistance of the Hastelloy X to fluoride attack was less than that of Haynes Alloy 25. Exposure to high-purity nonradioactive SrF_2 resulted in limited metal attack which appeared to increase slightly with exposure temperature. Each specimen showed evidence of surface dissolution with some grain boundary attack and pitting (Figure 26). Microprobe data showed no evidence of strontium diffusion into the alloy. Both the electron micrographs and microprobe data indicated a reaction zone up to 4 mils thick at the surface of each specimen which was depleted in the normal carbide precipitates. In the specimens tested at 1000 and 1100°C there was a narrow

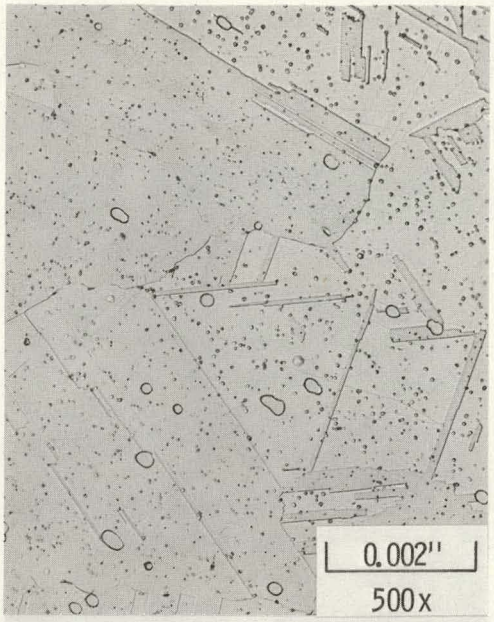

(a) "As Received"

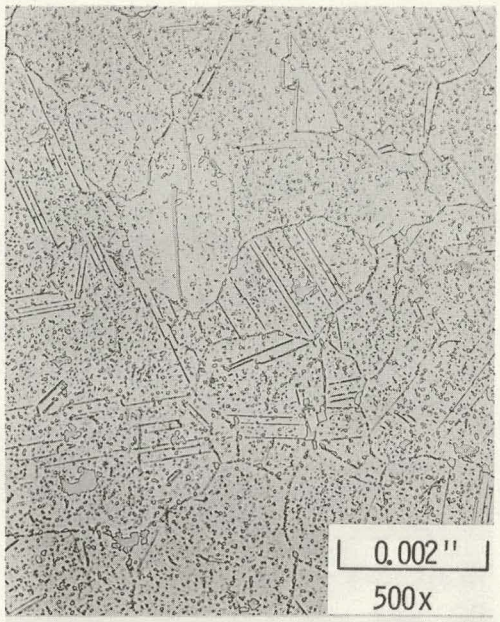

(b) 800°C, 4400 Hours

(c) 1000°C, 4400 Hours

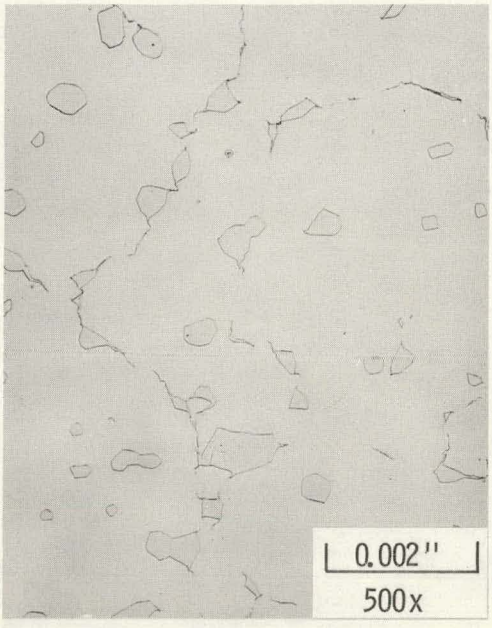

(d) 1100°C, 4400 Hours

FIGURE 25. The Effect of Thermal Aging on the Microstructure of Hastelloy X

(a) 800°C, 4400 Hours

(b) 1100°C, 4400 Hours

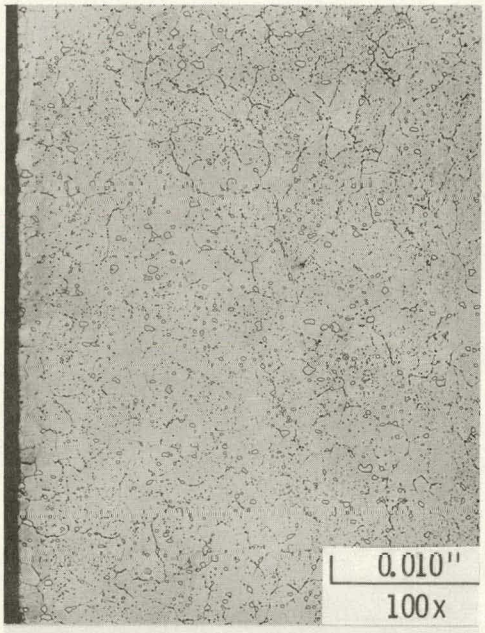

(c) 1000°C, 4400 Hours

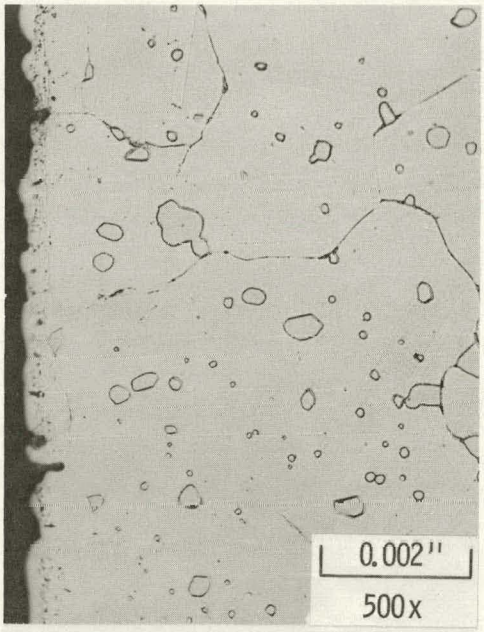

(d) 1000°C, 4400 Hours

FIGURE 26. Hastelloy X Specimens Tested with High-Purity Nonradioactive SrF_2

band <1 mil thick just below the surface which contained a finely dispersed precipitate that was very high in chromium and iron and may have been sigma phase (Figure 26d). Exposure to the high-purity SrF_2 did not affect the hardness of the Hastelloy X except possibly to increase the hardness slightly at 1100°C compared to the reference specimen.

Testing of the Hastelloy X with the high-purity and WESF-grade $^{90}SrF_2$ resulted in substantially more metal attack than was observed with the non-radioactive SrF_2. Overall, specimens exposed to the high-purity $^{90}SrF_2$ exhibited more attack than those tested with the WESF-grade $^{90}SrF_2$, although the types of attack were quite similar (Figure 27). Surface dissolution, grain boundary attack and subsurface void formation were found in all specimens. Changes in the microstructure were also apparent in all specimens, especially those exposed to the high-purity $^{90}SrF_2$. Dissolution of normal alloy precipitates occurred in all samples and reached a depth of 20 mils in samples exposed to high-purity $^{90}SrF_2$ at 1100°C. Heavy discrete precipitates were found in the grain boundaries of all specimens to depths up to 12 to 13 mils. The precipitates were not characterized but did not appear to be carbides. In each of the samples tested at 1100°C there was a zone at the surface about 10 to 12 mils thick where the average grain size was less than that of the bulk material. A comparison with the "as received" material showed that little grain growth had occurred in the affected zone, probably because of the stabilizing influence of the precipitates present.

Exposure of Hastelloy X to the SrF_2-impurity mixtures produced no significant increase in chemical attack compared to the SrF_2 alone, except when SrO or FeF_3 was present. However, the presence of impurities did result in significant changes in the microstructure of the alloy. All of the specimens exposed to the SrF_2-impurity mixtures suffered some surface dissolution and grain boundary attack. Subsurface voids were present in most of the specimens. Typical examples of specimens exposed to the fluoride-impurity mixtures are shown in Figure 28. The only specimens showing extensive chemical attack were those exposed to SrF_2 containing FeF_3 or SrO.

(a) High Purity $^{90}SrF_2$
800°C, 4400 Hours

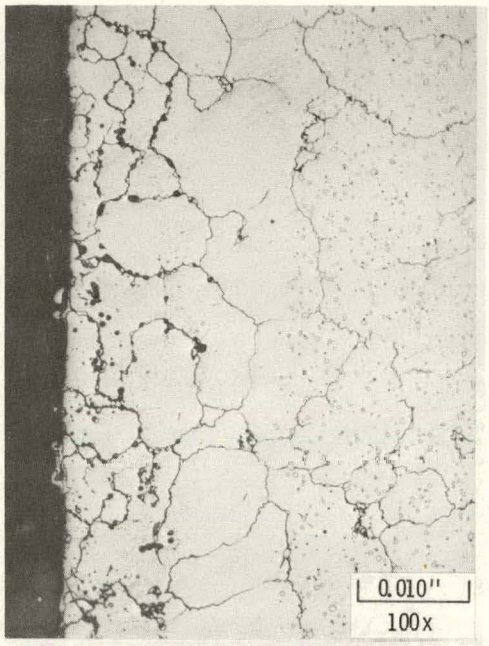

(b) High Purity $^{90}SrF_2$
1100°C, 4400 Hours

(c) WESF Grade $^{90}SrF_2$
1000°C, 4400 Hours

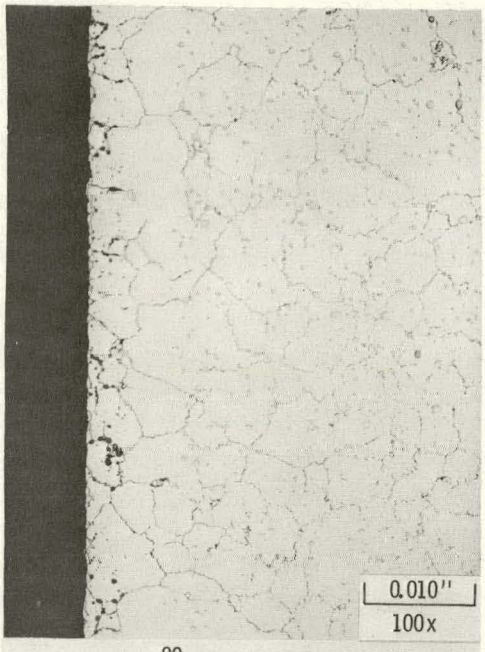

(d) WESF Grade $^{90}SrF_2$
1100°C, 4400 Hours

FIGURE 27. Hastelloy X Specimens Exposed to $^{90}SrF_2$

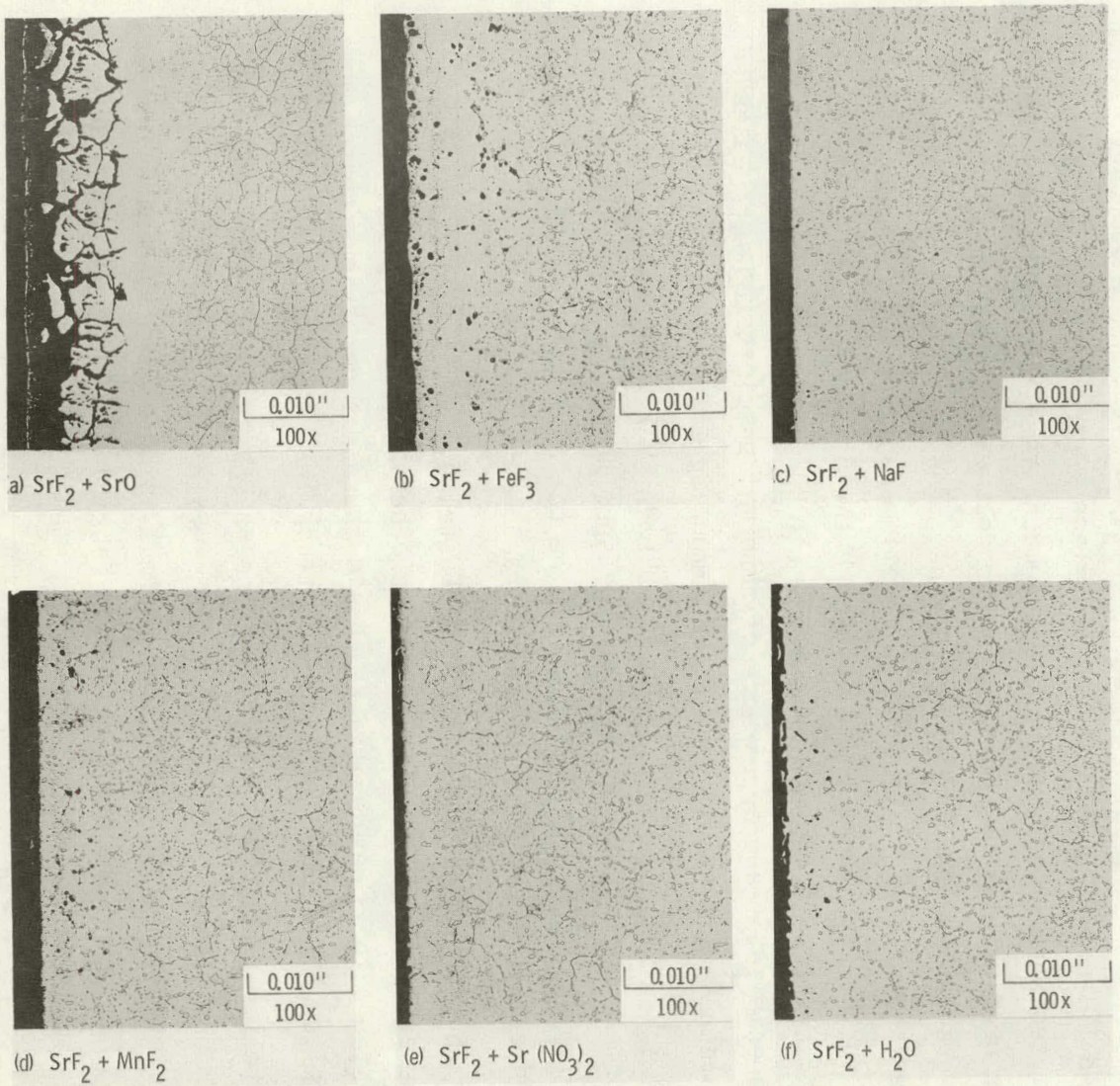

FIGURE 28. Hastelloy X Specimens Exposed to SrF_2-Impurity Mixtures at 1000°C for 4400 hr

The presence of SrO produced extensive grain boundary attack (Figure 28a). Microprobe data showed a diffusion of strontium into the grain boundaries and grain matrices, and a depletion of chromium and nickel in the matrix adjacent to the affected areas. Normal alloy precipitates had almost completely disappeared in the reaction zone. Surface dissolution was extensive in the specimens exposed to SrF_2-FeF_3, but less grain boundary attack was found (Figure 28b). There was a surface layer where the normal alloy precipitates were greatly reduced and a much wider zone where heavy discrete globular precipitates had formed. Microprobe data showed an iron concentration gradient across the affected zone. Analysis of the globular precipitates showed them to be high in chromium and iron with a composition similar to the FeCr sigma phase, although the presence of the sigma phase does not seem likely in specimens aged at 1000°C. The disappearance of normal precipitates and appearance of abnormal precipitates were observed in the other specimens exposed to SrF_2-impurity mixtures but the affected zone was much less than that found in couples containing FeF_3. Analysis of the abnormal precipitates in the various specimens showed them to be high in chromium and iron. No diffusion of the cation impurity into the alloy was found except when copper or iron were present.

The thermodynamic analysis of the Hastelloy X-WESF $^{90}SrF_2$ system indicated the alloy should be similar to the other Ni- and Co-base alloys in its resistance to fluoride attack. Again there was no obvious reason why the Hastelloy X was less resistant to attack than the Haynes Alloy 25.

Hastelloy X provides good resistance to seawater corrosion and good oxidation resistance up to 1000°C. It has fair high temperature strength characteristics, but the effects of thermal aging on its mechanical properties have not been completely defined. Fabricability and weldability of the alloy is good.

7.2.7 Hastelloy N-SrF_2

The Hastelloy N test specimens were fabricated from material that had been solution heat-treated at 2165°F and water quenched. The microstructure

of the "as received" material is shown in Figure 29a. The scattered grain boundary and matrix precipitates appear to be carbides of the M_6C and possibly M_2C types. Microprobe data show the precipitates are very high in molybdenum with a lesser amount of chromium. Thermal aging at 800°C resulted in continuous grain boundary precipitation and a moderate increase in bulk precipitation (Figure 29b). The data indicate the precipitates are principally M_6C carbide phase with molybdenum the predominant component. Specimens aged at 1000 and 1100°C no longer exhibited the continuous grain boundary precipitation, but bulk precipitation was similar to that at 800°C (Figure 29c-d).

Grain size stability was good at 800°C, but selective grain growth occurred at 1000°C and increased still further at 1100°C. Hardness of the "as received" material was higher than expected for the solution heat-treated alloy. The hardness decreased with increasing exposure temperature, and at 1000°C and above the hardness was typical of the solution annealed alloy.

Since Hastelloy N was developed at ORNL as a container material for molten fluoride salts in the MSRE program, it was expected to be resistant to attack by the strontium fluoride. However, this was not the case. Overall, the Hastelloy N was less resistant to attack by the various grades of strontium fluoride than any of the other containment materials tested. Exposure to the high-purity nonradioactive SrF_2 produced some unusual results in that the chemical attack of the Hastelloy N decreased sharply with increasing temperature (Figure 30). Specimens tested at 800°C exhibited heavy grain boundary attack and subsurface void formation, while the normal alloy precipitates were largely depleted in the affected zone. At 1000°C the grain boundary attack was reduced and there was little subsurface void formation. Dissolution of normal alloy precipitates was similar to that observed at 800°C. At 1100°C there was no evidence of grain boundary attack and only slight subsurface void formation. Dissolution of normal alloy precipitates occurred at the specimen surface, and was accompanied

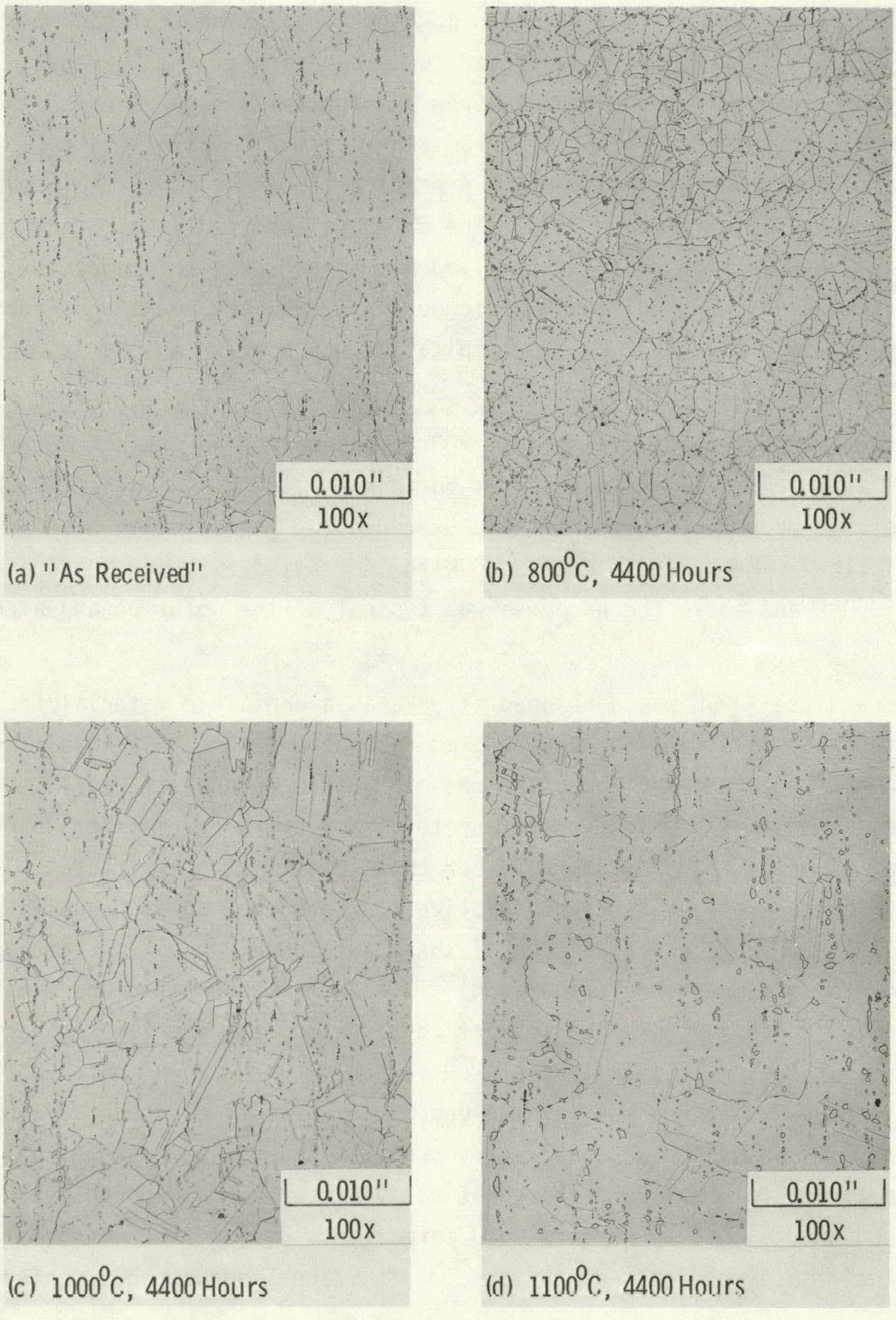

(a) "As Received"

(b) 800°C, 4400 Hours

(c) 1000°C, 4400 Hours

(d) 1100°C, 4400 Hours

FIGURE 29. Effects of Thermal Aging on the Microstructure of Hastelloy N

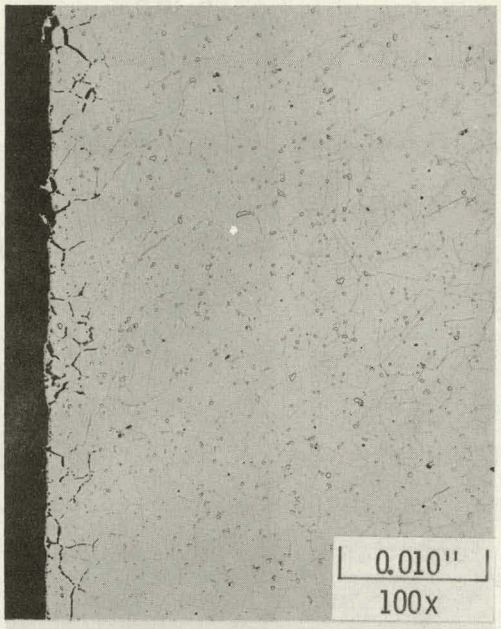

(a) 800°C, 4400 Hours

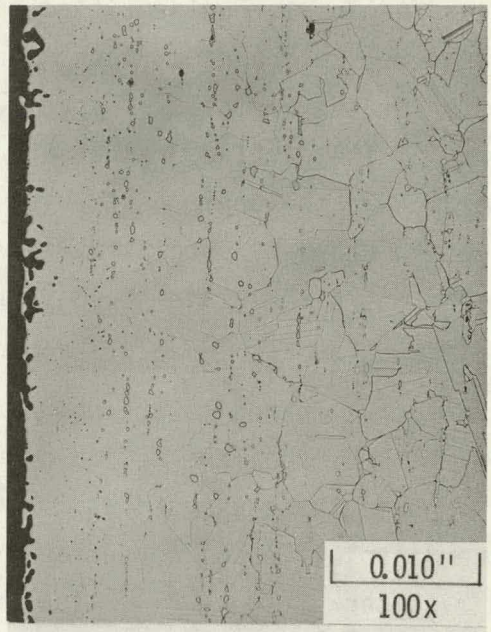

(b) 1000°C, 4400 Hours

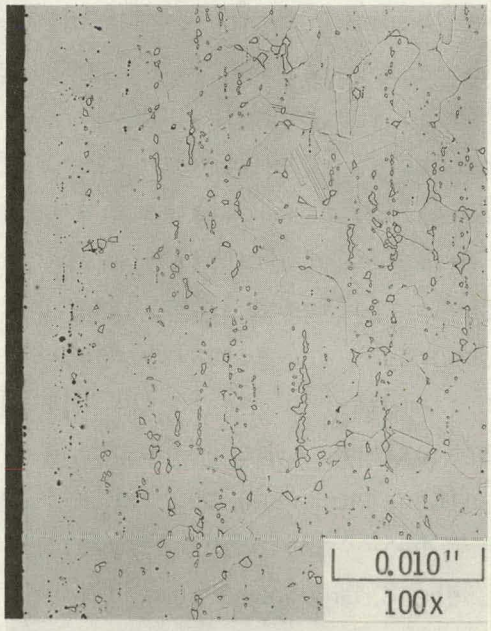

(c) 1100°C, 4400 Hours

FIGURE 30. Hastelloy N Specimens Exposed to High-Purity Nonradioactive SrF_2

by the appearance of unidentified precipitates, which were high in chromium and iron, in the grain matrices. Grain boundary attack and subsurface void formation of the Hastelloy N specimens could be attributed directly to the presence of the carbide grain boundary precipitates. Some diffusion of strontium into the grain boundaries was observed in those specimens in which grain boundary precipitates were present (800 and 1000°C), but not in specimens where the grain boundary precipitates were absent (1100°C).

Exposure to the radioactive strontium fluoride resulted in increased metal attack compared to the nonradioactive SrF_2, but the attack mechanisms were similar. Specimens tested at 800°C suffered heavy grain boundary attack, while those exposed at the higher temperatures exhibited general surface dissolution and subsurface void formation but much less grain boundary attack (Figure 31). Isolated voids occurred to considerable depth in the 1000 and 1100°C specimens, as did the dissolution of normal alloy precipitates. Maximum attack was observed in the specimens exposed at 1000°C.

The addition of impurities to high-purity nonradioactive SrF_2 did not appreciably increase the chemical attack of the Hastelloy N except when SrO or FeF_3 was present. In fact some impurities appeared to decrease the chemical attack [i.e., AlF_3, $(Ba,Ca,Mg)F_2$, H_2O]. A number of the impurities produced substantial changes in the microstructure of the alloy, typically the dissolution of normal alloy precipitates and the appearance of abnormal precipitates. Typical examples of Hastelloy N specimens exposed to SrF_2-impurity mixtures are shown in Figure 32. What appear to be voids in several of the photomicrographs are actually discrete globular precipitates. Strontium oxide was extremely corrosive to the Hastelloy N resulting in very heavy grain boundary attack. Microprobe data indicated extensive diffusion of strontium along the grain boundaries. The addition of FeF_3 to the SrF_2 also produced heavy grain boundary attack as well as subsurface void formation. Microprobe data showed some diffusion of iron into the grain boundaries and grain matrices but little or no diffusion of strontium

WESF GRADE $^{90}SrF_2$

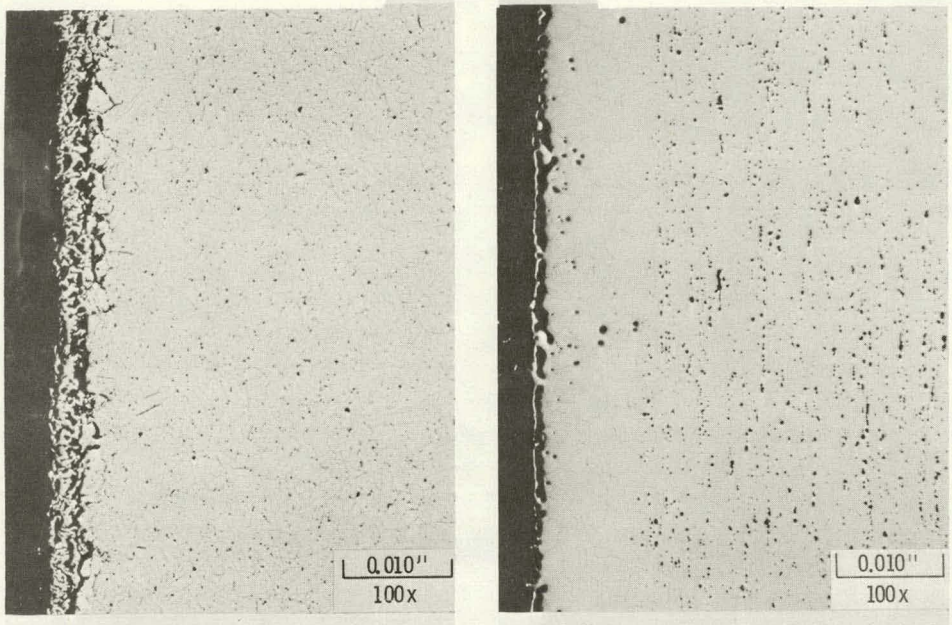

(a) 800°C, 4400 Hours

(b) 1000°C, 4400 Hours

HIGH PURITY $^{90}SrF_2$

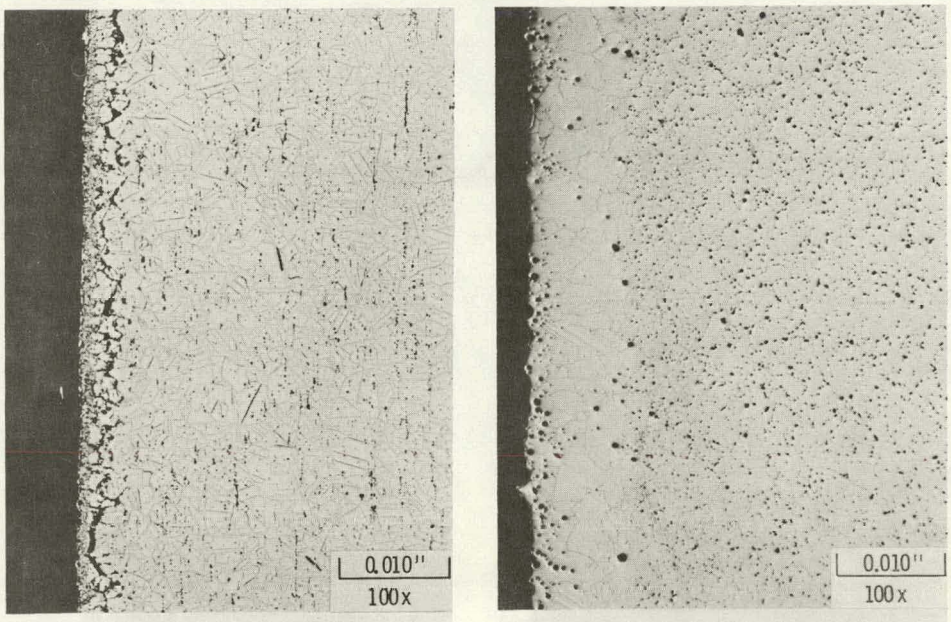

(c) 800°C, 4400 Hours

(d) 1000°C, 4400 Hours

FIGURE 31. Hastelloy N Specimens Exposed to $^{90}SrF_2$

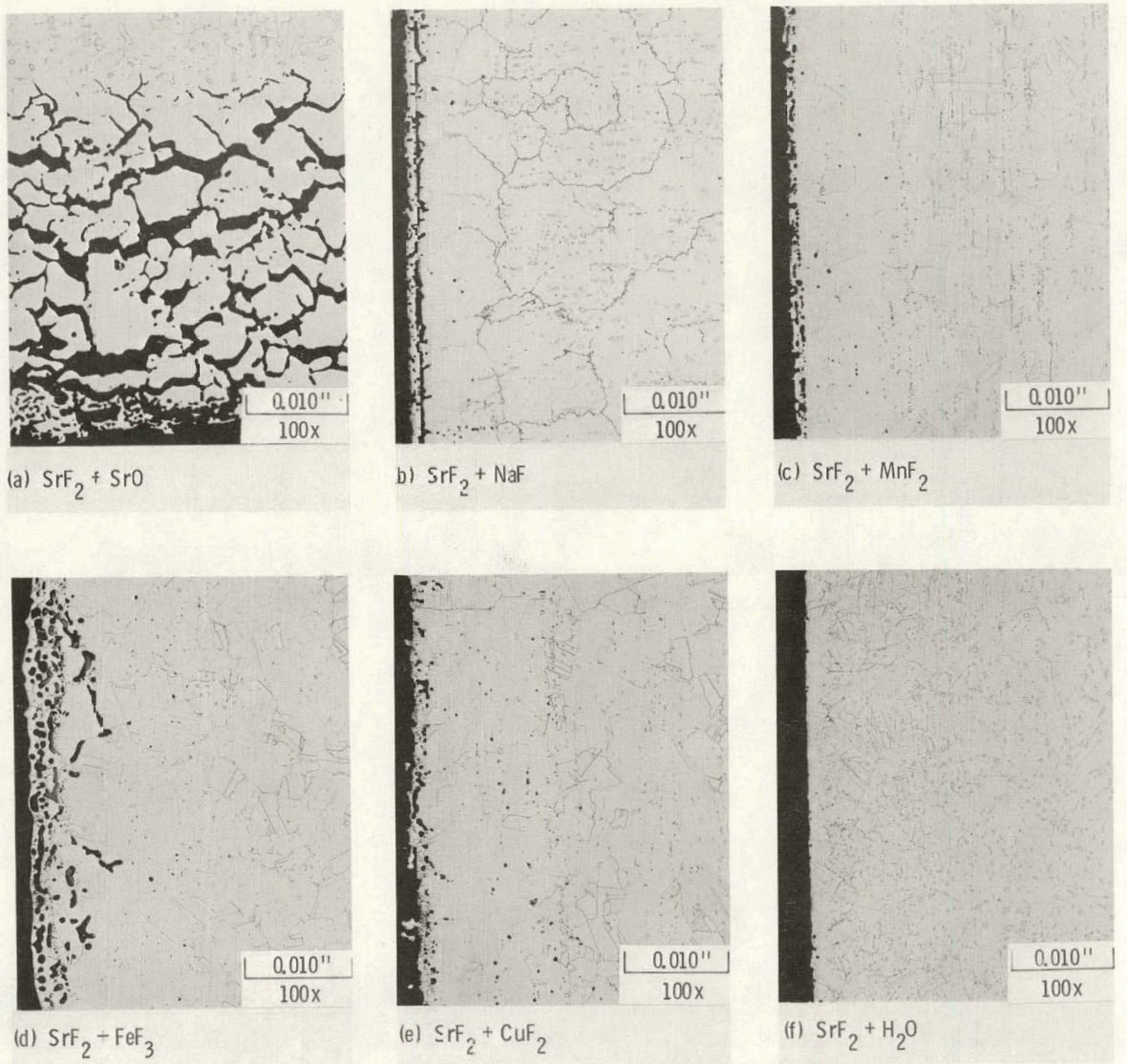

FIGURE 32. Hastelloy N Specimens Exposed to SrF_2-Impurity Mixtures at 1100°C for 4400 hr

into the alloy. There was no indication in the other specimens of diffusion of the cation impurity into the alloy, but slight diffusion of strontium was found. Analysis of the discrete globular precipitates found in the various specimens showed them to be high in chromium and iron, approximating the sigma phase in composition.

The Hastelloy N suffers a loss of impact strength and ductility upon thermal aging at 650 to 900°C, although to a lesser extent than the Haynes Alloy 25.[9] Its resistance to oxidation and seawater corrosion is less than that of some of the other Ni-base alloys, such as Hastelloy C-276 and Hastelloy X. These facts, combined with its poor combatibility with $^{90}SrF_2$, make the Hastelloy N a poor choice as the containment material for $^{90}SrF_2$.

7.2.8 Inconel 600-SrF_2

The Inconel 600 test specimens were fabricated from hot rolled, pickled and annealed bar stock. Microstructure of the "as received" material is presented in Figure 33a and shows a very fine grain structure with occasional discrete precipitates of titanium nitride, titanium carbide (or cyanonitride) and chromium carbide (probably Cr_7C_3). While the certified report of chemical analysis for the lot of Inconel 600 used in the tests and the manufacturer's brochures do not list titanium as a component of the alloy, the alloy does contain a slight amount of titanium which usually is present as discrete carbide or nitride inclusions. Thermal aging at 800°C produced some bulk precipitation, Cr_7C_3 and $Cr_{23}C_6$, but very little grain boundary precipitation (Figure 33b). At 1000°C grain boundary precipitation increased, but bulk precipitation was less than at 800°C (Figure 33c). At 1100°C both the grain boundary and bulk precipitates are much less apparent, except for the titanium nitride-cyanonitride inclusions which were stable at all temperatures (Figure 33d). At temperatures above 800°C, Cr_7C_3 is the predominant carbide phase.

Grain size stability of the Inconel 600 was the worst of all the Ni- and Co-base alloys tested. Aging at 800°C produced only a slight increase in grain size, but very large grain growth occurred at 1000 and 1100°C.

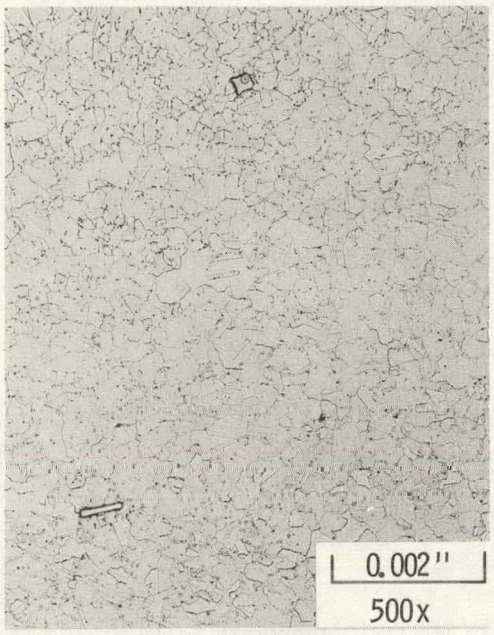

(a) "As Received"

(b) 800°C, 4400 Hours

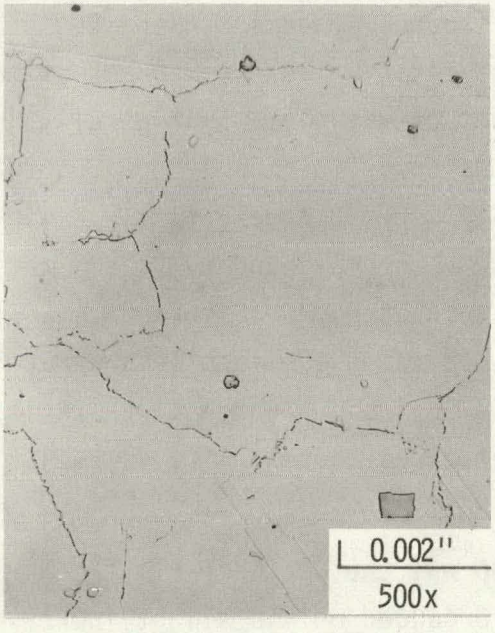

(c) 1000°C, 4400 Hours

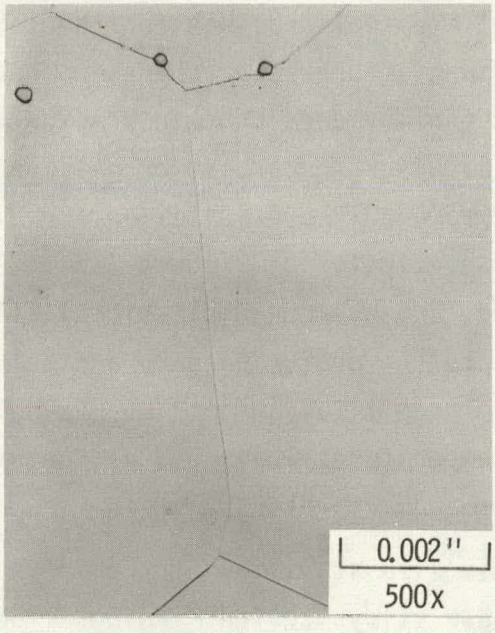

(d) 1100°C, 4400 Hours

FIGURE 33. Effect of Temperature on the Microstructure of Inconel 600

The hardness of the alloy decreased with increasing exposure temperature. The hardness of the reference specimens was lowest at the specimen surface and increased toward the center.

The Inconel 600 was quite resistant to chemical attack by the strontium fluoride, but changes in the microstructure were apparent to considerable depths in most test specimens. Exposure to the high-purity nonradioactive SrF_2 produced only slight chemical attack which did not increase significantly with temperature (Figure 34). At 800°C there was some surface dissolution with slight grain boundary attack. At 1000 and 1100°C the grain boundary attack increased slightly but surface dissolution was about the same. The specimens tested at 1000 and 1100°C all exhibited a very thin surface layer 1 to 2 mils wide where the average grain size was much smaller than in the body of the specimens. The specimens tested at the various temperatures all exhibited a surface layer where normal alloy bulk precipitates were largely dissolved but that contained finely dispersed irregular precipitates high in iron and chromium. The microprobe data showed no evidence of strontium diffusion into the alloy grain boundaries or matrix. Exposure to the SrF_2 appeared to cause a slight decrease in specimen hardness, especially at 800°C.

Exposure of Inconel 600 to the WESF-grade and high-purity $^{90}SrF_2$ resulted in substantially more attack than was observed with the nonradioactive SrF_2, but the amount of attack did not increase significantly with temperature. The attack mechanisms appeared to be similar to those found in the nonradioactive couples (Figure 35). Specimens exposed at 800°C suffered a general grain boundary attack. At 1000 and 1100°C grain boundary attack was greatly reduced, but there was some subsurface void formation and surface dissolution. Every specimen exposed to $^{90}SrF_2$ exhibited a surface reaction zone up to 20 mils deep where the normal alloy precipitates were depleted and other precipitates had formed. In addition, the specimens exposed at 1000 and 1100°C exhibited a thin surface layer where the average grain size was greatly reduced compared to the body of the specimen.

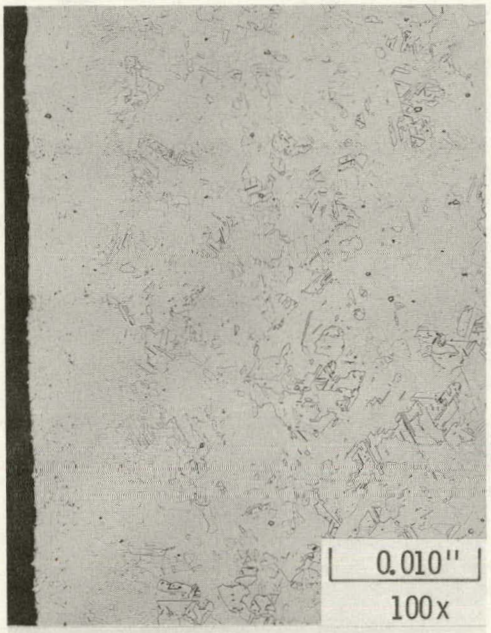

(a) 800°C, 4400 Hours

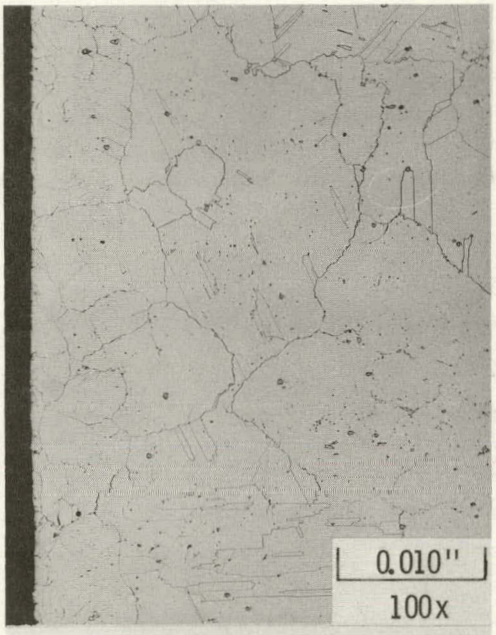

(b) 1000°C, 4400 Hours

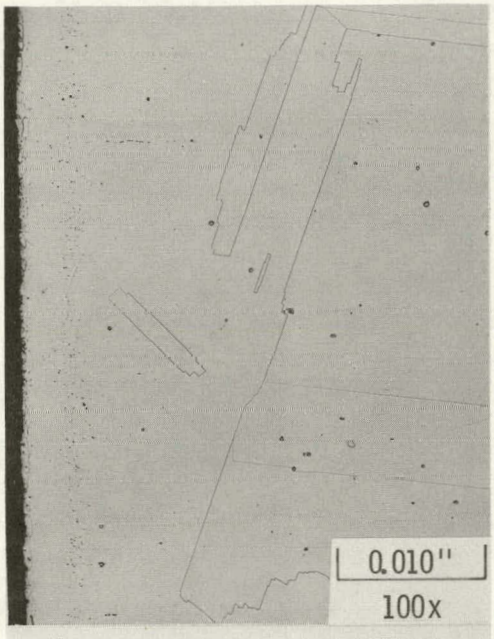

(c) 1100°C, 4400 Hours

FIGURE 34. Inconel 600 Specimens Exposed to High-Purity Nonradioactive SrF_2

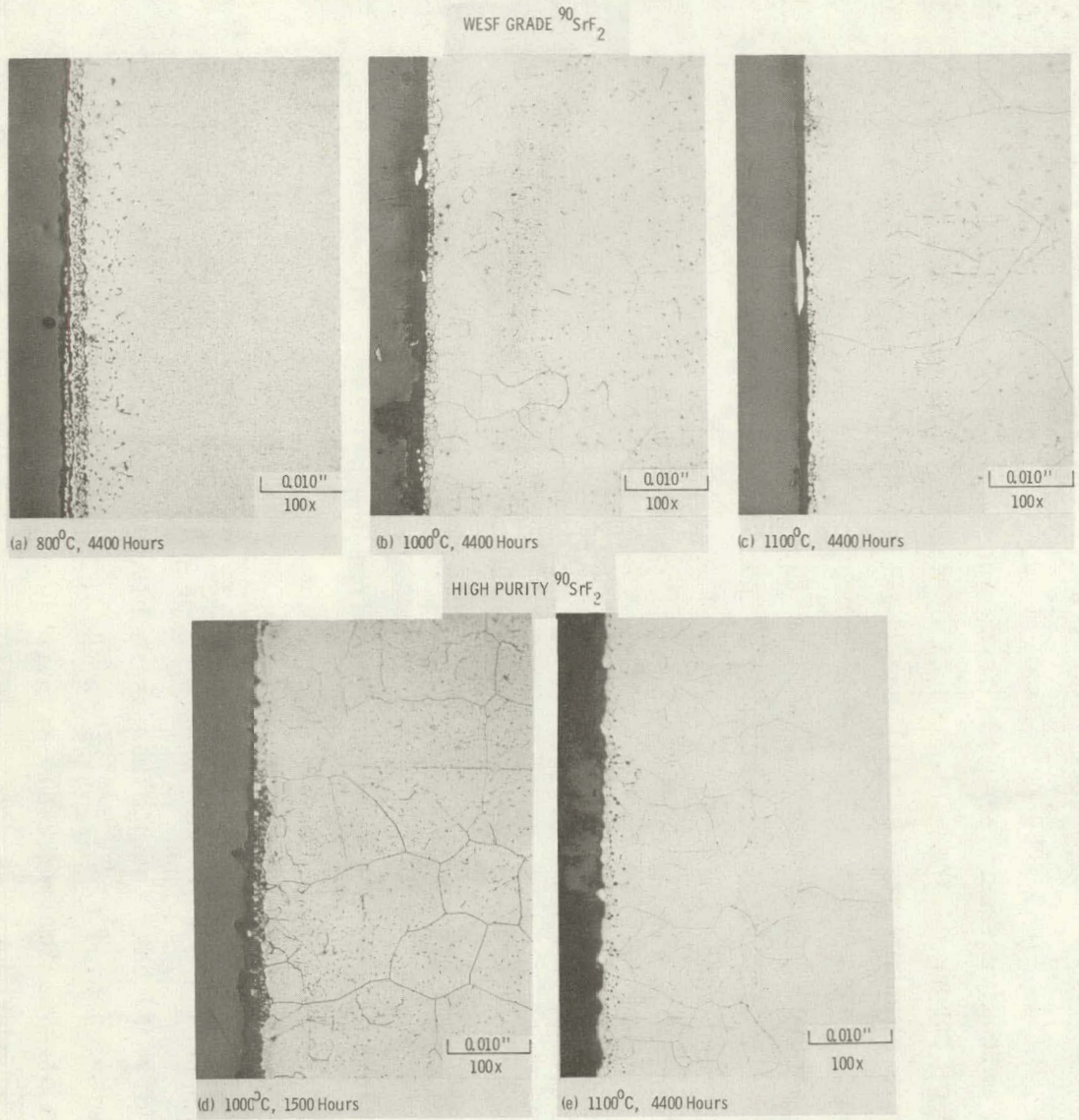

FIGURE 35. Inconel 600 Specimens Exposed to $^{90}SrF_2$

The addition of impurities to the high-purity nonradioactive SrF_2 did not increase the chemical attack of Inconel 600 except when the test mixture contained SrO, FeF_3 or CuF_2 (Figure 36). As was the case with the other Ni- and Co-base alloys, the addition of SrO to the SrF_2 greatly increased the attack of the Inconel 600 resulting in extensive grain boundary penetration. Microprobe data showed extensive diffusion of strontium into the grain boundaries. Test specimens exposed to SrF_2 containing FeF_3 or CuF_2 exhibited extensive subsurface void formation. Analytical data showed diffusion of copper or iron into the alloy matrix. The voids are probably due to grain boundary attack, although the photomicrographs give little indication of such attack. Changes in microstructure were apparent in most specimens exposed to the impurity-SrF_2 mixtures but changes varied depending on the impurity involved. Dissolution of normal precipitates, changes in grain size, and appearance of unidentified precipitates were all found in varying degrees in the various specimens. In all cases the unidentified precipitates were high in iron and chromium.

Inconel 600 is very resistant to oxidation up to 1000°C and is easily fabricated and welded. Because it can suffer pitting when exposed to stagnant seawater, Inconel 600 is rarely used in seawater applications. Although the strength of Inconel 600 is not as great as some of the other Ni- and Co-base alloys it appears to suffer less from thermal aging effects than many of the alloys.

7.2.9 Inconel 625-SrF_2

The Inconel 625 test specimens were prepared from hot rolled and annealed (1950°F) bar stock. The "as received" material was a fine grained material with carbide precipitates in the grain boundaries and discrete inclusions of titanium, probably as nitride or cyanonitride (Figure 37a). The grain boundary precipitates are rich in molybdenum and columbium and are probably MC and M_6C carbides and possibly Ni_3Cb. Thermal aging at 800°C increased the grain boundary and bulk precipitates which appear to be molybdenum, niobium and chromium carbides (Figure 37b). Aging at 1000 and 1100°C

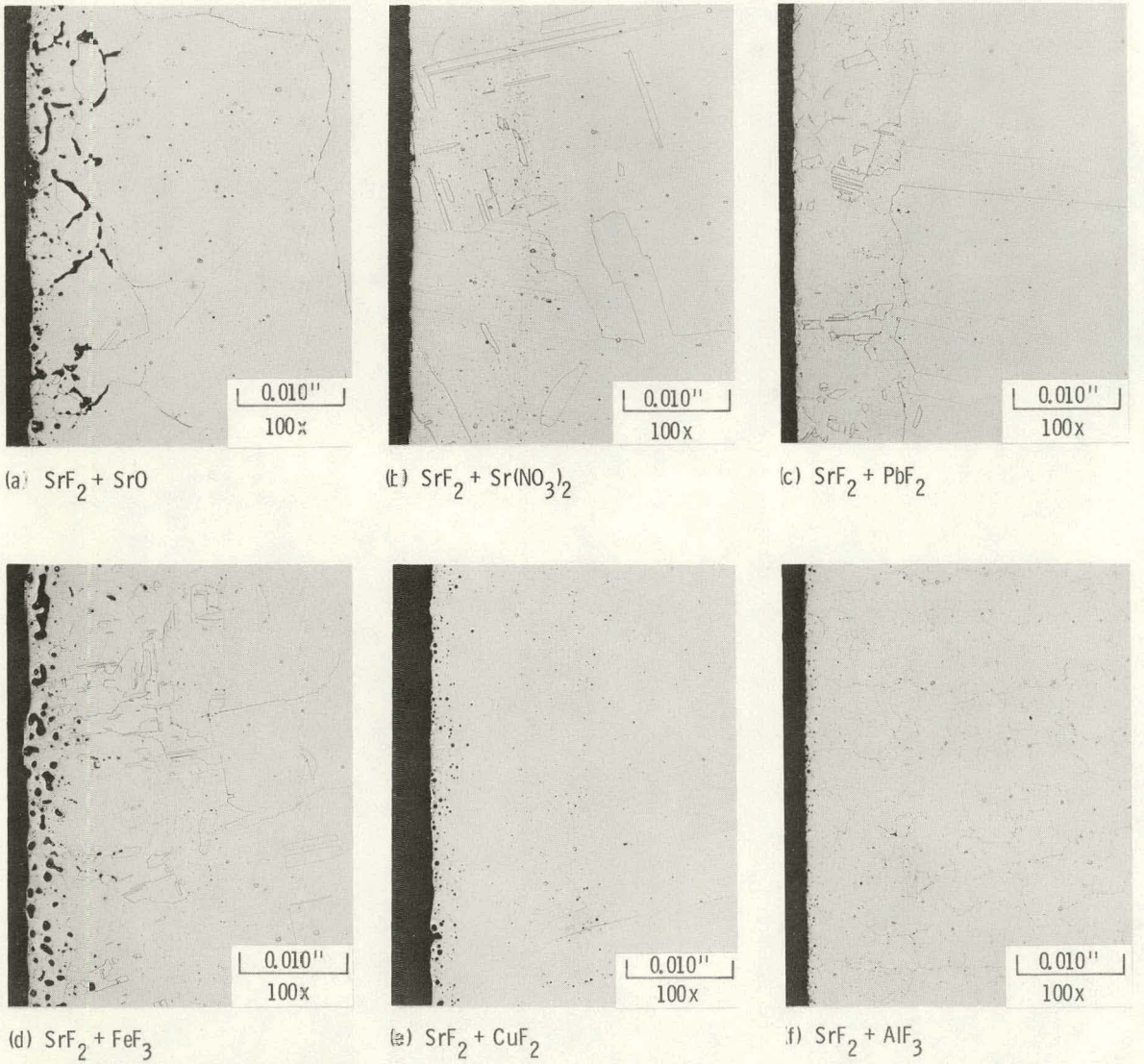

(a) $SrF_2 + SrO$ (b) $SrF_2 + Sr(NO_3)_2$ (c) $SrF_2 + PbF_2$

(d) $SrF_2 + FeF_3$ (e) $SrF_2 + CuF_2$ (f) $SrF_2 + AlF_3$

FIGURE 36. Inconel 600 Specimens Exposed to SrF_2-Impurity Mixtures at 1000°C for 4400 hr

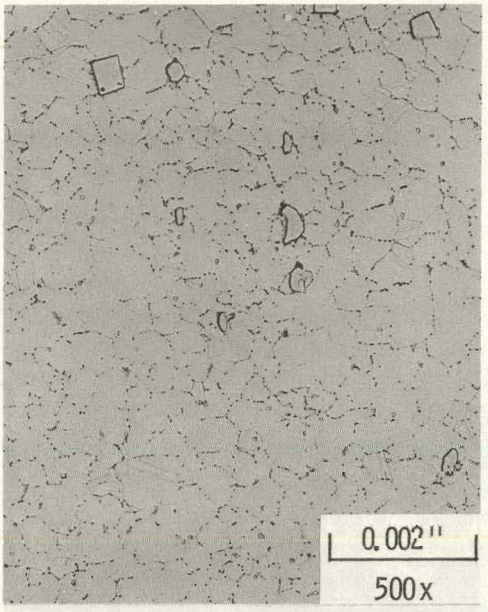

(a) "As Received"

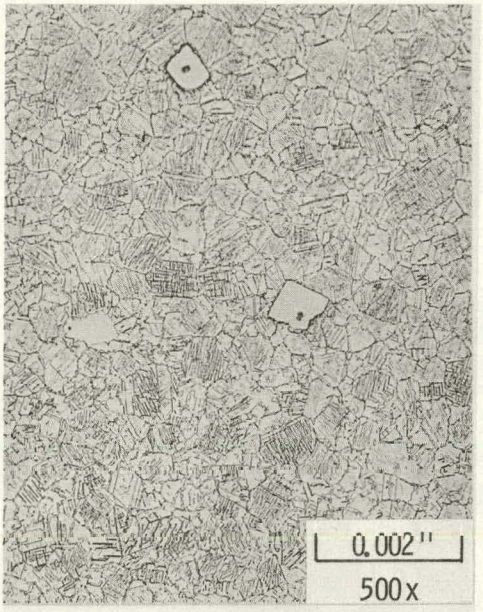

(b) 800°C, 4400 Hours

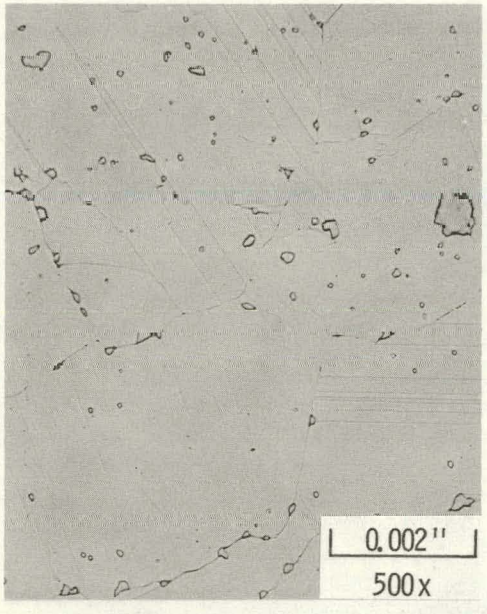

(c) 1000°C, 4400 Hours

(d) 1100°C, 4400 Hours

FIGURE 37. The Effect of Thermal Aging on the Microstructure on Inconel 625

resulted in the dissolution of most of the precipitates except for the titanium inclusions (Figure 37c-d). Very little grain growth was observed in the specimens aged at 800°C, but extensive grain growth occurred at the higher temperatures. Hardness of the "as received" material was higher than normal for the annealed alloy and decreased from the surface toward the center of the specimen. Aging at 800°C increased the overall hardness. Aging at 1000 and 1100°C decreased the hardness to the range expected of the annealed alloy.

The Inconel 625 was less resistant to fluoride attack than the Inconel 600. Exposure to high-purity nonradioactive SrF_2 resulted in moderate chemical attack on the Inconel 625, but had only limited effect on the alloy microstructure (Figure 38). Specimens tested at 800°C suffered limited grain boundary attack and some dissolution of normal alloy precipitates. Specimens exposed at 1000°C suffered extensive grain boundary attack and subsurface void formation to a depth of 3 mils, while dissolution of normal alloy precipitates occurred to a depth of 4 mils. At 1100°C grain boundary attack was less extensive, but subsurface void formation increased. Microporosity not visible in the low magnification photomicrographs occurred to a depth of 3 mils. No changes in microstructure were apparent in the 1100°C specimens. There was no evidence of strontium diffusion into the grain boundaries and grain matrices of the alloy. Microprobe data did show, however, a high chromium concentration in the alloy matrix near the voids in the 1000 and 1100°C specimens. Exposure to the fluoride did not have a significant effect on the hardness of the alloy.

Exposure to the WESF-grade and high-purity $^{90}SrF_2$ resulted in increased attack of the Inconel 625 as compared to the nonradioactive SrF_2, especially with regard to effects on the microstructure. Overall, the WESF-grade $^{90}SrF_2$ appeared to be more corrosive than the high-purity $^{90}SrF_2$ (Figure 39). Specimens exposed to the $^{90}SrF_2$ at 800°C suffered extensive grain boundary attack and subsurface void formation. At 1000 and 1100°C grain boundary attack was apparently much less but subsurface void formation was substantially greater. However, the void formation was probably due to grain

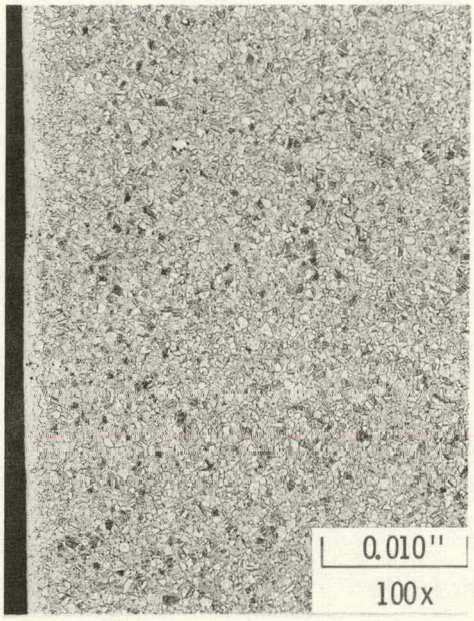

(a) 800°C, 4400 Hours

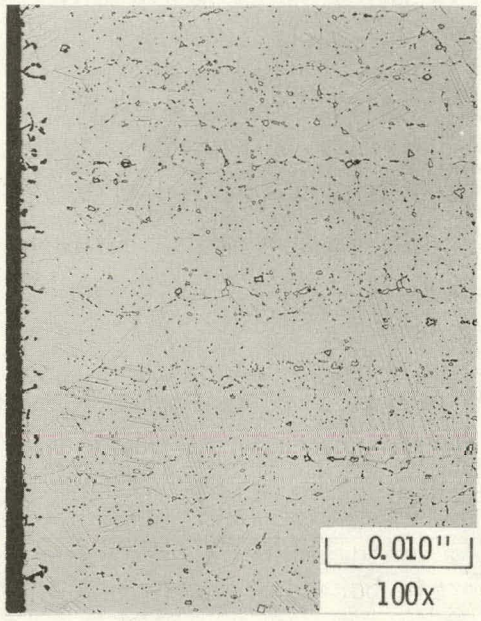

(b) 1000°C, 4400 Hours

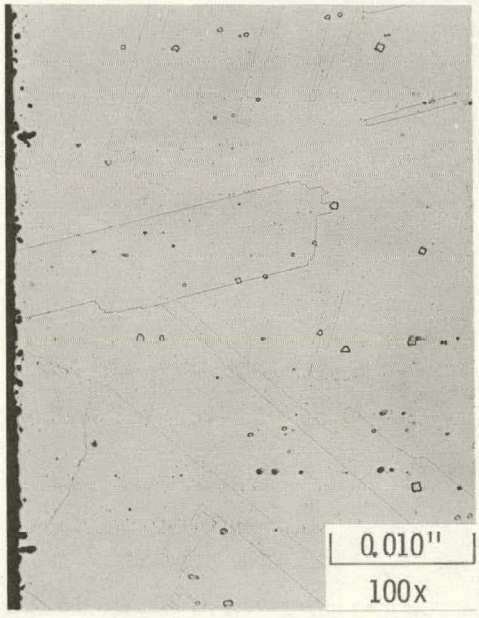

(c) 1100°C, 4400 Hours

FIGURE 38. Inconel 625 Specimens Exposed to High-Purity Nonradioactive SrF_2

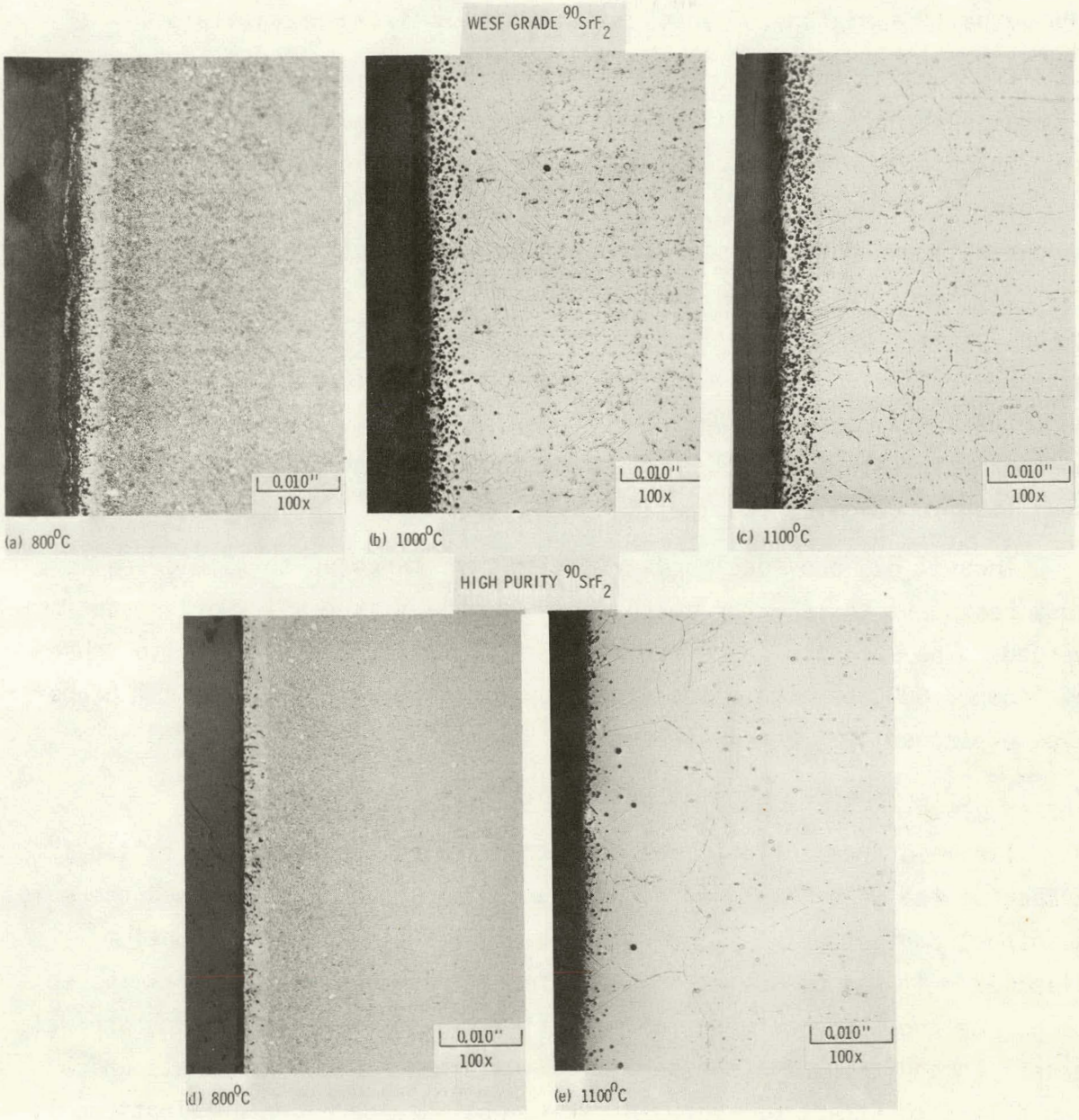

FIGURE 39. Inconel 625 Specimens Exposed to $^{90}SrF_2$ for 4400 hr

boundary attack which was not visually identifiable from the photomicrographs. Changes in microstructure were extensive in the 1000 and 1100°C test specimens. Dissolution of normal alloy precipitates occurred up to a depth of 20 mils, while unidentified discrete globular precipitates occurred up to a depth of 5 mils. In Figure 39b, c, and e what appear to be voids are actually a mixture of voids and the unidentified precipitates.

Exposure of the Inconel 625 to the SrF_2-impurity mixtures resulted in increased changes in the alloy microstructure (compared to SrF_2 alone), but had little effect on the chemical attack (except where SrO was present). In some cases the addition of impurities such as NaF and AlF_3 to the SrF_2 appeared to decrease chemical attack. As was the case with the other Ni- and Co-base alloys the addition of SrO to the SrF_2 resulted in extensive grain boundary attack. All of the specimens exposed to the SrF_2-impurity mixtures exhibited a surface layer where normal alloy precipitates were depleted and a much narrower zone where unidentified precipitates were present. In each case microprobe data show that the abnormal precipitates were high in chromium and iron.

Inconel 625 provides good oxidation resistance up to 1000°C and is very resistant to seawater corrosion. The alloy is easily worked and welded. The strength characteristics of the alloy are superior to those of Inconel 600, but the effects of thermal aging on the mechanical properties of Inconel 625 have not been well defined.

7.2.10 Effects of Welding on Compatibility

The weld areas of a number of test capsules were examined to see if attack of the weld metal had occurred. In the couple design used there is no direct contact between the weld metal and the compacted strontium fluoride. It was possible, however, for strontium fluoride particles to penetrate the space between the capsule wall and lid and approach the weld zone. In addition, the possibility of gas-metal reactions exists which could lead to attack of the weld metal, while temperature gradients could lead to diffusion of reactants to the weld area.

In general, metal attack in the weld areas was found to be much less than that observed with the test specimens. Figure 40 shows the weld areas of a number of capsules that contained high-purity nonradioactive SrF_2. There is very limited attack of the weld metal by the high-purity SrF_2. The only case where extensive attack of the weld metal was apparent was in the couples containing CuF_2 or FeF_3 as impurities in the SrF_2 (Figure 41). In each case the attack mechanism was similar to that observed with the equivalent test specimens. The notches observed in the Haynes Alloy 25 specimen shown in Figure 41 are the result of machining rather than attack.

The Ni- and Co-base alloy capsules containing the SrF_2-SrO mixture showed little evidence of weld metal attack. This is surprising considering the extensive attack of the test specimens exposed to the SrF_2-SrO mixture. The results indicate there was little movement or diffusion of the SrO in the test couples, whereas considerable movement of the CuF_2 or FeF_3 must have occurred.

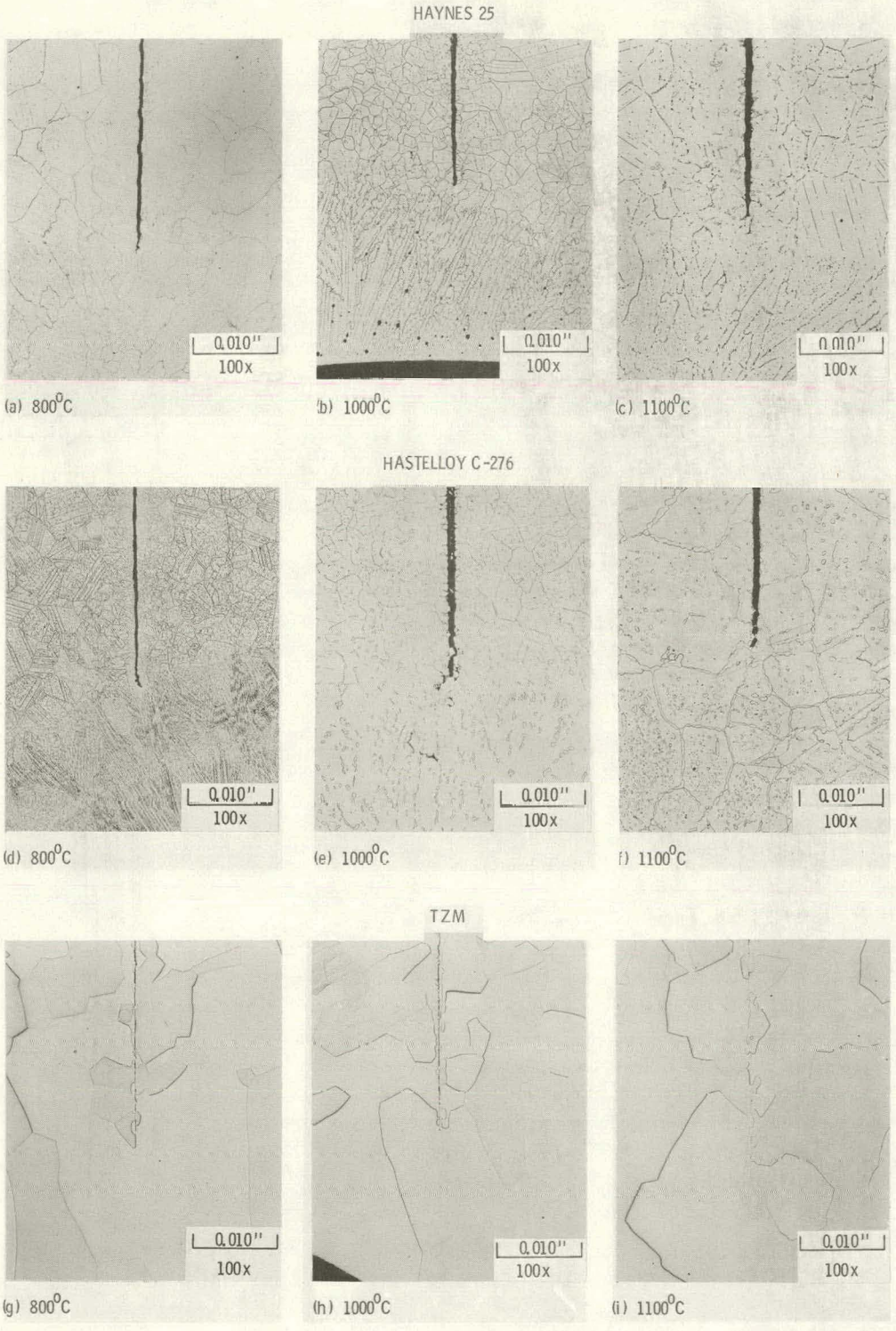

FIGURE 40. Welded Specimens after Exposure to High-Purity Nonradioactive SrF_2 for 4400 hr

(a) Hastelloy C-276
$SrF_2 + CuF_2$

(b) Hastelloy C-276
$SrF_2 + FeF_3$

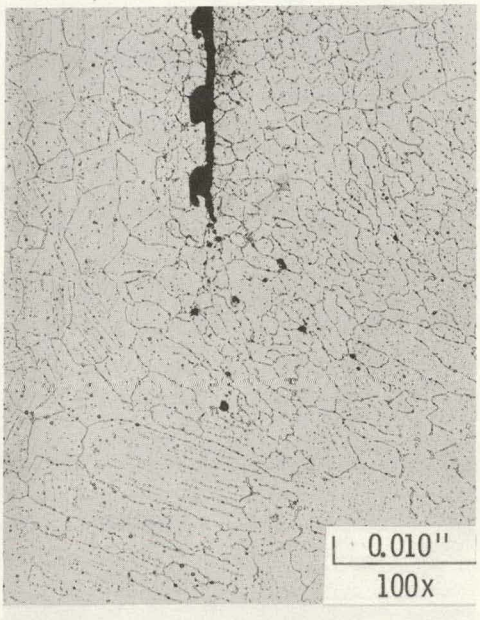

(c) Haynes 25
$SrF_2 + FeF_3$

(d) TZM
$SrF_2 + FeF_3$

FIGURE 41. Welded Specimens Exposed to SrF_2-Impurity Mixtures at 1000°C for 4400 hr

8.0 CONCLUSIONS

Sufficient data were obtained from the short-term compatibility tests to accomplish the objectives set forth in Section 5.0. Based on the overall results, three containment materials were identified as the prime candidates for long-term compatibility testing. They are Haynes Alloy 25, TZM and Hastelloy C-276, with Inconel 600 and Hastelloy X as possible alternates. Selection of three candiates was based on the following considerations:

- Of all the containment materials evaluated, tungsten was the most compatible with the various grades of strontium fluoride at 800 to 1100°C. Chemical attack of the tungsten was very slight. The only tungsten specimens exhibiting significant chemical attack were those exposed to SrF_2 containing CuF_2 as an impurity. Exposure to the fluoride had almost no effect on the microstructure of the tungsten. No difference in compatibility with the fluoride could be detected between the wrought and arc cast tungsten specimens.

  Other properties of tungsten, such as its poor oxidation resistance and difficulties in fabrication and welding, reduce its usefulness as a container material for $^{90}SrF_2$. Because of its many limitations tungsten is not considered to be a practical material to use in the WESF process to contain the $^{90}SrF_2$, and it was not selected as one of the materials to be evaluated in the long-term compatibility tests. However, tungsten can be considered as a potential container material for $^{90}SrF_2$ in special applications.

- TZM is almost as resistant to attack by strontium fluoride as tungsten. Chemical attack of the TZM specimens was minimal except when exposed to strontium fluoride containing CuF_2 or FeF_3. No significant effect on the microstructure was observed except in the specimens exposed to SrF_2 containing CuF_2 or FeF_3.

  TZM suffers some of the same disadvantages as tungsten, such as poor oxidation resistance. However, TZM is more easily fabricated and welded than tungsten and can probably be adapted for use in the WESF

process to contain the $^{90}SrF_2$. This would involve using TZM for the inner capsule and a different material that is oxidation resistant for the outer capsule. Because the TZM is compatible with $^{90}SrF_2$ and because it can probably be used in the WESF process, it was selected as one of the materials to be evaluated in the long-term tests.

- Of the seven Ni- and Co-base alloys tested, Haynes Alloy 25 was the most resistant to fluoride attack. On an overall basis, both chemical attack and changes in microstructure were much less with the Haynes Alloy 25 specimens than with the other Ni- and Co-base alloys. However, the Haynes Alloy 25 specimens suffered considerably more attack than the tungsten and TZM specimens.

  Haynes Alloy 25 suffers a serious loss of toughness and ductility when thermally aged at 650 to 900°C, which reduces its usefulness as a container material for $^{90}SrF_2$ in heat source applications. However, the alloy can be considered for use when the $^{90}SrF_2$ is doubly encapsulated. The Haynes Alloy 25 can be used for the inner capsule to provide $^{90}SrF_2$ compatibility, and a different material used for the outer capsule to provide the needed strength requirements. In addition, the alloy can be used in the WESF production operation with a minimum of development effort. Based on the above consideration Haynes Alloy 25 was selected as one of the materials to be evaluated in the long-term compatibility tests.

- The other six Ni- and Co-base alloys were much less resistant to fluoride attack than the Haynes Alloy 25. Ranking the six in order of their resistance to fluoride attack is difficult because the ranking would vary depending on the grade of strontium fluoride being considered. Overall, the Inconel 600, Hastelloy C-276 and Hastelloy X appear to be about equal in their resistance to fluoride attack; while the other three alloys, Haynes Alloy 188, Inconel 625 and Hastelloy N, are substantially less resistant to attack.

Because Hastelloy C-276 possesses many attractive properties, such as good oxidation resistance and excellent seawater corrosion resistance, and since it is currently being used at WESF to contain the $^{90}SrF_2$, it was selected as the third containment material to be evaluated in the long-term compatibility tests. Inconel 600 and Hastelloy X also possess certain desirable properties and should be considered as possible alternates to Hastelloy C-276.

Overall, the experimental results show that the impurities that are normally present in the WESF $^{90}SrF_2$ in high concentration, i.e., Na, Ca, Ba, have relatively little effect on the compatibility of the strontium fluoride with the containment materials at 800 to 1100°C. The results also show that certain impurities can have a serious adverse effect on strontium fluoride compatibility. SrO, for example, when present in the SrF_2 produces extensive chemical attack of the Ni- and Co-base alloys. Fluorides of the multivalent cations, such as Cu and Fe, generally cause increased chemical attack of the containment materials tested. They also produce substantial microstructural changes in the Ni- and Co-base alloys. Water and nitrate ion had a suprisingly small effect on compatibility, possibly because they were present in low concentrations. Fortunately, the impurities which were shown to have an adverse effect on compatibility are normally present in the WESF $^{90}SrF_2$ in low concentrations. It does not appear likely that additional purification steps will be needed in the WESF process to improve the quality of the $^{90}SrF_2$ product. However, close control of the purification steps and other process operations will be needed to insure that the harmful impurities are reduced to the lowest practical levels.

In addition to the foregoing there are a number of other conclusions that can be reached from the test data:

- In general metal attack was greater in the couples containing $^{90}SrF_2$ than in the equivalent couples containing high-purity nonradioactive SrF_2. Changes in the microstructure increased to a greater degree than did the chemical attack. The increased attack probably resulted from impurities and decay products in the $^{90}SrF_2$, and not from the radiation.

- Overall, chemical attack of the test specimens did not increase appreciably with increasing exposure temperatures to 1100°C, and there were instances where the attack was less at the higher temperatures. Microstructural changes were generally greater at the higher temperatures.
- The slope of the rate curves could not be predicted from the limited data available, but in almost every case the rate of metal attack appeared to decrease with increasing exposure time.
- As a general rule, the presence of impurities in the SrF_2 produced significant changes in the microstructure of the Ni- and Co-base alloy specimens, and the microstructural changes affected the specimens to greater depths than did the chemical attack.
- While it was impossible to identify the reactions producing the chemical attack of the Ni- and Co-base alloys, in most cases they involved the precipitates in the alloy grain boundaries. This could be one possible explanation why the chemical attack of the alloys did not increase substantially above 800°C, since less precipitates formed at the higher test temperatures.

In order to provide reliable estimates of long-term metal attack in $^{90}SrF_2$ heat sources, additional data will be needed. The kinetics of the reactions involved in metal attack will have to be determined and the reaction mechanisms identified. The effects of fluoride attack on the mechanical properties of the container materials will also have to be determined. The long-term compatiblity tests, which are the second phase of this program are designed to supply the needed information. The tests will be carried out using fuel-grade $^{90}SrF_2$ produced at WESF. TZM, Haynes Alloy 25 and Hastelloy C-276 will be evaluated in the tests which will last up to 30,000 hr. Test temperatures will be 600, 800 and 1000°C. Tensile and Charpy specimens will be tested to determine the effects of fluoride attack on the mechanical properties of the alloys. The effect of varying the test couples surface to volume ratio (S/V) will also be investigated. In addition, a more detailed thermodynamic analysis of the three WESF $^{90}SrF_2$-alloy systems is being carried out by Dr. Carl Alexander and his associates at Battelle-Columbus.

9.0 REFERENCES

1. F. J. Maraglia, Compatibility of Strontium Space Fuel Forms, MND-3062-27, Martin Marietta Corp., Baltimore, MD, June 1966, (Declassified).
2. H. T. Fullam, Compatibility of Cesium Chloride and Strontium Fluoride with Containment Materials, BNWL-1673, Battelle-Northwest, Richland, WA, October 1972.
3. T. Rosenqvist, Thermochemical Data for Metallurgists, Tapir Forlag, 1970.
4. A. Glassner, The Thermochemical Properties of the Oxides, Fluorides, and Chlorides to 2500°C, ANL-5750, Argonne National Laboratory, Argonne, IL, 1957.
5. C. J. Smithells, Metals Reference Book, Vol. 1, Butterworth's, London, 1967.
6. O. Kubaschewski and E. L. Evans, Metallurgical Thermochemistry, Pergamon, London, 1958.
7. F. K. McTaggart and A. G. Turnbull, Aust. J. Chem., vol. 17, pp. 727-30, 1964.
8. D. T. Bourgette, Effect of Aging Time and Temperature On the Impact and Tensile Behavior of L-605-A Cobalt Base Alloy, ORNL-TM-3734, Oak Ridge National Laboratory, Oak Ridge, TN, April 1973.
9. H. E. McCoy and D. T. Bourgette, Influence of Aging on the Impact Properties of Hastelloy N, Haynes Alloy No. 25 and Haynes Alloy No. 188, ORNL-TM-4380, Oak Ridge National Laboratory, Oak Ridge, TN.

10.0 ACKNOWLEDGMENTS

Several organizations and many individuals contributed to the work covered in this report. Much of the experimental work was performed by R. J. Elovich, while preparation of the $^{90}SrF_2$ and radioactive test couples was carried out by members of the Applied Chemistry Section under the direction of J. L. Green. Metallographic examination and microprobe analysis of the nonradioactive couples was provided by R. H. Beauchamp and J. L. Daniels of BNW and W. I. Clark of HEDL. Analysis of the radioactive couples was provided by J. W. Goffard of HEDL, R. S. Crouse and the Radiation and Electron Metallography group at ORNL, and V. W. Storhok of Battelle-Columbus. K. R. Wheeler of BNW and J. D. Watrous of the Donald W. Douglas Laboratories provided valuable help in evaluating the experimental data.

H. H. Van Tuyl of BNW was program manager through FY-74 at which time program responsibility was transferred to J. H. Jarrett. Initially, overall program guidance was provided by L. A. Miller of the AEC's Division of Applied Technology, and subsequently by A. P. Litman of ERDA's Division of Space Nuclear Systems.

11.0 APPENDIX

11.1 THERMODYNAMIC ANALYSIS OF WESF $^{90}SrF_2$-CONTAINER SYSTEMS

As discussed in Section 4.0, an attempt was made to predict, on the basis of thermodynamic considerations, the possible reactions that might occur between WESF-produced $^{90}SrF_2$ and the nine containment materials evaluated in the short-term compatibility tests. The potential for a given reaction to occur was estimated by calculating the Gibbs free energy of reaction (ΔG_R°) over the temperature range of 25 to 1200°C.

Each of the nine fluoride-metal systems to be considered is extremely complex because of the many components present. The WESF $^{90}SrF_2$ contains a great many impurities as well as decay products. Each of the seven Ni- and Co-base alloys contains at least eight components. Even the simplest of the nine systems, tungsten-WESF $^{90}SrF_2$, contains at least 24 constituents which must be considered in a thermodynamic analysis.

Because of the large number of constituents in each of the nine systems under consideration, a rigorous analysis of a given system could involve literally hundreds or thousands of potential reactions. Carrying out a rigorous analysis is prevented by two factors:

1. The chemical species present in the WESF $^{90}SrF_2$ have not been identified, and the compounds formed in the Ni- and Co-base alloys as a function of time and temperature are not completely known.
2. Thermochemical data are not available for most of the complex compounds, intermetallics and solid solutions which are potentially possible in the various systems.

In order to analyze each system, it was necessary to make a number of simplifying assumptions to reduce the reactions to be considered to those involving compounds for which thermochemical data are available:

- The impurities in the WESF $^{90}SrF_2$ are present as simple compounds of unit activity; they are not present as complex compounds or solid solutions with the SrF_2, decay products or each other.

- The decay products are ZrF_4, ZrF_2 and zirconium metal.
- The alloys are solid solutions, and there is no compound formation between alloy components at temperatures up to 1200°C.
- The solid reaction products are simple fluorides and oxides of unit activity or free metal. Complex fluorides, complex oxides, oxyfluorides or intermetallic compounds are not considered to be possible reaction products.
- There is no liquid phase present up to 1200°C.
- Each fluoride-metal system is assumed to be a closed system, as would be the case with an operating $^{90}SrF_2$ heat source.

The above assumptions preclude the presence of complex compounds and intermetallic compounds in the reaction system. They also preclude the existence of solid solutions of fluorides or oxides in the systems. A superficial examination of the various systems will show that some of the assumptions are only partially valid. For example, some components of the Ni- and Co-base alloys do interact to form compounds of various types, such as carbides and intermetallics, when the alloys are thermally aged. The assumptions were necessary, however, to allow the thermodynamic analysis of the nine systems to be completed with the level of effort that was possible within program funding limitations.

The impurities present in the WESF $^{90}SrF_2$, their probable forms, and concentration ranges are given in Table 1A. The cationic impurities are present primarily as fluorides. Since the WESF $^{90}SrF_2$ also contains a small amount of oxygen, some metal oxides may also be present. However, analysis of the fluoride shows that the bulk of the oxygen is present as water. Therefore, the concentration of metal oxides should be very low. For the thermodynamic analyses, however, it was assumed that metal oxides could be present in the fluoride.

Free energy of formation data on the fluorides and oxides of interest in the nine alloy-fluoride systems are given in Tables 2A and 3A. The data are given in kilocalories per gram atom (kcal/g-atom) of anion and were

TABLE 1A. Probable Impurities in WESF $^{90}SrF_2$

Impurity	Probable Form	Concentration Range (wt%)
Al	AlF_3	<0.5
Ba	BaF_2	0.1-2.0
Ca	CaF_2	0.1-2.0
Cd	CdF_2	<0.1
Cr	CrF_3	<0.2
Cu	CuF_2	<0.01
Fe	FeF_3	<0.1
H	H_2O	<0.01
K	KF	<0.1
Mg	MgF_2	0.05-0.5
Mn	MnF_2	<0.1
Na	NaF	1-4
Ni	NiF_2	<0.1
O	H_2O	<0.05
Pb	PbF_2	<0.2
R[(a)]	RF_3	<2.0
Si	SiO_2 or $SiF_6^=$	<0.02
Zr	ZrF_4,Zr	Variable (decay product)

(a) Rare earths

TABLE 2A. Free Energy of Formation of Various Fluorides

Compound	$-\Delta G_f^\circ$, kcal/g-atom of fluorine					
	25°C	600°C	800°C	1000°C	1100°C	1200°C
AlF_3	113	101	97	93	91	89
BF_3	90	87	86	85	85	84
BaF_2	137	125	122	119	117	116
CF_4	40	36	35	34	33	32
CaF_2	140	129	125	121	119	117
CbF_5	64	59	58	57	56	55
CdF_2	77	66	63	56	53	50
CoF_2	74	65	61	58	57	55
CrF_2	86	77	74	70	69	68
CrF_3	83	73	70	67	66	64
CuF	56	48	45	43	43	42
CuF_2	59	50	47	45	44	43
FeF_2	79	70	67	64	62	61
FeF_3	73	63	60	57	55	54
HF	65	65	66	66	67	67
KF	129	114	109	102	99	95
LaF_3	134	124	120	117	115	113
MgF_2	128	116	112	108	106	103
MnF_2	90	81	78	76	75	74
MnF_3	74	64	61	58	57	56
MoF_5	63	58	57	56	55	54
MoF_6	64	58	56	54	53	52
NaF	129	115	110	104	101	97
NiF_2	74	64	61	58	57	55
PF_3	54	50	48	47	46	45
PbF_2	74	62	59	55	54	53
RF_3(a)	131	120	117	113	111	109
SF_6	40	33	28	25	23	22
SiF_4	94	89	87	86	85	84
SrF_2	138	127	123	119	118	116
TiF_3	100	90	86	83	81	79
TiF_4	93	86	85	83	83	82
VF_3	85	75	72	68	67	65
VF_4	76	70	68	67	67	66
WF_4	58	48	47	45	45	44
WF_5	52	47	46	45	45	44
WF_6	47	41	39	37	36	35
ZrF_2	109	99	96	92	90	89
ZrF_4	108	97	93	91	90	89

(a) RF_3 = Rare Earth Fluoride - Typically NdF_3

TABLE 3A. Free Energy of Formation of Various Oxides

Compound	$-\Delta G_f^\circ$, kcal/g-atom of oxygen					
	25°C	600°C	800°C	1000°C	1100°C	1200°C
Al_2O_3	126	112	106	101	99	96
B_2O_3	94	83	80	77	75	73
BaO	129	116	111	105	103	100
CO	33	45	49	53	56	58
CO_2	47	47	47	47	47	47
CaO	144	131	126	121	118	116
CbO	92	80	77	73	71	69
CdO	54	41	36	25	20	16
CoO	51	41	36	34	33	31
Co_3O_4	46	34	30	25	23	21
Cr_2O_3	83	71	67	63	61	59
Cu_2O	35	24	21	18	16	14
CuO	30	19	15	11	9	7
FeO	58	49	46	43	42	40
Fe_3O_4	60	49	45	41	39	38
Fe_2O_3	59	48	43	39	37	35
K_2O	76	58	52	44	40	36
La_2O_3	136	125	121	117	115	112
MgO	137	122	117	112	109	104
MnO	87	77	73	70	68	66
Mn_3O_4	77	64	60	56	53	52
Mn_2O_3	72	59	55	51	49	47
MoO_2	64	52	46	44	42	40
MoO_3	54	42	38	35	34	33
Na_2O	90	70	64	51	46	40
Nb_2O_5	85	75	68	64	62	60
NiO	52	38	33	29	26	24
P_2O_3	81	70	67	64	62	60
P_2O_5	66	53	49	45	43	42
PbO	45	31	26	23	21	19
R_2O_3(a)	137	125	121	117	115	113
SO_2	41	36	34	32	32	31
SiO_2	102	90	86	81	79	77
SrO	134	121	116	111	108	106
TiO	116	103	99	93	92	90
Ti_2O_3	113	102	98	92	91	89
TiO_2	103	93	89	84	83	81
VO	97	90	86	82	79	77
V_2O_3	93	82	78	74	72	70
WO_2	64	54	50	46	44	42
WO_3	61	49	46	42	40	38
ZrO_2	123	110	105	101	99	97
H_2O	55	48	45	42	41	39

(a) Rare Earth Oxide - Typically Nd_2O_3

were taken primarily from Rosenqvist,[1] Glassner,[2] Smithells,[3] Kubaschewski and Evans,[4] and Richardson and Jeffes.[5] When the references gave different ΔG_f° values for a given compound, an average value was used (unless some values were obviously incorrect).

The accuracy of the thermochemical data that is available on the metal fluorides is relatively poor. Only a small fraction of the data was based on experimental measurements, and most of the thermochemical data available on the fluorides was estimated by various theoretical techniques. To illustrate the accuracy of the fluoride data, the following values have been published recently for the free energy of formation of CaF_2, CoF_2, NaF and ZrF_4 at 298°K:

Compound	ΔG_f°, kcal/moles	Reference
CaF_2	-280 ± 10	Rosenqvist[1]
CaF_2	-277.6 ± 4	Smithells[3]
CoF_2	-148 ± 10	Rosenqvist
CoF_2	-147.9 ± 6	Smithells
NaF	-130 ± 5	Rosenqvist
NaF	-128.5 ± 3	Smithells
ZrF_4	-434 ± 2	Rosenqvist
ZrF_4	-434.7 ± 3	Smithells

In the case of the metal oxides the same problems apply, although to a lesser degree than with the fluorides. The available data on the oxides has somewhat better accuracy than the data on the fluorides and a greater fraction of the data was based on experimental measurements.

Because of the limited accuracy of the thermochemical data, the ΔG_f° values given in Tables 2A and 3A have been rounded off to the nearest whole number. This may cause a few apparent anomalies in the thermodynamic calculations but does not affect the overall results to any appreciable degree.

As stated previously, it was assumed that there was no compound formation between constituents of a given alloy, even at high temperatures. Instead it was assumed that each alloy was a solid solution, and the partial

molar free energy of mixing ($\Delta\bar{G}_M$) was calculated for each alloy constituent using the method developed by Hildebrand and Scott.[6] Since the alloy compositions can vary somewhat from heat to heat, $\Delta\bar{G}_M$ for a given alloy component can vary depending on the actual concentration. The $\Delta\bar{G}_M$ data presented in subsequent tables were calculated using the alloy compositions given in Table 4A. The compositions listed in Table 4A vary somewhat from those given in Table 11 (Section 6.2.3). The data in Table 4A are typical compositions for the alloys under consideration, while the compositions given in Table 11 are those of specific heats of alloys that were used in the short-term compatibility tests.

The potential for a fluoride-metal or oxide-metal reaction to occur can be predicted very roughly by comparing the appropriate free energies of formation. In Table 5A the fluorides and oxides of interest are listed in order of decreasing free energy of formation at 25 and 1200°C. Theoretically any element should be capable of reducing the fluoride or oxide of any element below it on the table. For temperatures between 25 and 1200°C the relative order of the fluorides and oxides may vary somewhat from those given in Table 5A. These shifts should not be too significant, however. In the WESF $^{90}SrF_2$-alloy systems under consideration the problem is somewhat more complicated because of alloy solid solutions, and the partial molar free energy of mixing of alloy components must be considered in the free energy of reaction calculations.

Before discussing the individual $^{90}SrF_2$-alloy systems there are certain factors to be considered which apply to all nine systems. If ZrF_2 is assumed to be present in the fluoride as a decay product of $^{90}SrF_2$, it would represent a powerful reducing agent. A comparison of the free energies of formation given in Table 2A shows that ZrF_2 could theoretically reduce many of the impurity fluorides present in WESF $^{90}SrF_2$ to the metallic state. Typical examples of such potential reactions are given in Equations (1) through (4).

TABLE 4A. Composition of Containment Materials Evaluated in the Thermodynamic Analysis

Element	Typical Composition, wt%								
	Hastelloy C-276	Hastelloy X	Hastelloy N	Haynes Alloy 25	Haynes Alloy 188	Inconel 600	Inconel 625	TZM	Tungsten
Al			0.16				0.21		
B		0.001	0.01						
C	0.02	0.09	0.07	0.09	0.08	0.06	0.04		
Cb							3.6		
Co	2.4	1.5	0.16	Bal	Bal				
Cr	16.0	21.4	6.2	19.7	21.8	15.7	22.0		
Cu			0.30			0.30			
Fe	6.4	19.0	4.7	2.2	1.6	7.5	3.4		
La					0.05				
Mn	0.50	0.60	0.60	1.4	1.1	0.40	0.05		
Mo	15.3	8.9	16.8				8.9	Bal	
Ni	Bal	Bal	Bal	10.3	22.3	Bal	Bal		
P	0.025	0.015	0.01	0.019	0.01		0.01		
S	0.006	0.006	0.01	0.007	0.006	0.007	0.007		
Si	0.04	0.47	0.72	0.26	0.30	0.24	0.24		
Ti			0.24				0.28	0.5	
V	0.20								
W	3.2	0.44	0.42	14.6	14.1				99.9
Zr								0.1	

TABLE 5A. Fluorides and Oxides Listed in Order of Decreasing Thermodynamic Stability at 25 and 1200°C

Fluorides		Oxides	
25°C	1200°C	25°C	1200°C
Ca	Ca	Ca	Ca
Sr	Sr	R(a)	R(a)
Ba	Ba	Mg	La
La	La	La	Sr
R(a)	R(a)	Sr	Mg
Na	Mg	Ba	Ba
K	Na	Al	Zr
Mg	K	Zr	Al
Al	Al	Ti(II)	Ti(II)
Zr(II)	Zr(IV)	Ti(III)	Ti(III)
Zr(IV)	Zr(II)	Ti(IV)	Ti(IV)
Ti(III)	B	Si	Si
Si	Si	V(II)	V(II)
Ti(IV)	Ti(IV)	B	B
B	Ti(III)	V(III)	V(III)
Mn(II)	Mn(II)	Nb(II)	Nb(II)
Cr(II)	Cr(II)	Na	Mn(II)
V(III)	H	Mn(II)	Cb(V)
Cr(III)	V(IV)	Cb(V)	P(III)
Fe(II)	V(III)	Cr	Cr
Cd	Cr(III)	P(III)	C(II)
V(IV)	Fe(II)	Mn_3O_4	Mn_3O_4
Co	Mn(III)	K	C(IV)
Mn(III)	Co	Mn(III)	Mn(III)
Ni	Ni	P(V)	P(V)
Pb	Cb(V)	W(IV)	W(IV)
Fe(III)	Fe(III)	Mo(IV)	Mo(IV)
H	Mo(V)	W(VI)	Na
Mo(VI)	Pb	Fe_3O_4	Fe(II)
Cb(V)	Mo(VI)	Fe(III)	H
Mo(V)	Cd	Fe(II)	W(VI)
Cu(II)	P	H	Fe_3O_4
W(IV)	W(IV)	Mo(VI)	K
Cu(I)	W(V)	Cd	Fe(III)
P	Cu(II)	Ni	Mo(VI)
W(V)	Cu(I)	Co(II)	S
W(VI)	W(VI)	C(IV)	Co(II)
S	C	Co(III)	Ni
C	S	Pb	Co(III)
		S	Pb
		Cu(I)	Cd
		C(II)	Cu(I)
		Cu(II)	Cu(II)

(a) R = Rare Earth - Typically Nd_2O_3

$$2FeF_3 + 3ZrF_2 \rightleftarrows 3ZrF_4 + 2Fe \quad (1)$$

$$MnF_2 + ZrF_2 \rightleftarrows ZrF_4 + Mn \quad (2)$$

$$NiF_2 + ZrF_2 \rightleftarrows ZrF_4 + Ni \quad (3)$$

$$2AlF_3 + 3ZrF_2 \rightleftarrows 3ZrF_4 + 2Al \quad (4)$$

The calculated free energies of reaction (ΔG_R°) for Equations (1) through (4) (obtained using the data shown in Table 2A) are presented in Table 6A. Since the calculated ΔG_R° values for Equations (1) through (3) are strongly negative over the temperature range of interest (25 to 1200°C), ZrF_2 present in $^{90}SrF_2$ could theoretically reduce any iron, manganese or nickel fluorides present to the corresponding metals. Fluorides of cadmium, copper, chromium and lead could be reduced by the ZrF_2 in similar fashion. The metals formed by the reduction of the fluorides could, in turn, alloy with each other or the containment material to form solid solutions (or intermetallic compounds). In the case of Equation (4), ΔG_R° is positive at the lower temperatures and reaches a value of zero at 1200°C. Therefore, the ZrF_2 would react with AlF_3 only at the higher temperatures. The ZrF_2 would not react with any of the other impurity metal fluorides present in WESF $^{90}SrF_2$ to any appreciable extent up to 1200°C in a closed system.

TABLE 6A. Calculated Free Energy of Reaction for Equations (1) Through (4)

Equation	ΔG_R°, kcal/Equation as Written					
	25°C	600°C	800°C	1000°C	1100°C	1200°C
1	-204	-192	-180	-198	-210	-210
2	-34	-28	-24	-28	-30	-30
3	-66	-62	-58	-64	-66	-68
4	36	36	42	18	6	0

If zirconium metal is present in the $^{90}SrF_2$ as a decay product, it could react with impurity fluorides in the $^{90}SrF_2$ in the same manner as the ZrF_2. Zirconium metal could, theoretically, reduce the same fluorides to the metallic state. The zirconium could also alloy directly with the containment material, and could react with some of the less stable oxides, if they are present, to form ZrO_2 and the corresponding metal.

Analysis of strontium fluoride shows that it contains a small amount of water even after being fired at 1100°C for several hours. The water could react with some of the impurity fluorides to form hydrogen fluoride and the corresponding oxides.

$$2FeF_3 + 3H_2O \rightleftarrows Fe_2O_3 + 6HF \quad (5)$$

$$CuF_2 + H_2O \rightleftarrows CuO + 2HF \quad (6)$$

$$MnF_2 + H_2O \rightleftarrows MnO + 2HF \quad (7)$$

$$NiF_2 + H_2O \rightleftarrows NiO + 2HF \quad (8)$$

$$2AlF_3 + 3H_2O \rightleftarrows Al_2O_3 + 6HF \quad (9)$$

The calculated free energies of reaction for Equations (5) through (9) are presented in Table 7A and show that, theoretically, water should react appreciably with the metal fluorides at the higher temperatures. In a closed system the reactions would proceed until an equilibrium partial pressure of HF is established, or until one or more of the reactants is completely consumed. The water could also react with the lead, chromium and cadmium fluorides in similar fashion, but would not react with the alkali, alkaline earth or rare earth fluorides to any appreciable extent in a closed system. The water could react at the higher temperature with any ZrF_4 present. It could also react with any zirconium metal to form ZrO_2 and hydrogen.

TABLE 7A. Calculated Free Energy of Reaction for Equations (5) through (9)

Equation	ΔG°_R, kcal/Equation as Written					
	25°C	600°C	800°C	1000°C	1100°C	1200°C
5	36	-12	-30	-45	-60	-66
6	13	-1	-8	-11	-14	-16
7	18	3	-4	-8	-11	-13
8	21	8	2	-3	-5	-9
9	75	24	3	-15	-30	-39

11.1.1 Tungsten-WESF $^{90}SrF_2$ System

The tungsten-WESF $^{90}SrF_2$ system is the simplest of the nine systems being investigated. Even so, the system contains at least 24 components and a great many reactions must be considered. Tungsten is reported to form five fluorides (WF_4, WF_5, WF_6, W_4F and W_5F) and two principal oxides (WO_2 and WO_3). It also forms several oxyfluorides, a number of intermediate oxide phases depending on the temperature, as well as a great many complex fluorides, complex oxyfluorides and tungstates. In accordance with the assumptions given earlier, it is assumed that only WF_4, WF_5, WF_6, WO_2 and WO_3 are possible reaction products.

Of the three tungsten fluorides to be considered, the free energy of formation per atom of fluorine is most negative for WF_4 throughout the temperature range of interest (25 to 1200°C). Therefore in any reactions involving tungsten metal and inorganic fluorides WF_4 is assumed to be the reaction product.

Tungsten is a relatively weak reducing agent. Comparing the relative stabilities of the metal fluorides, as given in Table 5A, it is apparent that tungsten should react with only a few of the fluorides in the WESF $^{90}SrF_2$. Potential tungsten-fluoride reactions are given in Equations (10) through (34).

$$2SrF_2 + W \rightleftarrows WF_4 + 2Sr \quad (10)$$

$$2ZrF_4 + W \rightleftarrows WF_4 + 2ZrF_2 \quad (11)$$

$$ZrF_4 + W \rightleftarrows WF_4 + Zr \quad (12)$$

$$2ZrF_2 + W \rightleftarrows WF_4 + 2Zr \quad (13)$$

$$4NaF + W \rightleftarrows WF_4 + 4Na \quad (14)$$

$$2CaF_2 + W \rightleftarrows WF_4 + 2Ca \quad (15)$$

$$2BaF_2 + W \rightleftarrows WF_4 + 2Ba \quad (16)$$

$$2MgF_2 + W \rightleftarrows WF_4 + 2Mg \quad (17)$$

$$2MnF_2 + W \rightleftarrows WF_4 + 2Mn \quad (18)$$

$$2PbF_2 + W \rightleftarrows WF_4 + 2Pb \quad (19)$$

$$4CuF_2 + W \rightleftarrows WF_4 + 4CuF \quad (20)$$

$$2CuF_2 + W \rightleftarrows WF_4 + 2Cu \quad (21)$$

$$4CuF + W \rightleftarrows WF_4 + 4Cu \quad (22)$$

$$4FeF_3 + W \rightleftarrows WF_4 + 4FeF_2 \quad (23)$$

$$4FeF_3 + 3W \rightleftarrows 3WF_4 + 4Fe \quad (24)$$

$$2FeF_2 + W \rightleftarrows WF_4 + 2Fe \quad (25)$$

$$4AlF_3 + 3W \rightleftarrows 3WF_4 + 4Al \quad (26)$$

$$2CdF_2 + W \rightleftarrows WF_4 + 2Cd \quad (27)$$

$$2CrF_2 + W \rightleftarrows WF_4 + 2Cr \quad (28)$$

$$4CrF_3 + W \rightleftarrows WF_4 + 4CrF_2 \quad (29)$$

$$4CrF_3 + 3W \rightleftarrows 3WF_4 + 4Cr \quad (30)$$

$$2NiF_2 + W \rightleftarrows WF_4 + 2Ni \quad (31)$$

$$4KF + W \rightleftarrows WF_4 + 4K \quad (32)$$

$$4RF_3 + 3W \rightleftarrows 3WF_4 + 4R \quad (33)$$

$$4HF + W \rightleftarrows WF_4 + 2H_2 \quad (34)$$

The calculated free energies of reactions for the equations are given in Table 8A and indicate that the tungsten should only react with the fluorides of copper and iron. The iron and copper fluorides should be present in the WESF $^{90}SrF_2$ in very low concentrations; therefore, there should be little reaction between the tungsten and the WESF $^{90}SrF_2$.

Although the formation of intermetallic compounds is not considered in the analysis of the various systems, the possibility of reactions occurring which involve intermetallic compounds is not impossible. For example, if any ZrF_2 or free zirconium metal are present in the WESF $^{90}SrF_2$, as decay products, they could react with several of the less stable impurity fluorides to form ZrF_4 and the appropriate metals. The metals thus formed could alloy with the tungsten to form solid solutions or intermetallic compounds. In addition, the zirconium metal could react directly with the tungsten to form an intermetallic compound or solid solution.

$$Zr + 2W \rightleftarrows ZrW_2 \quad (35)$$

TABLE 8A. Calculated Free Energies of Reaction for Reactions (10) through (34)

Reaction Number	ΔG°_{R} (Reaction as Written), kcal					
	25°C	600°C	800°C	1000°C	1100°C	1200°C
10	320	316	304	296	292	288
11	196	188	172	180	180	180
12	200	196	184	184	180	180
13	204	204	196	188	180	180
14	284	268	252	236	224	212
15	328	324	312	304	296	292
16	316	308	300	296	288	288
17	280	272	260	252	244	236
18	128	132	124	124	120	120
19	64	56	48	40	36	36
20	16	16	8	8	0	0
21	4	8	0	0	-4	-4
22	8	0	-8	-8	-8	-8
23	12	4	-4	-8	-16	-16
24	180	180	156	144	120	120
25	84	88	80	76	68	68
26	660	636	600	576	552	540
27	76	72	64	44	32	24
28	112	116	108	100	96	96
29	76	68	60	54	48	48
30	300	300	276	264	240	240
31	64	64	56	52	48	44
32	284	264	248	228	216	204
33	876	864	840	816	792	780
34	28	68	76	84	88	92

The WESF $^{90}SrF_2$ may contain small amounts of metal oxides. Possible reactions involving tungsten and the oxides are listed below. Since the free energy of formation of WO_2 is more negative per atom of oxygen than that of WO_3 between 25 and 1200°C, only the reactions involving WO_2 are considered.

$$2SrO + W \rightleftarrows WO_2 + 2Sr \quad (36)$$

$$ZrO_2 + W \rightleftarrows WO_2 + Zr \quad (37)$$

$$2Al_2O_3 + 3W \rightleftarrows 3WO_2 + 4Al \quad (38)$$

$$2BaO + W \rightleftarrows WO_2 + 2Ba \quad (39)$$

$$2CaO + W \rightleftarrows WO_2 + 2Ca \quad (40)$$

$$2CdO + W \rightleftarrows WO_2 + 2Cd \quad (41)$$

$$2Cr_2O_3 + 3W \rightleftarrows 3WO_2 + 4Cr \quad (42)$$

$$2Cu_2O + W \rightleftarrows WO_2 + 4Cu \quad (43)$$

$$4CuO + W \rightleftarrows WO_2 + 2Cu_2O \quad (44)$$

$$2CuO + W \rightleftarrows WO_2 + 2Cu \quad (45)$$

$$2FeO + W \rightleftarrows WO_2 + 2Fe \quad (46)$$

$$2Fe_2O_3 + W \rightleftarrows WO_2 + 4FeO \quad (47)$$

$$2Fe_3O_4 + W \rightleftarrows WO_2 + 6FeO \quad (48)$$

$$2Fe_2O_3 + 3W \rightleftarrows 3WO_2 + 4Fe \quad (49)$$

$$Fe_3O_4 + 2W \rightleftarrows 2WO_2 + 3Fe \quad (50)$$

$$2H_2O + W \rightleftarrows WO_2 + 2H_2 \quad (51)$$

$$2MgO + W \rightleftarrows WO_2 + 2Mg \quad (52)$$

$$2MnO + W \rightleftarrows WO_2 + 2Mn \quad (53)$$

$$2Mn_3O_4 + W \rightleftarrows WO_2 + 6MnO \quad (54)$$

$$Mn_3O_4 + 2W \rightleftarrows 2WO_2 + 3Mn \quad (55)$$

$$2Mn_2O_3 + W \rightleftarrows WO_2 + 4MnO \quad (56)$$

$$6Mn_2O_3 + W \rightleftarrows WO_2 + 4Mn_3O_4 \quad (57)$$

$$2NiO + W \rightleftarrows WO_2 + 2Ni \quad (58)$$

$$2PbO + W \rightleftarrows WO_2 + 2Pb \quad (59)$$

$$SiO_2 + W \rightleftarrows WO_2 + Si \quad (60)$$

$$2R_2O_3 + 3W \rightleftarrows 3WO_2 + 4R \quad (61)$$

The calculated free energies of reaction for Reactions (36) through (61) are given in Table 9A. From the results, it can be seen that the tungsten should react with several of the oxides if they are present in the fluoride. The metals formed by the reactions could react, in turn, with the tungsten or each other. Fortunately the analytical data show the oxygen concentration in the SrF_2 is very low, and the bulk of the oxygen is present as water. Even if hydrolysis reactions occur in the system between the water and some fluorides, the oxide concentrations would still be very low and there would be little interaction with the tungsten.

11.1.2 TZM-WESF $^{90}SrF_2$ System

The alloy TZM is a molybdenum alloy containing small amounts of titanium (~0.5 wt%) and zirconium (~0.1 wt%). A comparison of chemical stabilities of the fluorides (see Table 5A) shows that components of the TZM alloy should be more reactive than tungsten even after allowing for the partial molar free energies of mixing.

TABLE 9A. Calculated Free Energies of Reaction for Reactions (36) through (61)

Reaction Number	ΔG°_R (Reaction as Written), kcal					
	25°C	600°C	800°C	1000°C	1100°C	1200°C
36	140	134	132	130	128	128
37	118	112	110	110	110	110
38	372	348	336	330	330	324
39	130	124	122	118	118	116
40	160	154	152	150	148	148
41	-20	-26	-28	-42	-44	-52
42	114	102	102	102	102	102
43	-58	-60	-58	-56	-56	-56
44	-78	-80	-82	-84	-80	-84
45	-68	-70	-70	-70	-70	-70
46	-12	-10	-8	-6	-4	-4
47	-6	-16	-26	-30	-34	-34
48	+4	-10	-16	-22	-28	-20
49	-30	-36	-42	-42	-42	-42
50	-16	-20	-20	-20	-20	-16
51	-18	-12	-10	-8	-6	-6
52	146	136	134	132	130	124
53	46	46	46	48	48	48
54	-34	-58	-58	-64	-64	-64
55	52	40	40	40	36	40
56	-44	-62	-62	-66	-66	-66
57	-64	-70	-70	-70	-54	-70
58	-24	-32	-34	-34	-36	-36
59	-38	-46	-46	-46	-46	-46
60	76	72	72	70	70	70
61	438	426	426	426	426	426

Molybdenum is reported to form several fluorides, but on a thermodynamic basis the pentafluoride (MoF_5) and hexafluoride (MoF_6) appear to be the most stable. Since the free energy of formation (per atom of fluorine) is almost the same for both compounds, only the pentafluoride was considered in the analysis of the system. In the case of titanium and zirconium, TiF_4, TiF_3 and ZrF_4 were assumed to be the only potential reaction products. In the case of the oxides, the reaction products were assumed to be MoO_2, TiO and ZrO_2.

The partial molar free energies of mixing for the components of the TZM alloy were calculated using the method developed by Hildebrand and Scott[6] and the alloy composition given in Table 4A. The values obtained are shown in Table 10A for temperatures from 25 to 1200°C.

TABLE 10A. Calculated Partial Molar Free Energies of Mixing for TZM Alloy Components

	$-\Delta\bar{G}_M$, kcal/mole					
Component	25°C	600°C	800°C	1000°C	1100°C	1200°C
Mo	0	0	0	0	0	0
Ti	3	8	10	12	13	14
Zr	7	13	16	19	21	23

Free energy of reaction calculations, using the data given in Tables 2A and 10A, predict the molybdenum present in the TZM would react with only a few of the fluorides present in the WESF $^{90}SrF_2$ at temperatures from 25 to 1200°C.

$$5AlF_3 + 3Mo \text{ (in TZM)} \rightleftarrows 5Al + 3MoF_5 \quad (62)$$

$$5BaF_2 + 2Mo \text{ (in TZM)} \rightleftarrows 5Ba + 2MoF_5 \quad (63)$$

$$5CaF_2 + 2Mo \text{ (in TZM)} \rightleftarrows 5Ca + 2MoF_5 \quad (64)$$

$$5CdF_2 + 2Mo \text{ (in TZM)} \rightleftarrows 5Cd + 2MoF_5 \quad (65)$$

$$5CrF_3 + Mo \text{ (in TZM)} \rightleftarrows 5CrF_2 + MoF_5 \quad (66)$$

$$5CuF_2 + 2Mo \text{ (in TZM)} \rightleftarrows 5Cu + 2MoF_5 \quad (67)$$

$$5FeF_3 + Mo \text{ (in TZM)} \rightleftarrows 5FeF_2 + MoF_5 \quad (68)$$

$$5KF + Mo \text{ (in TZM)} \rightleftarrows 5K + MoF_5 \quad (69)$$

$$5MgF_2 + 2Mo \text{ (in TZM)} \rightleftarrows 5Mg + 2MoF_5 \quad (70)$$

$$5MnF_2 + 2Mo \text{ (in TZM)} \rightleftarrows 5Mn + 2MoF_5 \quad (71)$$

$$5NaF + Mo \text{ (in TZM)} \rightleftarrows 5Na + MoF_5 \quad (72)$$

$$5NiF_2 + 2Mo \text{ (in TZM)} \rightleftarrows 5Ni + 2MoF_5 \quad (73)$$

$$5PbF_2 + 2Mo \text{ (in TZM)} \rightleftarrows 5Pb + 2MoF_5 \quad (74)$$

$$5RF_3 + 3Mo \text{ (in TZM)} \rightleftarrows 5R + 3MoF_5 \quad (75)$$

$$5SrF_2 + 2Mo \text{ (in TZM)} \rightleftarrows 5Sr + 2MoF_5 \quad (76)$$

$$5ZrF_2 + 2Mo \text{ (in TZM)} \rightleftarrows 5Zr + 2MoF_5 \quad (77)$$

$$10HF + 2Mo \text{ (in TZM)} \rightleftarrows 5H_2 + 2MoF_5 \quad (78)$$

The calculated free energies of reaction for Equations (62) through (78) are presented in Table 11A. They show that only the fluorides of copper and iron could react with molybdenum throughout the entire temperature range, while the lead and cadmium fluorides would react at the higher temperatures. None of the other metal fluorides in the WESF $^{90}SrF_2$ should react with the molybdenum. If any HF were present in the system, due to hydrolysis reactions between water and the fluorides, it would not react with the molybdenum to any measurable degree.

TABLE 11A. Calculated Free Energy of Reaction for Equations (62) through (78)

Equation	ΔG_R° (Reaction as Written), kcal					
	25°C	600°C	800°C	1000°C	1100°C	1200°C
62	750	645	600	555	540	525
63	740	670	650	630	620	620
64	770	710	680	650	640	630
65	140	80	60	0	-20	-40
66	70	35	25	25	10	10
67	-40	-80	-100	-110	-110	-110
68	-10	-45	-55	-65	-70	-70
69	330	280	260	230	220	205
70	650	580	550	520	510	490
71	270	230	210	200	200	200
72	330	285	265	240	230	215
73	110	60	40	20	20	10
74	110	40	20	-10	-10	-10
75	1020	930	900	855	840	825
76	750	690	660	630	630	620
77	460	410	390	360	350	350
78	20	70	90	100	120	130

The titanium and zirconium in the TZM would be stronger reducing agents than the molybdenum (even allowing for substantial partial molar free energies of mixing). They could react, therefore, with some additional fluorides in the WESF $^{90}SrF_2$ which do not react with the molybdenum.

$$4FeF_3 + 3Ti\ (\text{in TZM}) \rightleftarrows 4Fe + 3TiF_4 \quad (79)$$

$$2MnF_2 + Ti\ (\text{in TZM}) \rightleftarrows 2Mn + TiF_4 \quad (80)$$

$$2NiF_2 + Ti\ (\text{in TZM}) \rightleftarrows 2Ni + TiF_4 \quad (81)$$

$$4HF + Ti\ (\text{in TZM}) \rightleftarrows 2H_2 + TiF_4 \quad (82)$$

$$FeF_3 + Ti\ (\text{in TZM}) \rightleftarrows Fe + TiF_3 \quad (83)$$

$$3MnF_2 + 2Ti\ (\text{in TZM}) \rightleftarrows 3Mn + 2TiF_3 \quad (84)$$

$$2MnF_2 + Zr\ (\text{in TZM}) \rightleftarrows 2Mn + ZrF_4 \quad (85)$$

$$4CrF_3 + 3Zr\ (\text{in TZM}) \rightleftarrows 4Cr + 3ZrF_4 \quad (86)$$

$$4AlF_3 + 3Zr\ (\text{in TZM}) \rightleftarrows 4Al + 3ZrF_4 \quad (87)$$

$$4NaF + Zr\ (\text{in TZM}) \rightleftarrows 4Na + ZrF_4 \quad (88)$$

The calculated free energy of reaction for Equations (79) through (88) are shown in Table 12A. While not all of the equations and ΔG_R° values have been shown, the thermodynamic calculations predict that the titanium and zirconium in the TZM could react with all of the fluorides in the WESF $^{90}SrF_2$ except AlF_3 and the alkali metal, alkaline earth and rare earth fluorides.

Although the concentration of metal oxides in the WESF $^{90}SrF_2$ would be very low, they could have an effect on $^{90}SrF_2$ containment and should be considered in the thermodynamic analyses of $^{90}SrF_2$-alloy systems. Assuming

TABLE 12A. Calculated Free Energy of Reaction for Equations (79) through (88)

Equation	ΔG°_R, (Reaction as Written), kcal					
	25°C	600°C	800°C	1000°C	1100°C	1200°C
79	-231	-252	-270	-276	-297	-294
80	-9	-12	-18	-16	-19	-18
81	-73	-80	-86	-88	-91	-94
82	-109	-76	-66	-56	-51	-46
83	-78	-73	-68	-65	-63	-61
84	-54	-38	-28	-16	-6	-2
85	-65	-51	-44	-41	-39	-37
86	-279	-249	-228	-231	-237	-239
87	-81	87	96	81	75	69
88	91	85	84	71	65	55

MoO_2, TiO and ZrO_2 are the possible reaction products, the thermodynamic calculations predict that molybdenum in TZM would react with the oxides of cadmium, copper, iron (III), manganese (III), nickel and lead if they are present in the fluoride. The molybdenum could also react to some degree with any water that might be present. The titanium and zirconium in the TZM could react with any of the oxides present except those of aluminum and the alkaline earth and rare earth elements.

In summary, the thermodynamic calculations predict that the components of the TZM alloy could react with some of the impurity fluorides (and oxides) present in WESF $^{90}SrF_2$, particularly those of the polyvalent ions such as copper, iron and manganese. Fortunately those impurities that the calculations predict should react with TZM are present in the WESF $^{90}SrF_2$ in low

concentrations. The calculations also indicate that no reactions should occur between the TZM components and $^{90}SrF_2$ or fluoride impurities present in high concentrations-- such as ZrF_4, ZrF_2, NaF, CaF_2, BaF_2, MgF_2 and AlF_3.

11.1.3 Ni- or Co-Base Alloy-WESF $^{90}SrF_2$ System

In analyzing the systems containing WESF $^{90}SrF_2$ and a Ni- or Co-base alloy it soon becomes obvious that if the alloys are assumed to be solid solutions then, on a thermodynamic basis, the systems are very similar. The alloys being evaluated contain a number of common components. Even though the concentration of a common component may vary substantially between alloys, the partial molar free energies of mixing ($\Delta\bar{G}_M$) do not vary by more than a few kilocalories. The calculated $\Delta\bar{G}_M$ values for the seven alloys, over a temperature range of 25 to 1200°C, are presented in Table 13A. The calculations were made using the alloy composition given in Table 4A.

In Table 14A the $\Delta\bar{G}_M$ values at 25°C and 1200°C are given for components that are common to all seven alloys. From the table it can be seen that the $\Delta\bar{G}_M$ values for a given component do not vary significantly for the various alloys. This means that reactions involving common alloy components which are theoretically possible in one alloy-fluoride system will probably also be possible in the other systems. The only major differences between the systems, therefore, will be when the alloys contain different components (assuming the alloys are solid solutions and no compounds form between alloy components). In considering the various alloy-fluoride systems only the Hastelloy C-276 WESF $^{90}SrF_2$ system will be described in detail. The other systems will only be mentioned when they differ markedly from the Hastelloy C-276-fluoride system.

11.1.4 Hastelloy C-276-WESF $^{90}SrF_2$ System

The Hastelloy C-276-WESF $^{90}SrF_2$ system is extremely complex because of the great many components present. Hastelloy C-276 is a Ni-base alloy containing 12 recognized components. Chemical analysis of the alloy at

TABLE 13A. Calculated Partial Molar Free Energies of Mixing for Components of Ni- and Co-Base Alloys

Alloy	Component	$-\Delta\bar{G}_M$, kcal/mole					
		25°C	600°C	800°C	1000°C	1100°C	1200°C
Hastelloy C-276	C	4	10	14	17	19	20
	Co	2	6	8	9	10	11
	Cr	1	3	4	4	5	5
	Fe	2	5	6	7	7	8
	Mn	3	9	11	13	14	15
	Mo	1	4	5	6	6	7
	Ni	0	1	1	1	1	2
	P	5	13	16	19	20	22
	S	5	16	19	23	25	27
	Si	4	12	15	18	19	20
	V	4	10	12	15	16	18
	W	3	3	10	12	13	13
Hastelloy X	B	6	17	21	24	26	28
	C	3	9	12	14	15	16
	Co	2	7	8	10	11	12
	Cr	1	3	3	4	4	4
	Fe	1	3	4	4	4	4
	Mn	3	9	11	13	14	15
	Mo	2	5	6	7	8	9
	Ni	0	1	2	2	2	2
	P	5	14	17	20	22	24
	S	5	16	19	23	25	27
	Si	3	8	10	12	13	14
	W	4	11	14	17	18	19
Hastelloy N	Al	3	10	12	14	15	16
	B	4	13	16	18	19	21
	C	3	10	12	14	15	16
	Co	4	11	14	16	17	18
	Cr	2	4	5	6	7	8
	Cu	4	10	13	15	16	17
	Fe	2	5	6	8	8	9
	Mn	3	9	11	13	14	15
	Mo	1	4	5	6	6	7
	Ni	0	0	1	1	1	1
	P	5	14	18	21	23	25
	S	5	14	17	21	22	24
	Si	3	7	9	10	11	12
	Ti	3	10	12	15	16	17
	W	4	11	14	17	18	19
Haynes Alloy 25	C	3	9	11	13	14	15
	Co	0	1	1	2	2	2
	Cr	1	2	3	3	4	4

TABLE 13A. (contd)

Alloy	Component	$-\Delta\bar{G}_M$, kcal/mole 25°C	600°C	800°C	1000°C	1100°C	1200°C
Haynes Alloy 25	Fe	2	6	7	9	9	10
	Mn	2	7	9	10	11	12
	Ni	1	4	5	6	6	7
	P	4	13	16	19	20	22
	S	4	13	16	18	19	21
	Si	3	8	10	13	14	15
	W	2	5	6	7	8	8
Haynes Alloy 188	C	3	9	11	13	14	16
	Co	1	2	2	2	2	3
	Cr	1	2	3	3	4	4
	Fe	2	7	8	10	11	12
	La	5	14	17	20	22	23
	Mn	2	7	9	11	12	12
	Ni	1	2	3	4	4	5
	P	5	14	17	20	22	23
	S	5	15	18	21	23	24
	Si	3	9	11	12	13	14
	W	2	5	6	8	8	9
Inconel 600	C	3	10	12	14	16	17
	Cr	1	3	4	4	4	5
	Cu	4	10	12	15	16	17
	Fe	2	4	5	6	6	7
	Mn	3	9	11	13	14	15
	Ni	0	0	1	1	1	1
	S	5	15	19	22	24	26
	Si	3	9	11	13	14	15
Inconel 625	Al	3	9	11	13	14	15
	C	3	10	13	15	16	17
	Cb	2	6	8	9	10	11
	Cr	1	2	3	3	3	4
	Fe	2	5	7	8	9	9
	Mn	4	13	16	19	20	23
	Mo	2	5	6	7	8	8
	Ni	0	1	1	1	1	1
	P	5	14	18	21	23	24
	S	5	15	19	22	24	25
	Si	3	9	11	13	14	15
	Ti	3	9	12	14	15	16

TABLE 14A. Partial Molar Free Energy of Mixing of Components in the Various Ni- and Co-Base Alloys

	$-\Delta\bar{G}_M$, kcal/mole													
	Chromium		Iron		Manganese		Carbon		Nickel		Silicon		Sulfur	
	25°C	1200°C	25°C	1200°C	25°C	1200°C	25°C	1200°C	25°C	1200°C	25°C	1200°C	25°C	1200°C
Hastelloy C-276	1	5	2	8	3	15	4	20	0	2	4	20	5	27
Hastelloy X	1	4	1	4	3	15	3	16	0	2	3	14	5	27
Hastelloy N	2	8	2	9	3	15	3	16	0	1	3	12	5	24
Haynes Alloy 25	1	4	2	10	2	12	3	15	1	7	3	15	4	21
Haynes Alloy 188	1	4	2	12	2	12	3	16	1	5	3	14	5	24
Inconel 600	1	5	2	7	3	15	3	17	0	1	3	15	5	26
Inconel 625	1	4	2	9	4	23	3	17	0	1	3	15	5	25

Battelle and ARHCO indicates the presence of at least two components, Al and Ti, not reported by the manufacturer. In the thermodynamic analysis only those components reported by the manufacturer were considered. Even using the simplifying assumptions previously stated, the number of reactions to be considered is still very large because of the many components present in the system.

A comparison of the free energy data given in Tables 2A and 3A and the fluoride-oxide stability rankings given in Table 5A makes it apparent that a number of reactions are potentially possible between components of the Hastelloy C-276 and constituents of the WESF $^{90}SrF_2$ [even allowing for the partial molar free energies of mixing of alloy components (Table 13A)]. Typical examples of fluoride reactions that must be considered in the Hastelloy C-276-WESF $^{90}SrF_2$ system are given in Equations (89) through (124). Of the various components of the alloy, silicon represents the strongest reducing agent, even after allowing for a substantial partial molar free energy of mixing. Fluoride impurities that do not react with silicon should not react with the other alloy components.

The calculated free energies of reaction for Equations (89) through (124), over the temperature range 25 to 1200°C, are given in Table 15A. The thermodynamic calculations predict that, as expected, the components of the Hastelloy C-276 will react with several of the impurity fluorides in the WESF $^{90}SrF_2$, especially those cations that can undergo valence changes such as Cu, Fe and Mn. However, the calculations also show that the only components of the WESF $^{90}SrF_2$ that will react with alloy components are those that are present in low concentrations; conversely, none of the fluorides that are present in relatively large concentrations (such as SrF_2, NaF, CaF_2, BaF_2, MgF_2 and R_2F_3) will react with alloy components.

If certain metals oxides are present in the WESF $^{90}SrF_2$ they may react with alloy components. Typical examples of oxide reactions that are potentially possible are listed in Equations (125) through (133).

$$2SrF_2 + C \quad (\text{in C-276}) \rightleftarrows CF_4 + 2Sr \tag{89}$$

$$2CuF_2 + C \quad (\text{in C-276}) \rightleftarrows CF_4 + 2Cu \tag{90}$$

$$4FeF_3 + C \quad (\text{in C-276}) \rightleftarrows CF_4 + 4FeF_2 \tag{91}$$

$$SrF_2 + Co \quad (\text{in C-276}) \rightleftarrows CoF_2 + Sr \tag{92}$$

$$2NaF + Co \quad (\text{in C-276}) \rightleftarrows CoF_2 + 2Na \tag{93}$$

$$CuF_2 + Co \quad (\text{in C-276}) \rightleftarrows CoF_2 + Cu \tag{94}$$

$$2FeF_3 + Co \quad (\text{in C-276}) \rightleftarrows CoF_2 + 2FeF_2 \tag{95}$$

$$SrF_2 + Cr \quad (\text{in C-276}) \rightleftarrows CrF_2 + Sr \tag{96}$$

$$CaF_2 + Cr \quad (\text{in C-276}) \rightleftarrows CrF_2 + Ca \tag{97}$$

$$PbF_2 + Cr \quad (\text{in C-276}) \rightleftarrows CrF_2 + Pb \tag{98}$$

$$ZrF_4 + Fe \quad (\text{in C-276}) \rightleftarrows FeF_2 + ZrF_2 \tag{99}$$

$$2NaF + Fe \quad (\text{in C-276}) \rightleftarrows FeF_2 + 2Na \tag{100}$$

$$NiF_2 + Fe \quad (\text{in C-276}) \rightleftarrows FeF_2 + Ni \tag{101}$$

$$SrF_2 + Mn \quad (\text{in C-276}) \rightleftarrows MnF_2 + Sr \tag{102}$$

$$CuF_2 + Mn \quad (\text{in C-276}) \rightleftarrows MnF_2 + Cu \tag{103}$$

$$2FeF_3 + Mn \quad (\text{in C-276}) \rightleftarrows MnF_2 + 2FeF_2 \tag{104}$$

$$2CrF_3 + Mn \quad (\text{in C-276}) \rightleftarrows MnF_2 + 2CrF_2 \tag{105}$$

$$5SrF_2 + 2Mo \quad (\text{in C-276}) \rightleftarrows 2MoF_5 + 5Sr \tag{106}$$

$$5FeF_3 + Mo \quad (\text{in C-276}) \rightleftarrows MoF_5 + 5FeF_2 \tag{107}$$

$$2NaF + Ni \quad (\text{in C-276}) \rightleftarrows NiF_2 + 2Na \tag{108}$$

$$CuF_2 + Ni \quad (\text{in C-276}) \rightleftarrows NiF_2 + Cu \tag{109}$$

$$PbF_2 + Ni \quad (\text{in C-276}) \rightleftarrows NiF_2 + Pb \tag{110}$$

$$3CuF_2 + 2P \quad (\text{in C-276}) \rightleftarrows 2PF_3 + 3Cu \tag{111}$$

$$3FeF_3 + P \text{ (in C-276)} \rightleftarrows PF_3 + 3FeF_2 \quad (112)$$

$$3CuF_2 + S \text{ (in C-276)} \rightleftarrows SF_6 + 3Cu \quad (113)$$

$$6FeF_3 + S \text{ (in C-276)} \rightleftarrows SF_6 + 6FeF_2 \quad (114)$$

$$2SrF_2 + Si \text{ (in C-276)} \rightleftarrows SiF_4 + 2Sr \quad (115)$$

$$4NaF + Si \text{ (in C-276)} \rightleftarrows SiF_4 + 4Na \quad (116)$$

$$2MnF_2 + Si \text{ (in C-276)} \rightleftarrows SiF_4 + 2Mn \quad (117)$$

$$2PbF_2 + Si \text{ (in C-276)} \rightleftarrows SiF_4 + 2Pb \quad (118)$$

$$6NaF_2 + 2V \text{ (in C-276)} \rightleftarrows 2VF_3 + 6Na \quad (119)$$

$$FeF_3 + V \text{ (in C-276)} \rightleftarrows VF_3 + Fe \quad (120)$$

$$3CdF_2 + 2V \text{ (in C-276)} \rightleftarrows 2VF_3 + 3Cd \quad (121)$$

$$2CdF_2 + W \text{ (in C-276)} \rightleftarrows WF_4 + 2Cd \quad (122)$$

$$2MgF_2 + W \text{ (in C-276)} \rightleftarrows WF_4 + 2Mg \quad (123)$$

$$4FeF_3 + W \text{ (in C-276)} \rightleftarrows WF_4 + 4FeF_2 \quad (124)$$

$$Cu_2O + C \text{ (in C-276)} \rightleftarrows CO + 2Cu \quad (125)$$

$$Fe_2O_3 + C \text{ (in C-276)} \rightleftarrows CO + 2FeO \quad (126)$$

$$2Fe_2O_3 + 3C \text{ (in C-276)} \rightleftarrows 3CO_2 + 4Fe \quad (127)$$

$$3PbO + 2Cr \text{ (in C-276)} \rightleftarrows Cr_2O_3 + 3Pb \quad (128)$$

$$NiO + Fe \text{ (in C-276)} \rightleftarrows FeO + Ni \quad (129)$$

$$Fe_2O_3 + 2P \text{ (in C-276)} \rightleftarrows P_2O_3 + 2Fe \quad (130)$$

$$2MnO + Si \text{ (in C-276)} \rightleftarrows SiO_2 + 2Mn \quad (131)$$

$$Cr_2O_3 + 3V \text{ (in C-276)} \rightleftarrows 3VO + 2Cr \quad (132)$$

$$2Fe_2O_3 + 3W \text{ (in C-276)} \rightleftarrows 3WO_2 + 4Fe \quad (133)$$

TABLE 15A. Calculated Free Energies of Reaction for Equations (89) through (124)

Equation	ΔG_R° (Reaction as Written), kcal					
	25°C	600°C	800°C	1000°C	1100°C	1200°C
89	396	374	366	357	359	356
90	80	66	62	61	63	64
91	88	62	58	53	51	52
92	130	130	132	131	132	133
93	112	106	106	101	98	95
94	-28	-24	-20	-17	-16	-13
95	-24	-26	-22	-21	-22	-19
96	105	103	102	102	103	101
97	109	107	106	106	105	103
98	-23	-27	-26	-26	-25	-25
99	58	55	52	59	63	63
100	102	95	92	92	85	80
101	-8	-8	-7	-6	-4	-5
102	99	101	101	99	100	99
103	-59	-53	-47	-49	-48	-47
104	-55	-55	-53	-53	-54	-53
105	-23	-23	-21	-17	-22	-21
106	752	698	670	642	642	634
107	-9	-41	-50	-59	-64	-63
108	110	106	103	98	94	91
109	-30	-27	-27	-25	-25	-22
110	0	-3	-3	-5	-5	-2
111	40	26	26	26	28	32
112	184	150	144	135	129	129
113	119	118	133	139	146	148
114	131	112	127	131	133	135
115	180	164	163	150	151	148
116	144	116	107	90	83	72
117	-17	-20	-21	-22	-21	-20
118	-76	-96	-97	-106	-105	-104
119	272	260	252	246	236	228
120	-32	-26	-24	-18	-12	-15
121	-40	-34	-30	-42	-52	-56
122	79	75	74	56	45	37
123	283	275	270	264	257	249
124	15	7	6	4	1	-3

The calculated free energies of reaction for Equations (125) through (133) are presented in Table 16A. The calculations show that several impurity oxides, especially those involving polyvalent reactions, would react with components of the alloy.

TABLE 16A. Calculated Free Energies of Reaction for Equations (125) through (133)

	ΔG_R° (Reaction as Written), kcal					
Equation	25°C	600°C	800°C	1000°C	1100°C	1200°C
125	+6	-11	-14	-18	-21	-24
126	32	11	12	-5	-10	-13
127	84	36	18	3	-3	-12
128	-112	-114	-115	-112	-110	-110
129	-4	-7	-8	-8	-10	-10
130	-56	-40	-40	-37	-35	-31
131	-32	-32	-33	-30	-31	-32
132	-32	-33	-29	-20	-16	-10
133	-21	-12	-12	-6	-3	-3

11.1.5 Hastelloy X-WESF $^{90}SrF_2$ System

On a thermodynamic basis, the Hastelloy X-WESF $^{90}SrF_2$ system should be very similar to the Hastelloy C-276-WESF $^{90}SrF_2$ system. This is to be expected since the two alloys contain, with two exceptions, the same components. The only differences are that the Hastelloy C-276 contains some vanadium not found in the Hastelloy X, while the latter contains a trace of boron which is not present in the former. The concentrations of common components vary somewhat between the two alloys which means the $\Delta\bar{G}_M$ values vary slightly (see Table 13A). The variations are insignificant, however, and reactions involving common components which are possible in one system should be possible in the other.

The boron which is present in the Hastelloy X is a fairly strong reducing agent, even allowing for a substantial partial molar free energy of mixing. The boron should be capable, therefore, of reacting with several impurity fluorides and oxides in the WESF $^{90}SrF_2$. Typical examples of fluoride reactions involving boron are given in Equations (134) through (146).

$$3SrF_2 + 2B \text{ (in Hast X)} \rightleftarrows 2BF_3 + 3Sr \quad (134)$$

$$3ZrF_4 + 4B \text{ (in Hast X)} \rightleftarrows 4BF_3 + 3Zr \quad (135)$$

$$3NaF + B \text{ (in Hast X)} \rightleftarrows BF_3 + 3Na \quad (136)$$

$$3CaF_2 + 2B \text{ (in Hast X)} \rightleftarrows 2BF_3 + 3Ca \quad (137)$$

$$AlF_3 + B \text{ (in Hast X)} \rightleftarrows BF_3 + Al \quad (138)$$

$$3CuF_2 + 2B \text{ (in Hast X)} \rightleftarrows 2BF_3 + 3Cu \quad (139)$$

$$3FeF_3 + B \text{ (in Hast X)} \rightleftarrows BF_3 + 3FeF_2 \quad (140)$$

$$3MnF_2 + 2B \text{ (in Hast X)} \rightleftarrows 2BF_3 + 3Mn \quad (141)$$

$$3PbF_2 + 2B \text{ (in Hast X)} \rightleftarrows 2BF_3 + 3Pb \quad (142)$$

$$3CdF_2 + 2B \text{ (in Hast X)} \rightleftarrows 2BF_3 + 3Cd \quad (143)$$

$$3CrF_3 + B \text{ (in Hast X)} \rightleftarrows BF_3 + 3CrF_2 \quad (144)$$

$$3NiF_2 + 2B \text{ (in Hast X)} \rightleftarrows 2BF_3 + 3Ni \quad (145)$$

$$RF_3 + B \text{ (in Hast X)} \rightleftarrows BF_3 + R \quad (146)$$

The calculated free energies of reaction for Equations (134) through (146) are given in Table 17A. The calculations show that the boron in the Hastelloy X should react only with the less stable fluorides and would not react with the alkaline earth, alkali metal and rare earth fluorides or the fluorides of zirconium and aluminum. A similar situation exists with the oxides and boron.

TABLE 17A. Calculated Free Energies of Reaction for Equations (134) through (146)

Equation	ΔG°_R (Reaction as Written), kcal					
	25°C	600°C	800°C	1000°C	1100°C	1200°C
134	300	274	264	252	250	248
135	240	188	168	168	164	176
136	123	101	93	81	74	65
137	312	286	276	264	258	254
138	75	59	54	48	44	43
139	-174	-188	-192	-192	-194	-190
140	-81	-97	-99	-102	-106	-104
141	12	-2	-6	-6	-8	-4
142	-84	-116	-120	-132	-134	-130
143	-66	-92	-96	-126	-140	-148
144	-33	-49	-51	-48	-58	-56
145	-84	-107	-114	-120	-122	-124
146	129	116	114	108	104	103

11.1.6 Hastelloy N-WESF $^{90}SrF_2$ System

The Hastelloy N is quite similar to the other Hastelloy alloys on a thermodynamic basis. The principal difference is that it contains three components not found in the other two: copper, titanium and aluminum. The copper would be a very weak reducing agent and should not react with components of the fluoride. The titanium would be a strong reducing agent, even allowing for a substantial partial molar free energy of mixing, and would react with a number of components in the fluoride. The reactivity of the titanium in the Hastelloy N would be similar to its reactivity in TZM, assuming no compound formation, and reactions which are possible in the TZM system should also be possible in the Hastelloy N system.

The aluminum would be a stronger reducing agent than the titanium and could react with all of the fluorides in the WESF $^{90}SrF_2$ except those of the alkali metals, the alkaline earths, the rare earths and possibly zirconium. It could also react with all of the oxides except those of the alkaline earths, rare earths and possibly zirconium.

11.1.7 Haynes Alloy 25-WESF $^{90}SrF_2$ System

Haynes Alloy 25 differs from the Hastelloy alloys in that it is a Co-base rather than a Ni-base alloy. It contains the same elemental constituents as Hastelloy C-276 except molybdenum or vanadium. While the $\Delta\bar{G}_M$ values for the common component of the two alloys vary somewhat, reactions involving common components which occur in one system should occur in the other. The one possible exception would involve cobalt which has a relatively large $\Delta\bar{G}_M$ value in the Hastelloy alloys as compared to Haynes Alloy 25.

11.1.8 Haynes Alloy 188-WESF $^{90}SrF_2$ System

Haynes Alloy 188 is another Co-base alloy. It differs from Haynes Alloy 25 principally in its nickel content (much higher) and in the fact that it contains a small amount of lanthanum. Except for the lanthanum, the Haynes Alloy 188-WESF $^{90}SrF_2$ system is very similar to the other Ni- and Co-base alloy system discussed above. The lanthanum is a very powerful reducing agent, even allowing for a substantial partial molar free energy of mixing. It could react with all of the fluorides in the WESF $^{90}SrF_2$ except the alkaline earth fluorides and some of the rare earth fluorides. It would also react with all of the oxides except those of Ca, Mg, Sr and some rare earth metals. Examples of possible fluoride and oxide reactions are given by Equations (147) through (154).

$$3BaF_2 + 2La \text{ (in Haynes 188)} \rightleftarrows 2LaF_3 + 3Ba \qquad (147)$$

$$3ZrF_4 + 4La \text{ (in Haynes 188)} \rightleftarrows 4LaF_3 + 3Zr \qquad (148)$$

$$AlF_3 + La \text{ (in Haynes 188)} \rightleftarrows LaF_3 + Al \qquad (149)$$

$$3CaF_2 + 2La \text{ (in Haynes 188)} \rightleftarrows 2LaF_3 + 3Ca \qquad (150)$$

$$3SrO + 2La \text{ (in Haynes 188)} \rightleftarrows La_2O_3 + 3Sr \quad (151)$$

$$3ZrO_2 + 4La \text{ (in Haynes 188)} \rightleftarrows 2La_2O_3 + 3Zr \quad (152)$$

$$Al_2O_3 + 2La \text{ (in Haynes 188)} \rightleftarrows La_2O_3 + 2Al \quad (153)$$

$$3BaO + 2La \text{ (in Haynes 188)} \rightleftarrows La_2O_3 + 3Ba \quad (154)$$

The calculated free energies of reaction for Equations (147) through (154) are presented in Table 18A. They show that the lanthanum in Haynes 188 would be very reactive and would react with all but the most stable fluorides and oxides in the WESF $^{90}SrF_2$.

TABLE 18A. Calculated Free Energies of Reaction for Equations (147) through (154)

Equation	ΔG_R° (Reaction as Written), kcal					
	25°C	600°C	800°C	1000°C	1100°C	1200°C
147	28	34	46	52	56	64
148	-292	-260	-256	-232	-212	-196
149	-58	-55	-52	-52	-50	-49
150	46	58	64	64	68	70
151	4	16	19	22	23	28
152	-58	-34	-28	-16	-8	+2
153	-20	-11	-11	-8	-4	-2
154	-11	1	4	4	8	10

11.1.9 Inconel 600-WESF $^{90}SrF_2$ System

Inconel 600 is a less complex alloy than the other Ni- and Co-base alloys under consideration since it contains only eight components. It is essentially a nickel-chromium-iron alloy with minor amounts of other components. All

components of the Inconel 600, except copper, are found in Hastelloy C-276. Reactions involving common components which occur in the Haynes and Hastelloy systems should also occur in the Inconel 600 system. The copper in the Inconel 600 is a weak reducing agent and should not react with any of the components of the WESF $^{90}SrF_2$.

11.1.10 Inconel 625-WESF $^{90}SrF_2$ System

The Inconel 625 is a more complex alloy than the Inconel 600 and contains several additional components. However, thermodynamically it is very similar to the Hastelloy and Haynes alloys, and reactions involving common components which are possible in the Hastelloy and Haynes alloy systems should also be possible in the Inconel 625 system. The only component in Inconel 625 which is not found in the other Ni- and Co-base alloys is columbium. The columbium would be a relatively weak reducing agent, and allowing for its partial molar free energy of mixing, would react with only the less stable fluorides and oxides in the WESF $^{90}SrF_2$.

11.2 SUMMARY

The WESF $^{90}SrF_2$ contains a number of fluoride impurities. Fortunately, the fluorides that are present in relatively high concentrations are the most stable of the metal fluorides (i.e., ZrF_2, ZrF_4, NaF, CaF_2, etc.). The thermodynamic analysis of the WESF $^{90}SrF_2$-alloy systems indicates a large number of reactions are possible between alloy components and impurity fluorides. With one exception, however, the potential reactions are restricted to impurity fluorides that are present in low concentrations. The only possible reactions involving fluorides present in large concentrations are limited to those involving lanthanum, which is found in trace levels in Haynes Alloy 188.

A number of reactions involving oxides are also possible in the various metal-fluoride systems. However, the concentration of oxygen in the fluoride is very low (<0.05 wt%), and most of the oxygen is present as water or nitrate. Therefore, the concentration of metal oxides in the fluoride should be very low, and of the oxides present, only the least stable should react with the components of the alloys.

Based on the thermodynamic calculations, TZM and tungsten should provide the greatest resistance to attack by WESF $^{90}SrF_2$. Because of the similarity in composition of the Ni- and Co-base alloys it is impossible to predict, on a thermodynamic basis, the relative resistance of these alloys to attack by WESF $^{90}SrF_2$. All of the Ni- and Co-base alloys will be attacked by the fluoride to some degree. The extent of attack of each alloy under a given set of conditions would depend on reaction kinetics. The reaction kinetics are almost impossible to estimate because of a lack of reliable data. A realistic evaluation of WESF $^{90}SrF_2$-alloy reactions can only be obtained by experimental studies.

The thermodynamic analysis of fluoride-alloy systems discussed above was based on a number of simplifying assumptions. A rigorous analysis which ignores these assumptions could provide significantly different results. Such an analysis is hampered by a lack of information on the compounds present in the WESF $^{90}SrF_2$, and a lack of thermochemical data on complex compounds, intermetallics and solid solutions which may be present in the systems.

11.3 REFERENCES

1. T. Rosenqvist, Thermochemical Data for Metallurgists, Tapir Forlag, 1970.
2. A. Glassner, Thermochemical Properties of the Oxides, Fluorides and Chlorides, to 2500°C, ANL-5750, Argonne National Laboratory, 1957.
3. C. J. Smithells, Metals Reference Book Vol. 1, Butterworth's, London, 1967.
4. O. Kubaschewski and E. L. Evans, Metallurgical Thermochemistry, Pergamon, London, 1958.
5. F. D. Richardson and J. H. E. Jeffes, J. Iron and Steel Inst., vol. 160, pp. 261-270, 1948.
6. J. H. Hildebrand and R. L. Scott, The Solubility of Nonelectrolytes, Reinhold Publishing Corp., New York, 1950.

DISTRIBUTION

No. of Copies

OFFSITE

1 ERDA Chicago Patent Attorney
9800 S. Cass Avenue
Argonne, IL 60439

A. A. Churm

1 ERDA Division of Biomedical and Environmental Research
Washington, DC 20545

J. N. Maddox

2 ERDA Division of Production and Materials Management
Washington, DC 20545

F. P. Baranowski
R. W. Ramsey, Jr.

11 ERDA Advanced Nuclear Energy Systems, Space and Special Purposes Division

R. T. Carpenter
G. P. Dix
T. J. Dobry, Jr.
N. Goldenberg
A. P. Litman (3)
J. J. Lombardo
G. A. Newby
B. J. Rock
E. J. Wahlquist

1 ERDA Oak Ridge Operations Office
P.O. Box E
Oak Ridge, TN 37830

D. C. Davis, Jr.

No. of Copies

3 ERDA Savannah River Operations Office
P.O. Box A
Aiken, SC 29801

R. H. Bass
T. B. Hindman
R. K. Huntoon

170 ERDA Technical Information Center

1 Department of the Army
Headquarters, U.S. Army
Facilities Engineering
Support Agency
Fort Belvoir, VA 22060

H. Musselman, Technical Director

1 Electronics and Applied Physics Division
Building 347.3, AERE Harwell
Oxfordshire OX11 ORA
Great Britain

E. H. Cooke-Yarborough

1 General Atomic Company
P.O. Box 81601
San Diego, CA 92138

H. C. Carney

1 General Electric Company MSVD
P.O. Box 8555
Philadelphia, PA 19101

P. E. Brown

1 General Electric Company, Vallecitos Laboratory
P.O. Box 846
Pleasanton, CA 94566

G. E. Robinson

3 Los Alamos Scientific Laboratory
P.O. Box 1663
Los Alamos, NM 87544

S. E. Bronisz
R. A. Kent
R. N. Mulford

No. of Copies	
1	Monsanto Research Corporation Mound Laboratory (ERDA) Nuclear Operations P. O. Box 32 Miamisburg, OH 45342 W. T. Cave
1	Naval Nuclear Power Unit P. O. Box 96 Ft. Belvoir, VA 22060 F. E. Rosell
1	Naval Facilities Engineering Command Nuclear Power Division (FAC04N) 200 Stovall Street Alexandria, VA 22332 G. E. Krauter
1	Navy Office of the Chief of Naval Operations Washington, D.C. 20390 Head, Reactor Branch
4	Holifield National Laboratory Oak Ridge, TN 37830 R. S. Crouse J. R. DiStefano E. Lamb A. C. Schaffhauser
3	Teledyne Energy Systems 110 W. Timonium Road Timonium, MD 21093 P. Dick R. Hannah P. Vogelberger
1	Westinghouse Astronuclear Laboratory P. O. Box 10864 Pittsburgh, PA 15236 C. C. Silverstein

No. of Copies	
2	ERDA Richland Operations
	W. C. Johnson
	B. J. Melton
7	Atlantic Richfield Hanford Company
	L. I. Brecke
	R. E. Isaacson
	L. M. Knights
	C. W. Malody
	J. D. Moore
	G. C. Oberg
	H. P. Shaw
31	Battelle-Northwest
	J. W. Bartlett
	R. E. Burns
	T. D. Chikalla
	R. L. Dillon
	J. W. Finnigan
	H. T. Fullam (10)
	K. M. Harmon
	A. J. Haverfield
	J. H. Jarrett
	R. S. Kemper
	R. P. Marshall
	R. W. McKee
	J. M. Nielsen
	R. E. Nightingale
	L. D. Perrigo
	A. M. Platt
	J. L. Simmons
	H. H. Van Tuyl
	Technical Information Files (3)
	Technical Publications